One- and three-dimensional measurements of the matter distribution from eBOSS and first DESI Lyman-α forest samples

Corentin Ravoux

Euclid France Galaxy Clustering
24 November 2022

CENTRE DE PHYSIQUE DES PARTICULES DE MARSEILLE
CPPM

SDSS

DARK ENERGY SPECTROSCOPIC INSTRUMENT
U.S. Department of Energy Office of Science

The Lyman-α forest

- Lyman-α: transition of neutral Hydrogen to first excited state $\lambda_\alpha = 1215.67$ Å
- Lines in quasar spectra at $\lambda_{\mathrm{obs}} = (1 + z_{\mathrm{abs}})\lambda_\alpha$ caused by absorber in the intergalactic medium (IGM) at z_{abs}

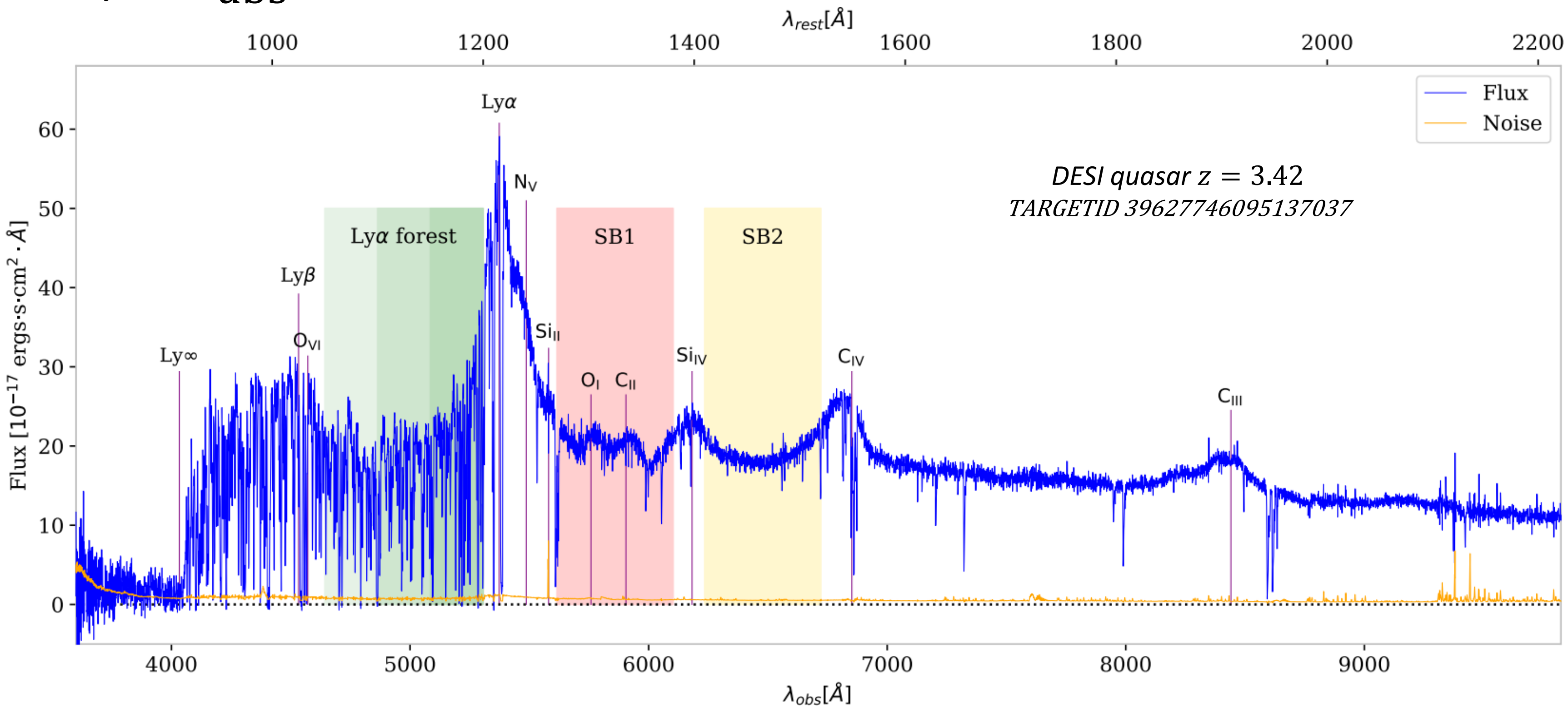

Lyman-α forest = Non-linear tracer of the neutral Hydrogen in the IGM

Definition of observational statistics

- <u>Lyman-α contrast</u>: Quasar continuum fitted to normalize absorptions in the flux

$$\delta_F(\lambda) = \frac{f(\lambda)}{\overline{F}(\lambda) C_{\mathrm{q}}(\lambda, z_{\mathrm{q}})} - 1$$

- Cross-correlation with a tracer X:

$$\xi_{\alpha X}(\vec{r}) = < \delta_F(\vec{x}) \delta_X(\vec{x} + \vec{r}) >_x$$

- One dimensional power spectrum:

$$P_{\mathrm{1D},\alpha}(k) = \langle |\delta_F(k)|^2 \rangle$$

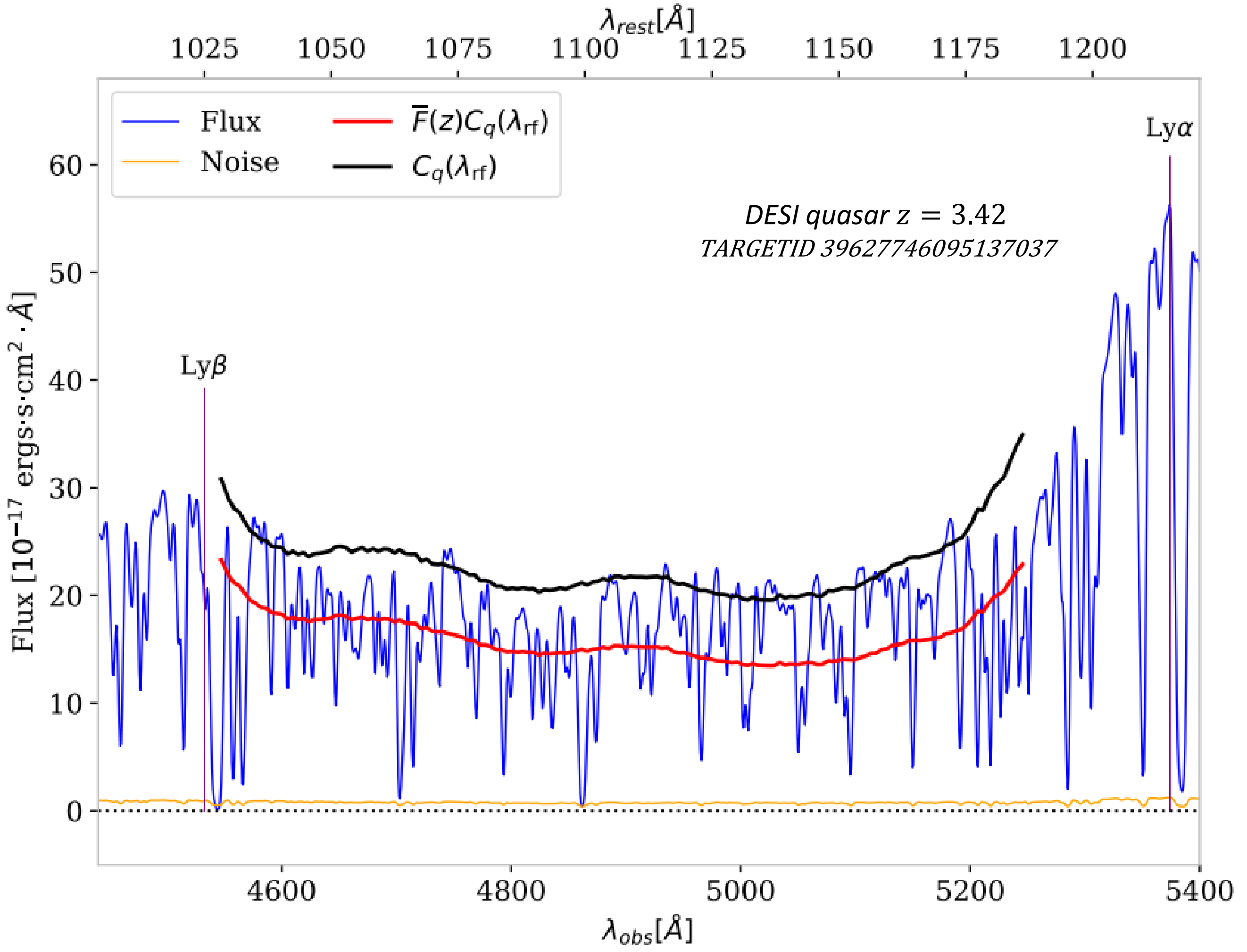

Contaminants

- Near the quasar:
  - Intrinsic continuum
  - Broad absorption line quasars (BAL)
- Along the line-of-sight:
  - Metal absorptions in the IGM
  - Damped Lyman-α systems (DLA)
- Near the telescope:
  - Atmospheric emission lines
  - Instrument noise
  - Spectrograph resolution

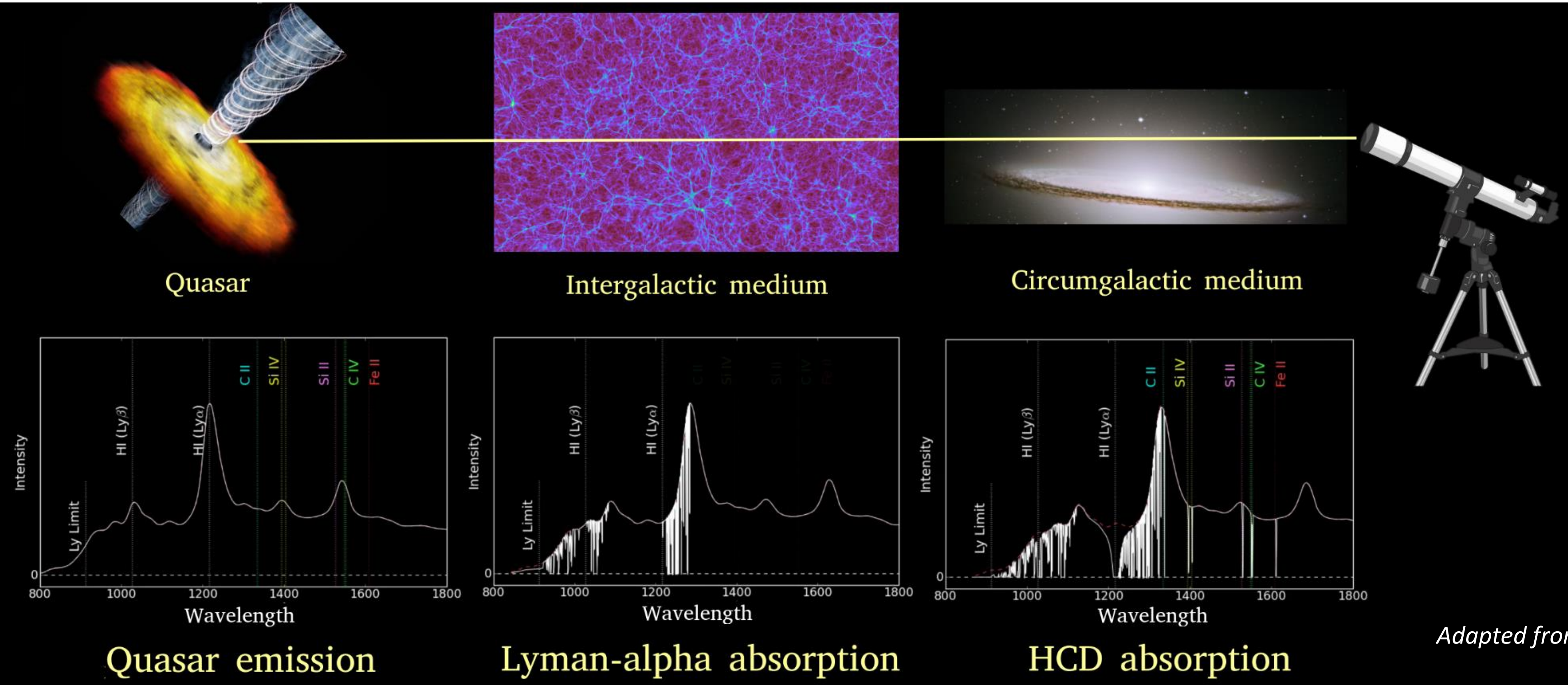

Adapted from A. Pontzen video

Lyman-α tomography and voids

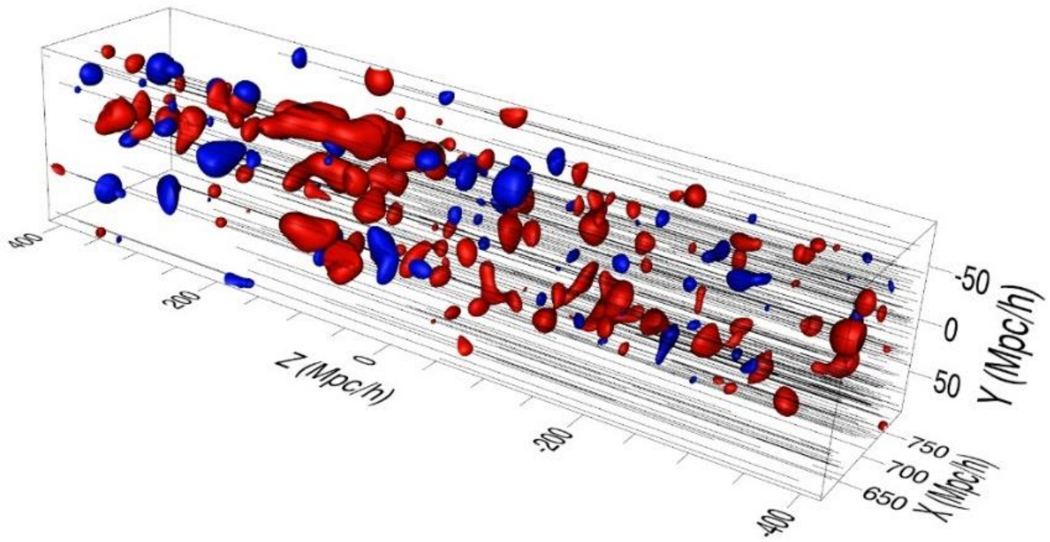

Ravoux et al. JCAP07(2020)010

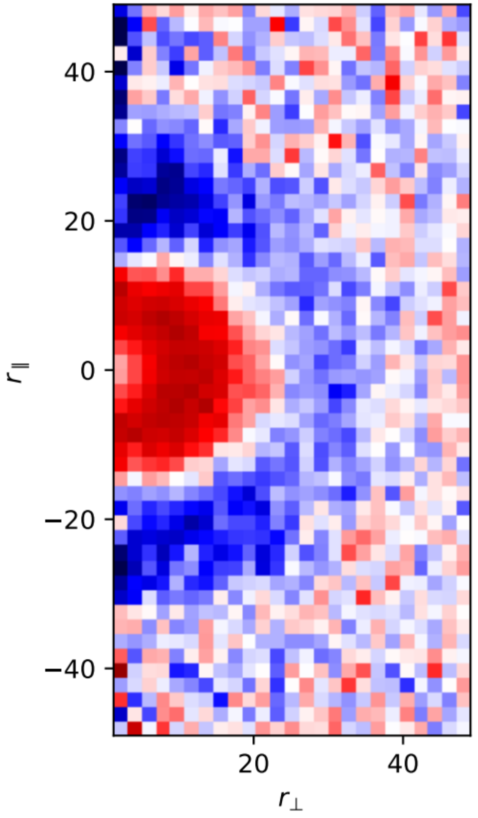

Ravoux et al. 2022

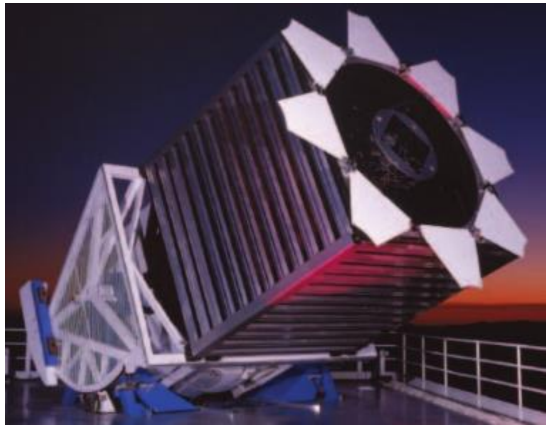

SDSS

eBOSS

CENTRE DE PHYSIQUE DES PARTICULES DE MARSEILLE
CPPM

SDSS

DARK ENERGY SPECTROSCOPIC INSTRUMENT
U.S. Department of Energy Office of Science

Lyman-α tomography

- 3D map of Lyman-α absorption from 1D spectra (*Pichon et al. 2001)*
- Initial goal: map the cosmic web ~ Mpc scale
- Example: CLAMATO (*Lee et al. 2018*)

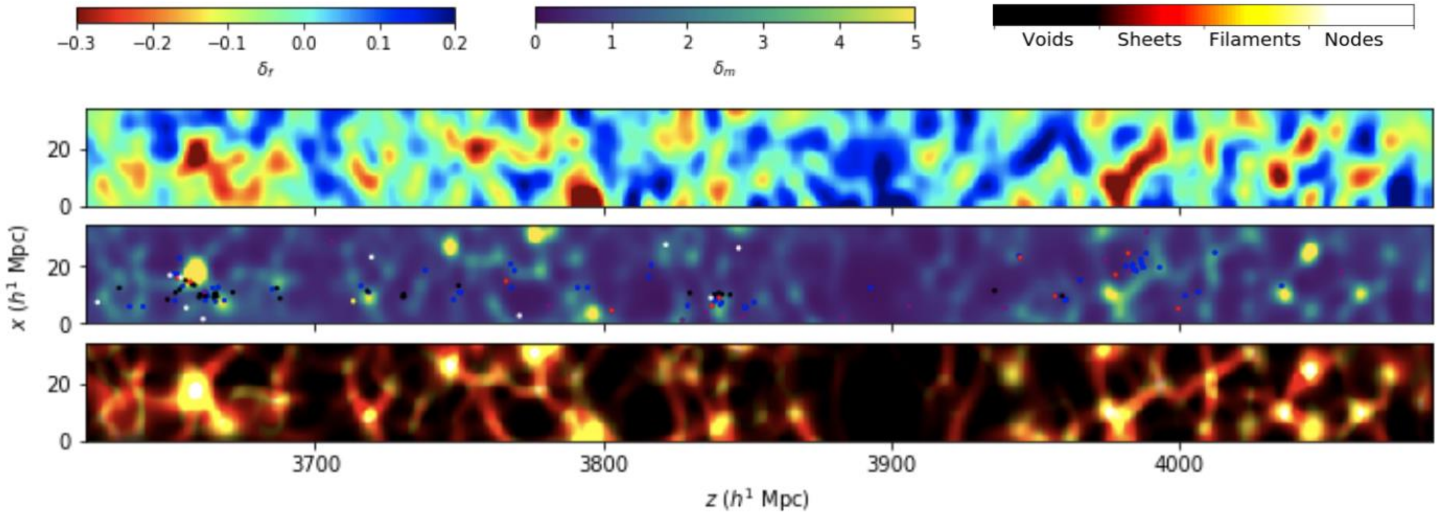

- Our objective: produce 3D map at large scales for large volumes ($\sim \mathrm{Gpc}^3 . h^{-3}$).
  - Need large volume surveys, with lower density of targets
  - Use of eBOSS DR16 data

Large-scale Lyman-α tomography with eBOSS

- Stripe 82 data:
  - Dense and homogeneous field
  - Mean separation 13 $h^{-1} \cdot \mathrm{Mpc}$

- Use of CLAMATO Wiener filter algorithm:
  - Noise-dependent interpolation of lines-of-sight with Gaussian kernels
  - Reconstruction length 13 $h^{-1} \cdot \mathrm{Mpc}$

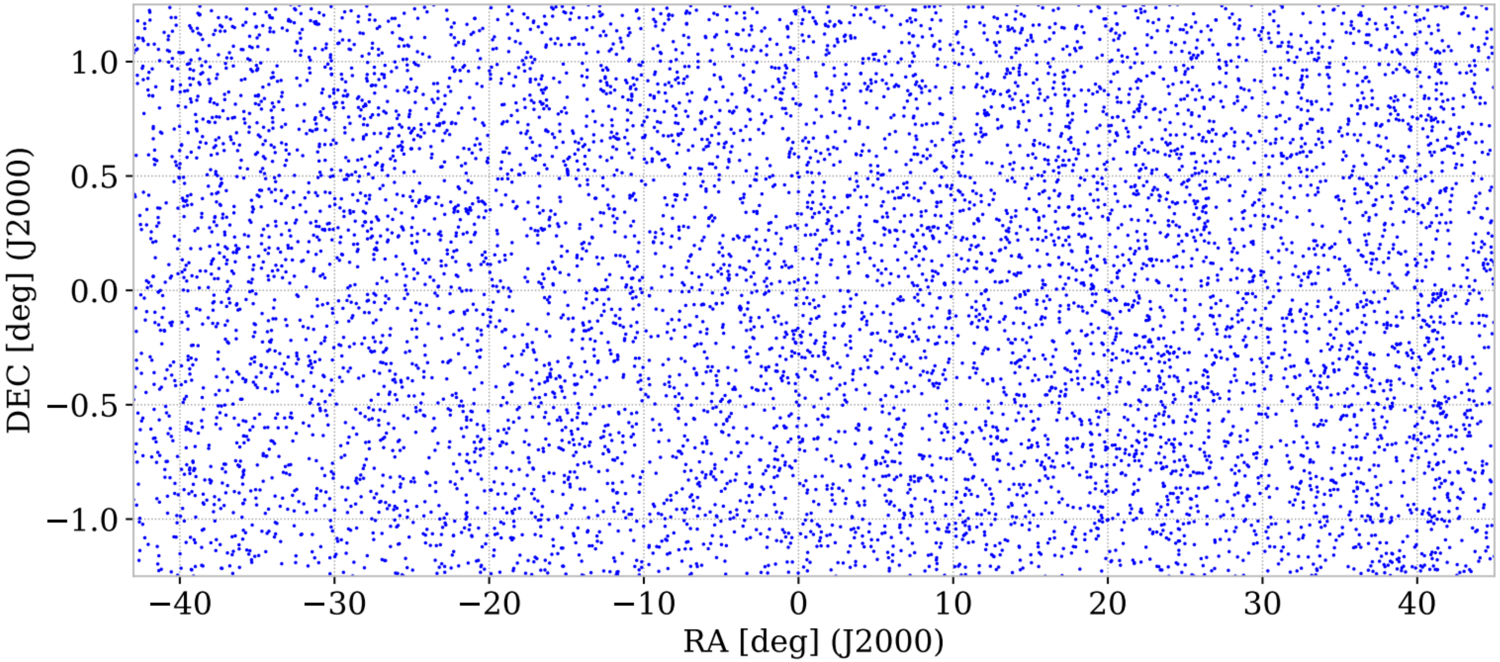

3D representation

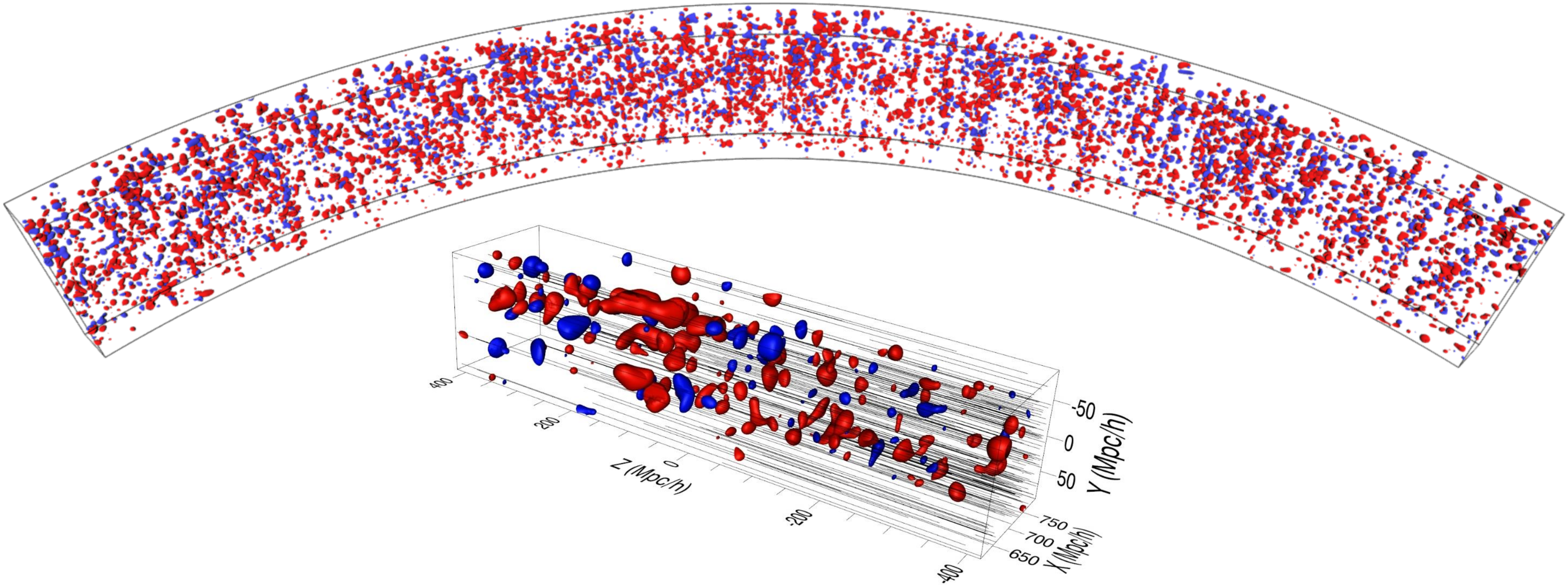

Largest 3D map tracing matter at redshift $z > 2$

Applications of Lyman-α tomography

- Average map of the reconstructed Lyman-α contrast around quasar positions:
  - Recast 3D view of cross-correlation between Lyman-α forest and quasars

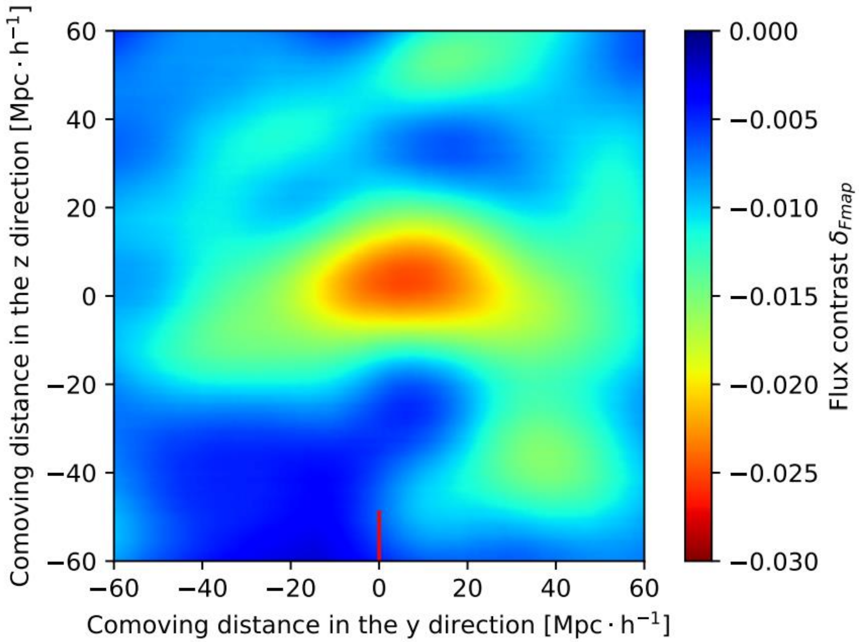

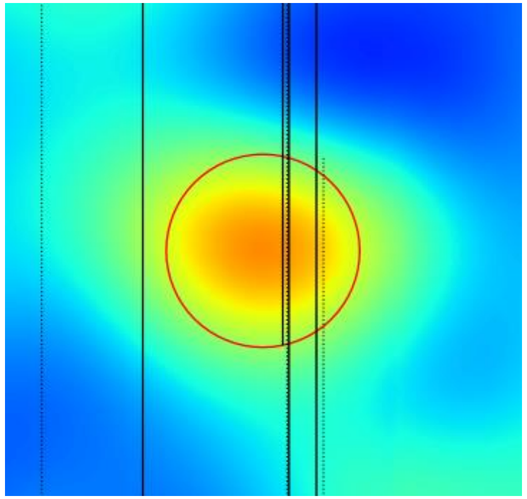

- Proto-cluster candidates identification:
  - Selection on Lyman-α contrast threshold and number of crossed lines-of-sight
  - **Identification of 8 proto-cluster candidates over Stripe 82**

High redshift voids

- Cosmic voids = 80 % in volume of the cosmic web
- Implementation of a 3D multi-threaded spherical void finder

First large void catalog at redshift $z > 2$

- Our objectives:
  - Study the shape of our voids and extend galaxy void analysis to redshift $z > 2$
  - Measure velocity flow around voids (redshift space distortions)

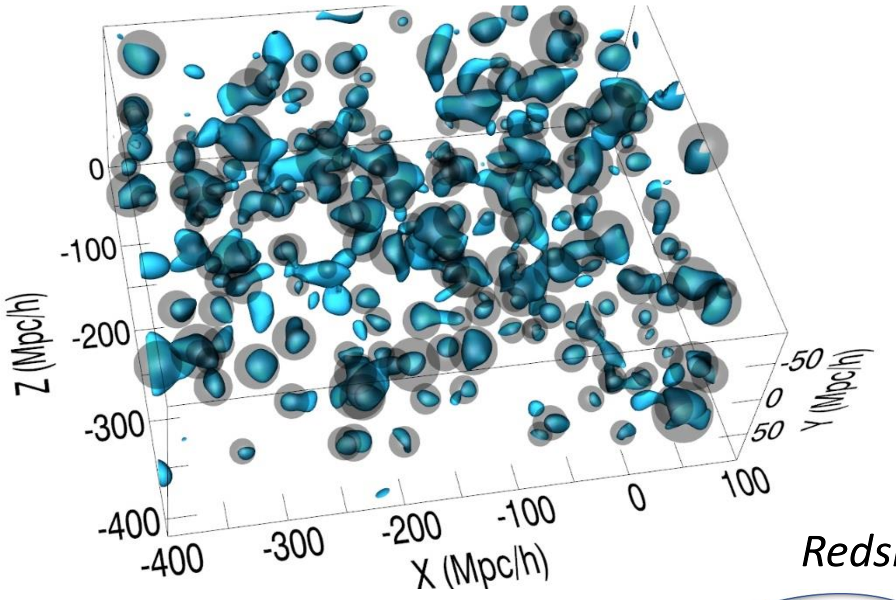

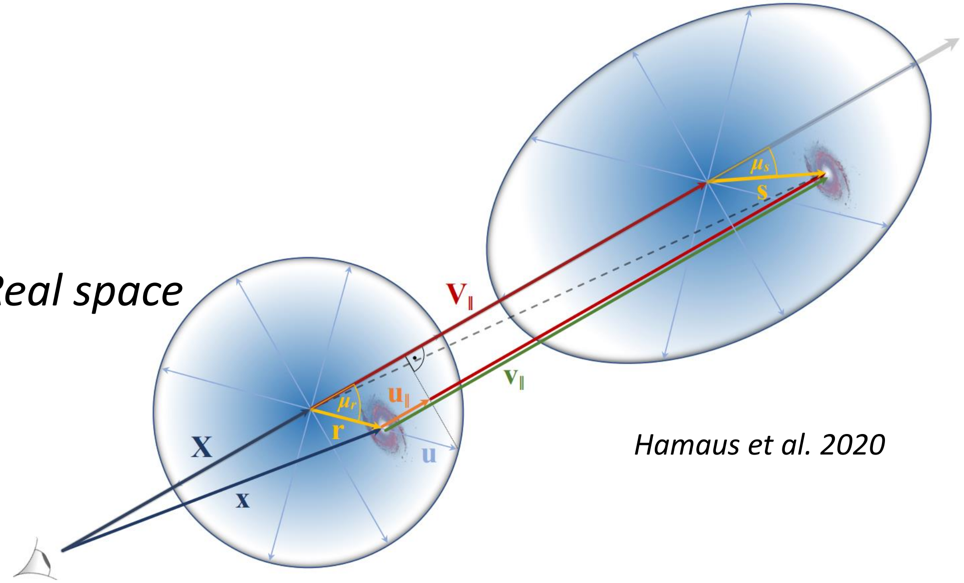

Lyman-α x void cross-correlation

- Cross-correlation between void centers and Lyman-α flux contrast:

$$\xi_{v\alpha}\left(A \equiv (r_\perp, r_\parallel)\right) = \frac{\sum_{(i,j)\in A} w_i \delta_{F,i}}{\sum_{(i,j)\in A} w_i}$$

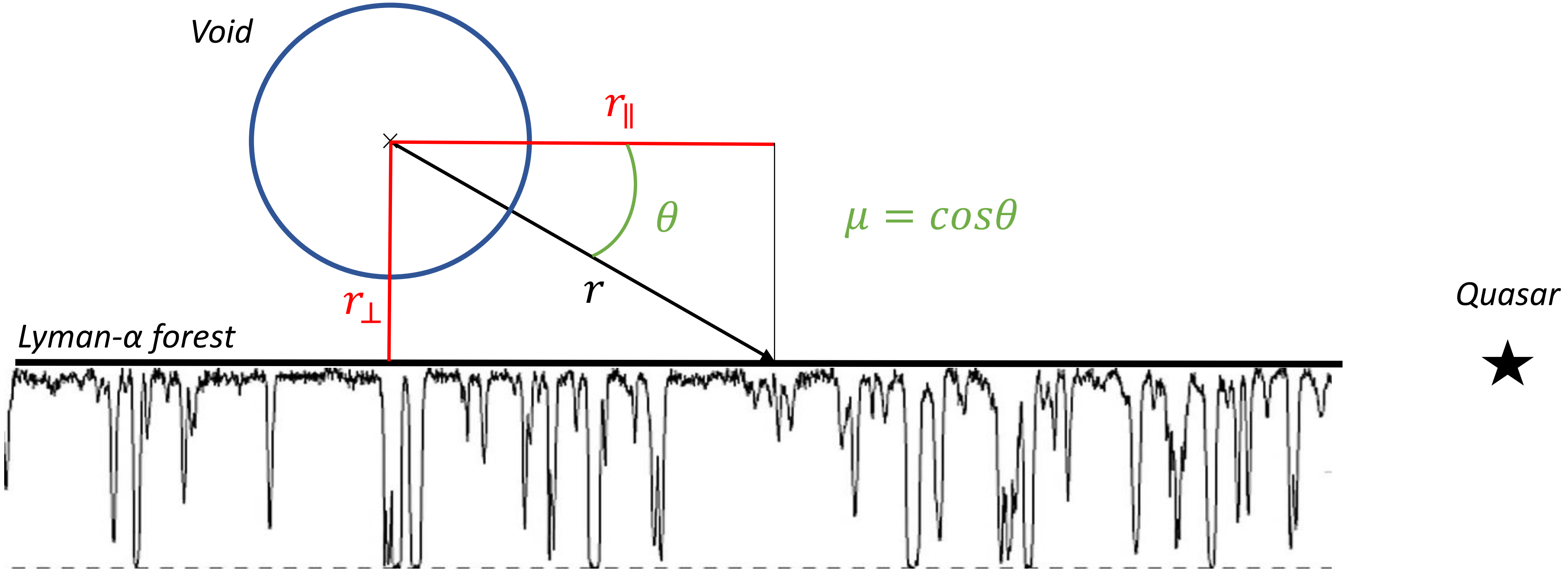

Measurement on eBOSS data

- Measure $\xi_{v\alpha}(r,\mu)$
- Decomposition into multipoles on Legendre basis:

$$\xi_\ell(r) = \int_{-1}^{1} \xi(r,\mu)\left(\frac{1+2\ell}{2}\right) P_\ell(\mu) d\mu$$

  - ξ_0 = Average void profile
  - ξ_2 = Measure departure from spherical symmetry, contains RSD signal

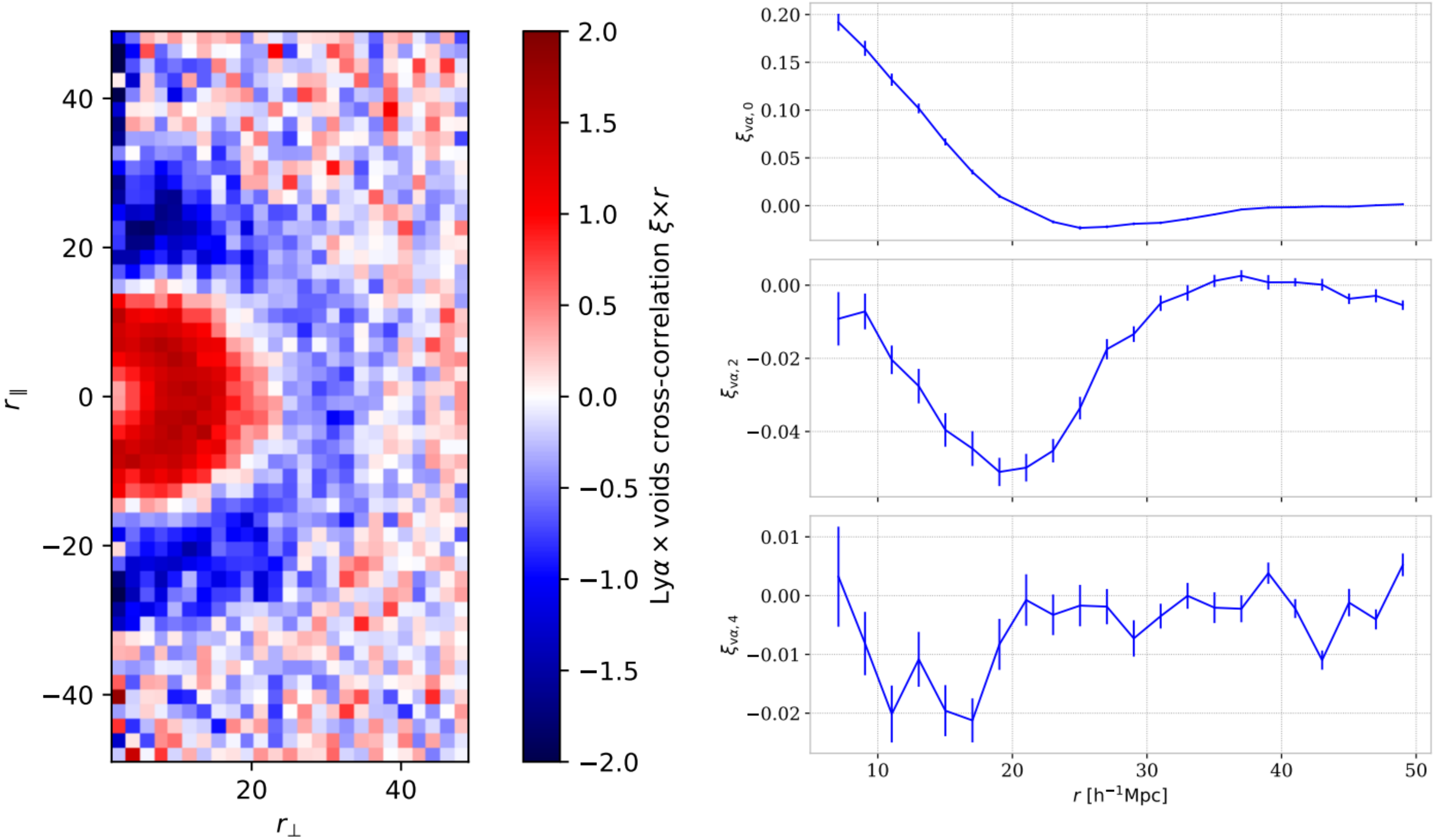

Study of cross-correlation with mocks

- Systematic effects:
  - Realizations on the same matter field adding systematics (Continuum fitting, Noise, Metals, DLA)
  - Relatively minor impact on the quadrupole which contains RSD signal
- Impact of RSD:
  - Mocks with and without RSD effect
  - Used 11 realizations to reduce statistical uncertainties
- **RSD impact seen on quadrupole**

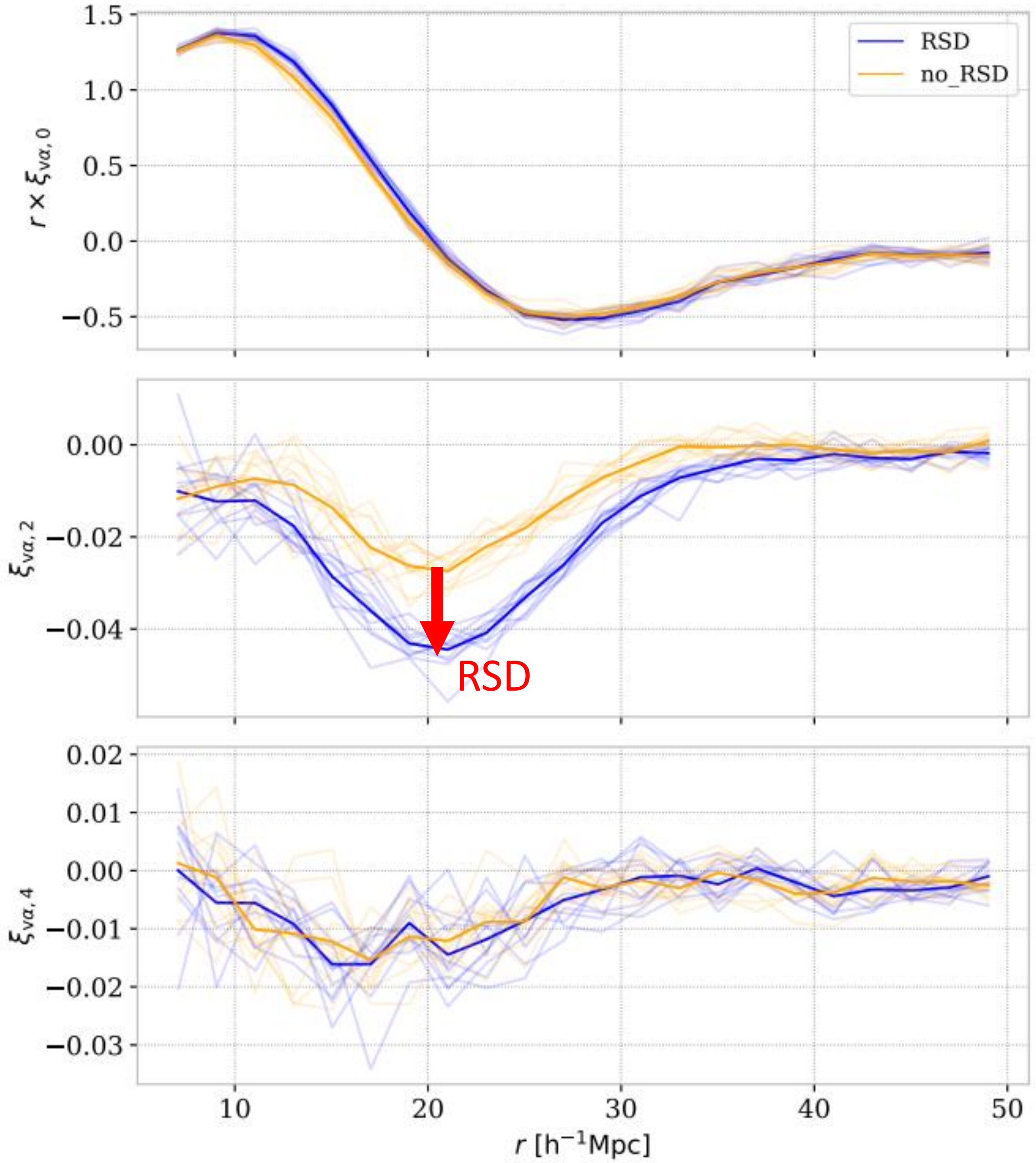

RSD parameter measurement

- Adaptation of a linear void model to Lyman-alpha forest:

$$\xi_2(r) = \left(\frac{2\beta}{3+\beta}\right)\left(\xi_0(r) - \bar{\xi}_0(r)\right)$$

- On eBOSS data:

$$\boldsymbol{\beta = 0.52 \pm 0.05}$$

First measurement of velocity flow around voids at $z > 2$

- Full interpretation of this value requires additional studies with cosmological simulations

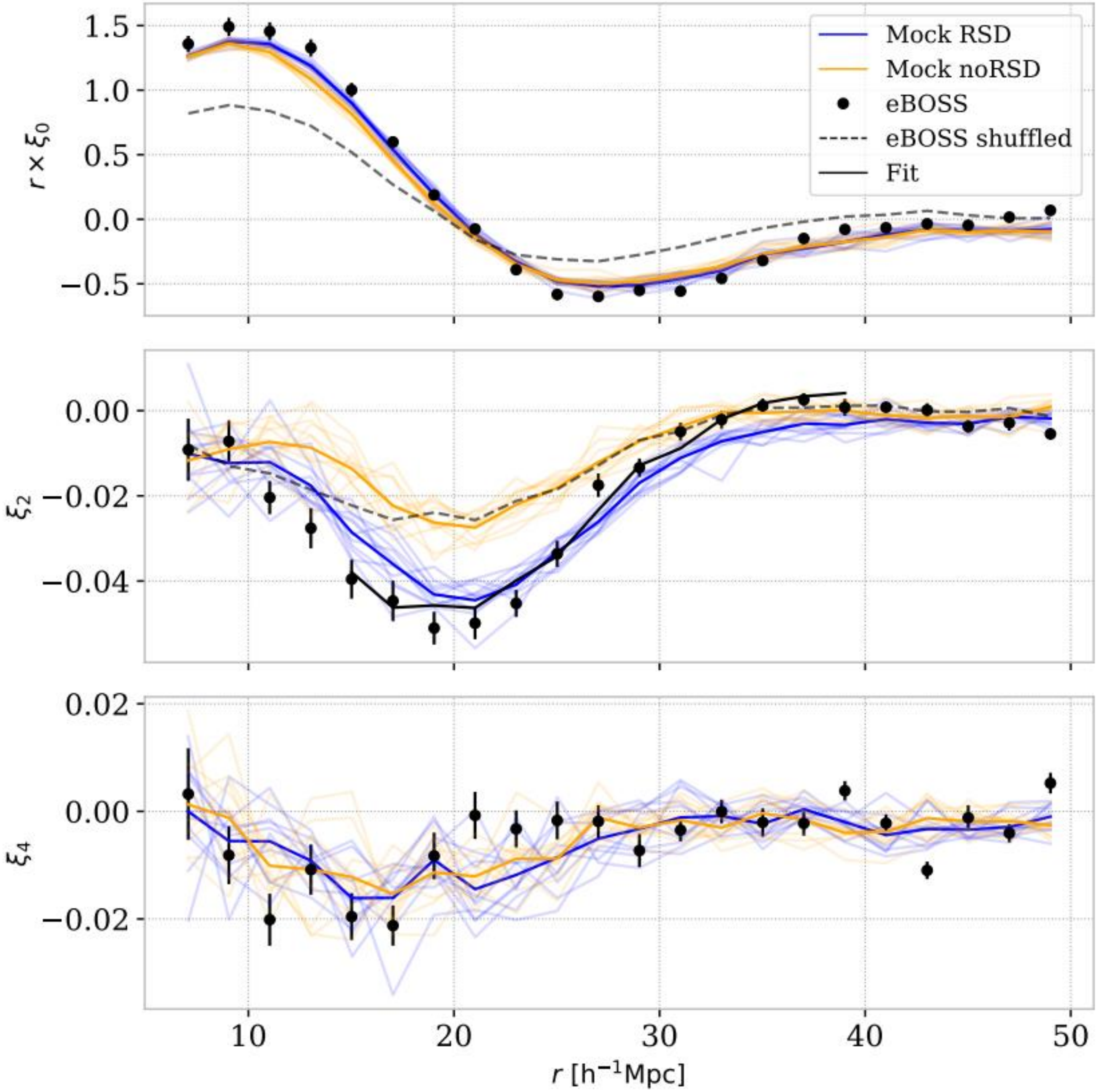

DARK ENERGY SPECTROSCOPIC INSTRUMENT

One dimensional power spectrum

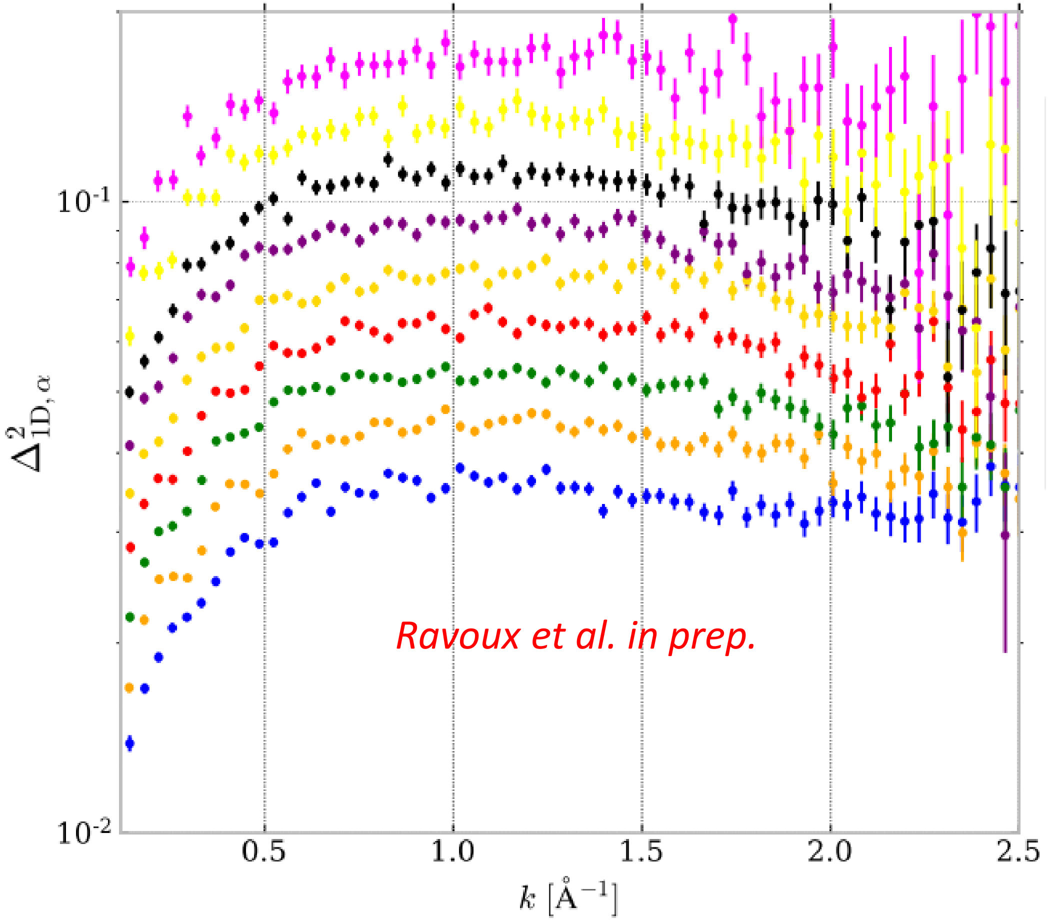

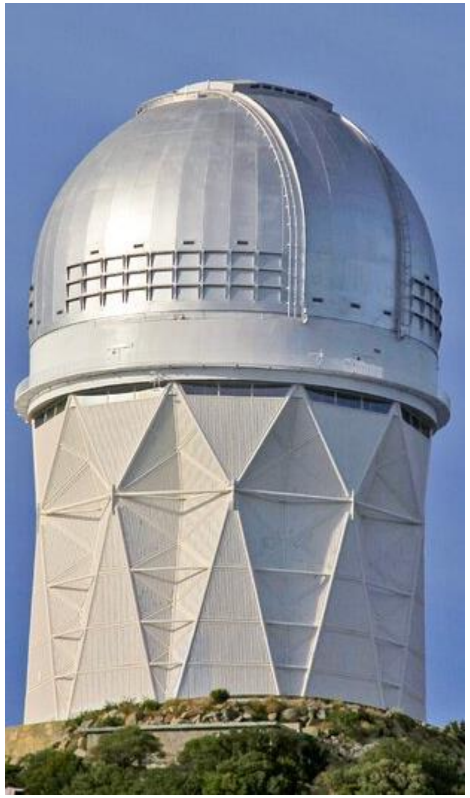

$P_{1\text{D},\alpha}$ measurement

- One dimensional power spectrum ($P_{1\text{D},\alpha}$)
  - Correlation along the line-of-sight
  - Probes small-scale matter clustering

- First measurement with DESI:
  - Increased statistics and resolution
  - Realize first measurement with method similar to eBOSS

- **Use to probe the small-scale matter power spectrum**

Latest measurement (eBOSS)

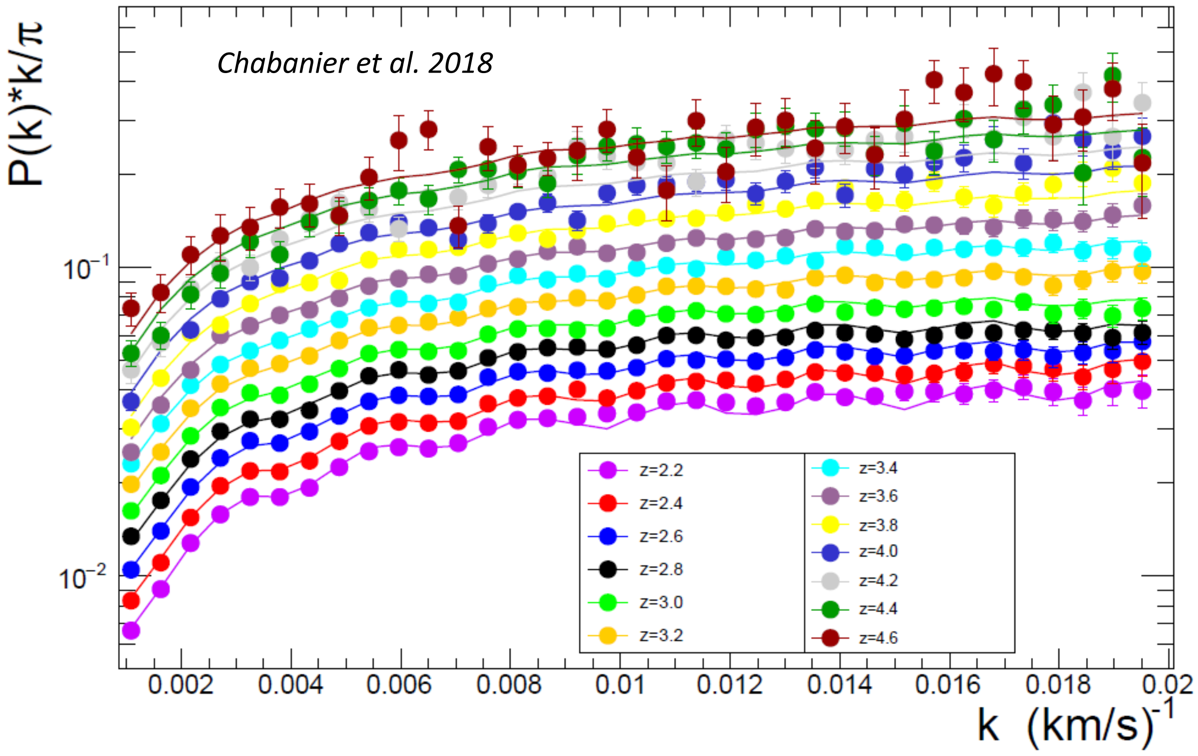

Large scales

Small scales

Application of $P_{1D,\alpha}$

- Matter power spectrum impacted by:
  - Sum of neutrino masses $\sum m_\nu$
  - Dark matter model (e.g. warm dark matter)

$P_{1D,\alpha}$ unique tool to constrain neutrino masses and dark matter properties

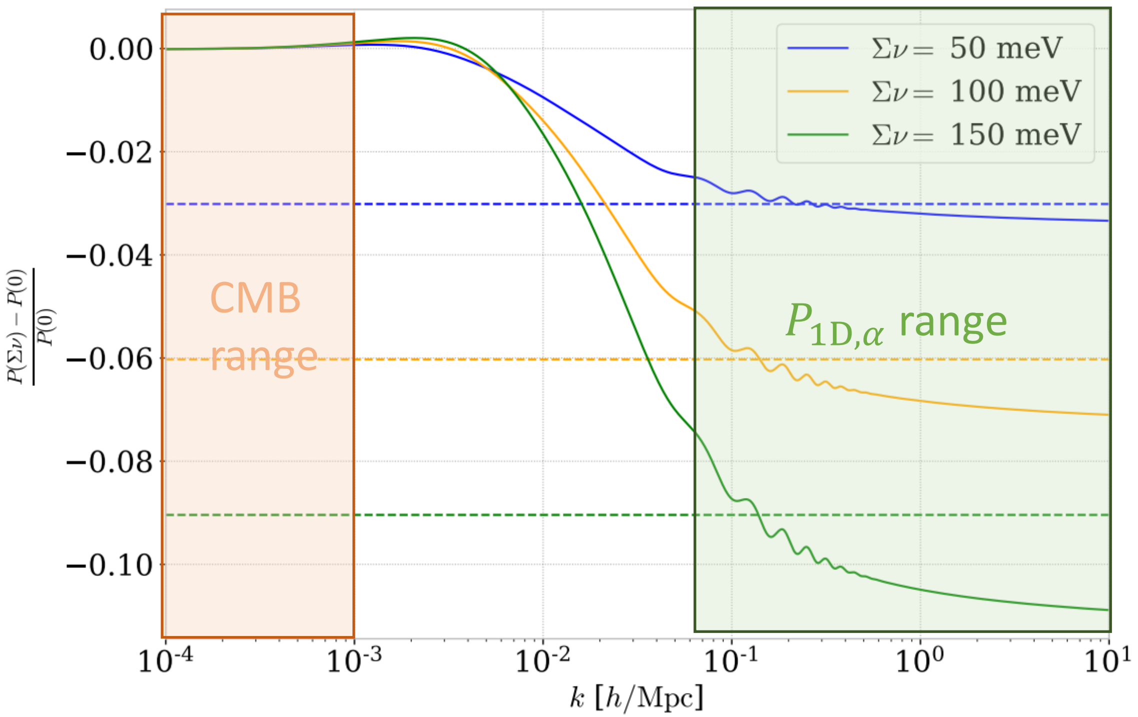

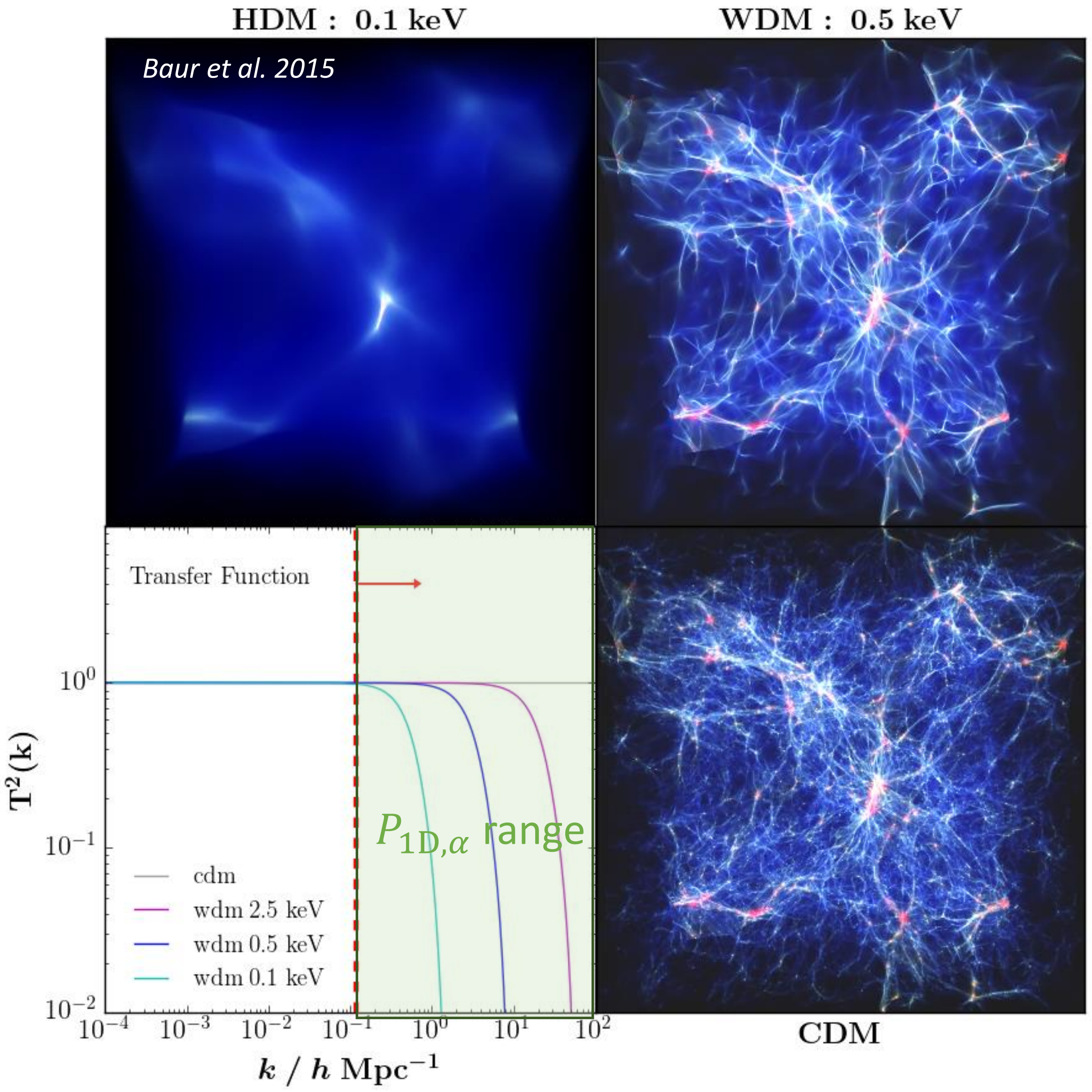

Systematic effects

- Instrumental:
  - Detector (spectrograph) noise
  - Finite spectrograph spectral resolution
- Astrophysical:
  - **Absorption by other IGM elements (metals)**
  - Damped Lyman-α systems (DLAs)
  - Missed broad absorption lines quasars (BALs)
- Analysis:
  - Masking of sky emission lines
  - Continuum fitting error

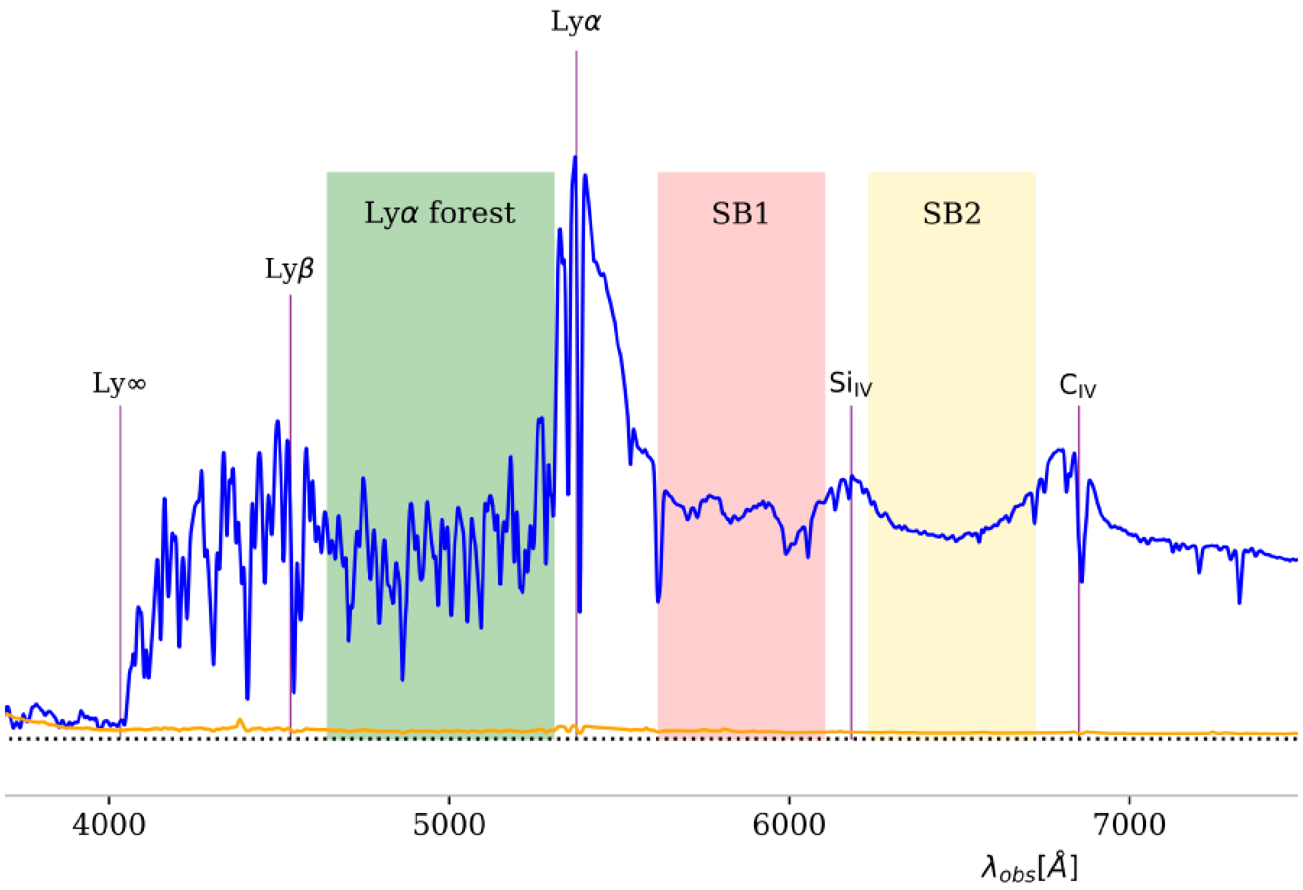

Example: effect of metals

- Contribution to $P_{1D,\alpha}$ from metals estimated using side bands
- Physically motivated parametrization to closely reproduce side band power spectrum
- Side band power spectrum subtracted to $P_{1D,\alpha}$ measurement

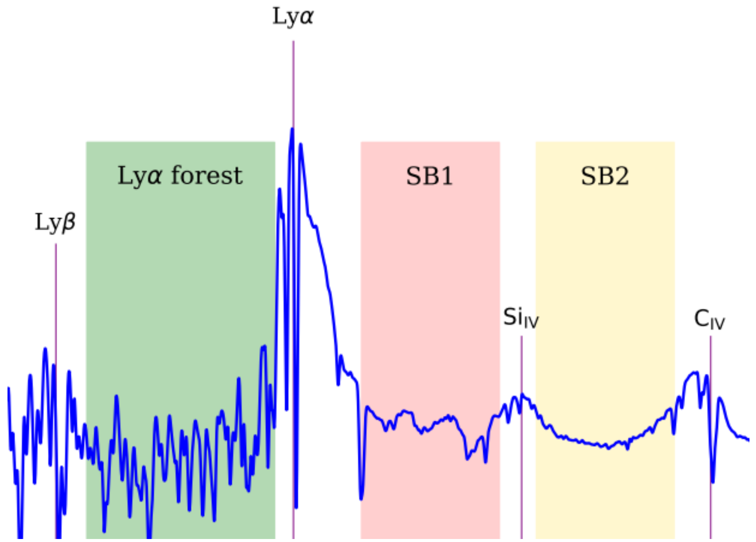

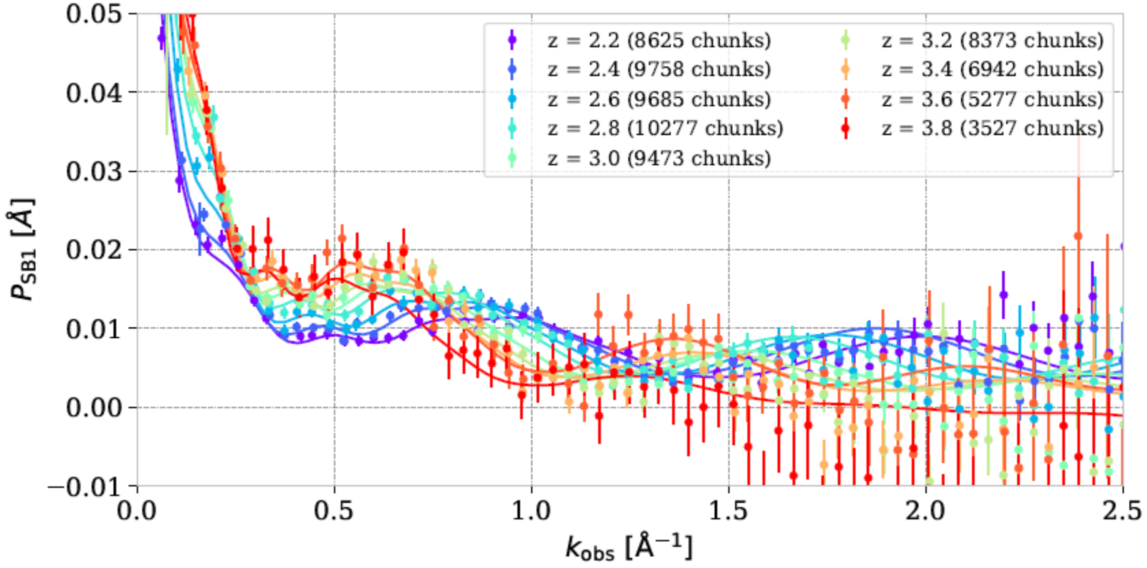

$P_{1D,\alpha}$ measurement with first DESI data

- Data used:
  - Quasar spectra from survey validation & first 2 months of main survey
  - SNR quality cut applied
  - ~7000 quasar spectra used

- In agreement with eBOSS and high-resolution measurements on respective wavenumber ranges

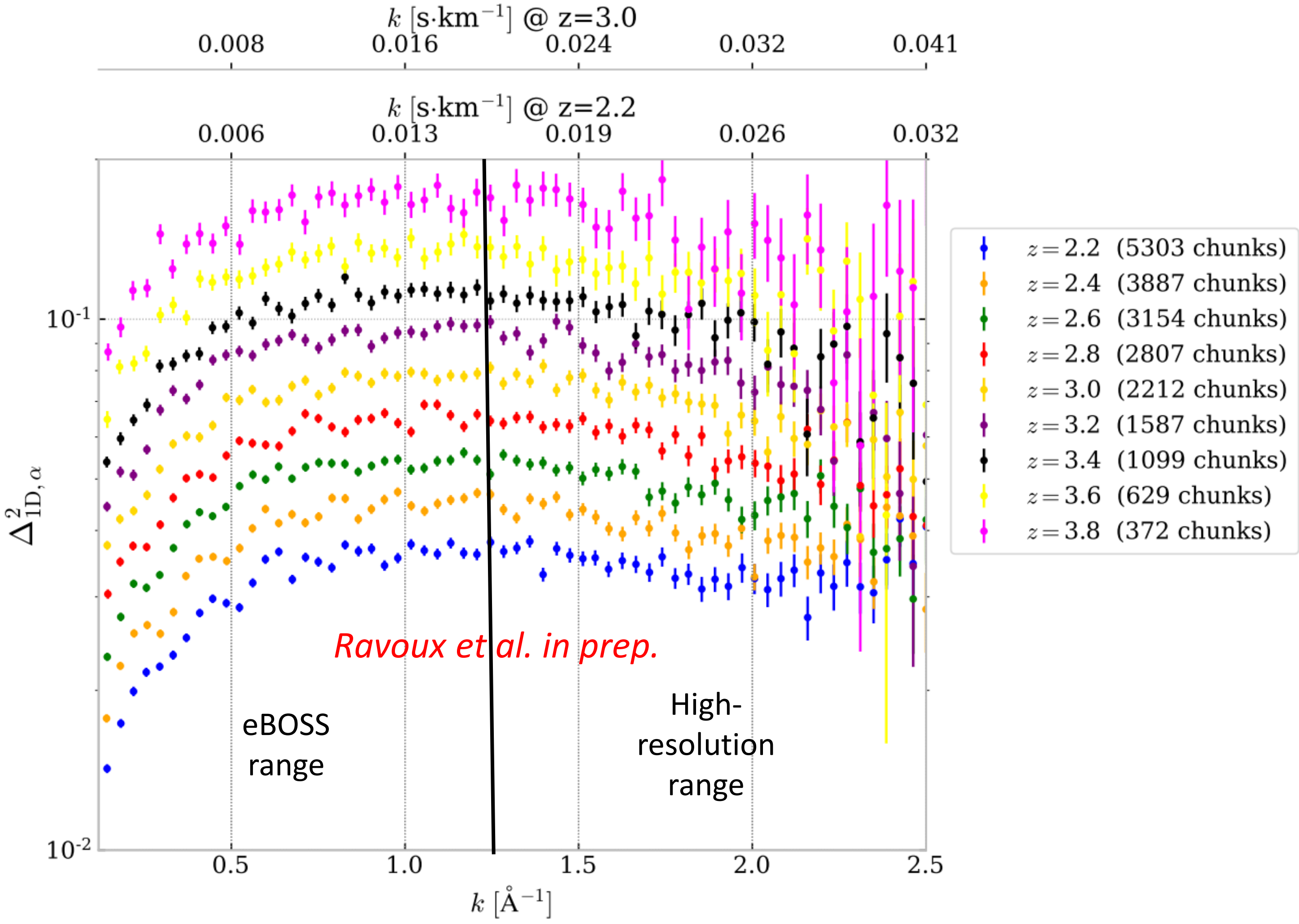

Interpreting this measurement with simulations will improve cosmological constraints

Conclusion

- Lyman-α tomography used to map a portion of the Universe
  Ravoux et al. JCAP07(2020)010

- Void cross-correlation, exploratory work to constrain growth of structures
  Ravoux et al. 2022

- $P_{1D,\alpha}$ will be used to improve constraints on neutrino mass and DM properties
  Ravoux et al. in prep.

Spectroscopic surveys for cosmology

- eBOSS: 2.5 m telescope at Apache Point Observatory
  - Observations end March 2019
- DESI: 4 m telescope at Kitt Peak Observatory
  - Automated targeting, 5000 spectra / observation
  - Survey validation (SV) early 2021
  - Main survey started in May 2021

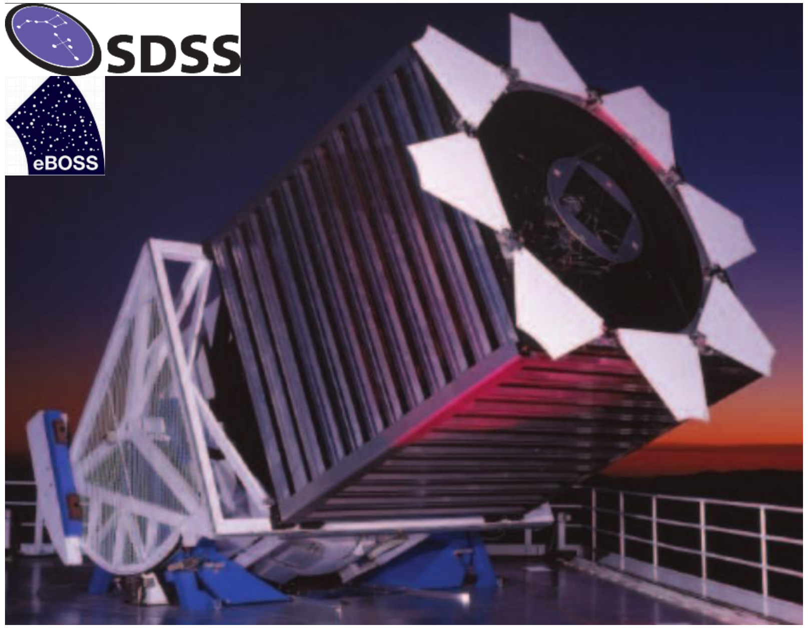

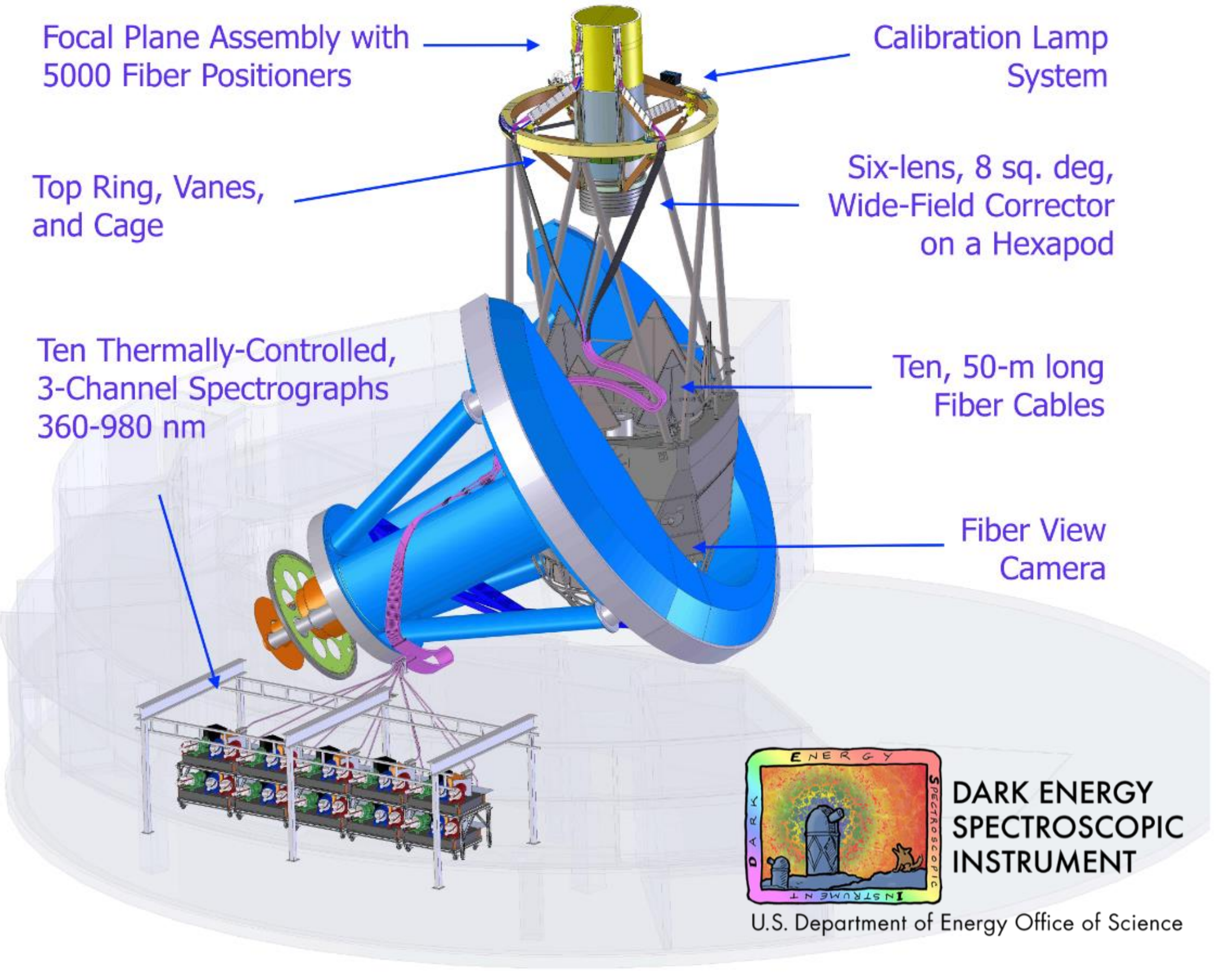

Lyman-α observations

- Moderate-resolution quasar surveys: Use of multi-object spectrographs
  - SDSS/eBOSS
  - DESI
  - WEAVE-QSO

- High-resolution quasar observations: SQUAD (VLT), KODIAQ (Keck), COS (HST), ANDES (ELT)

- Other target: Lyman- α forest from Lyman-Break Galaxies (CLAMATO, DESI-LBG)

High resolution observations

- <u>Currently</u> : R = 30 000 – 100 000, mean SNR per pixel ∼ 20
  - SQUAD survey (UVES,VLT), Murphy et al. 2019, 467 quasars
  - KODIAQ survey (HIRES,Keck), O'Meara et al. 2017, 300 quasars
  - COS instrument (HST), Danforth et al. 2016, 87 quasars

- <u>Future instruments</u>:
  - ESPRESSO instrument (VLT)
  - 4MOST Cosmology redshift survey (VISTA)
  - ANDES (ELT)

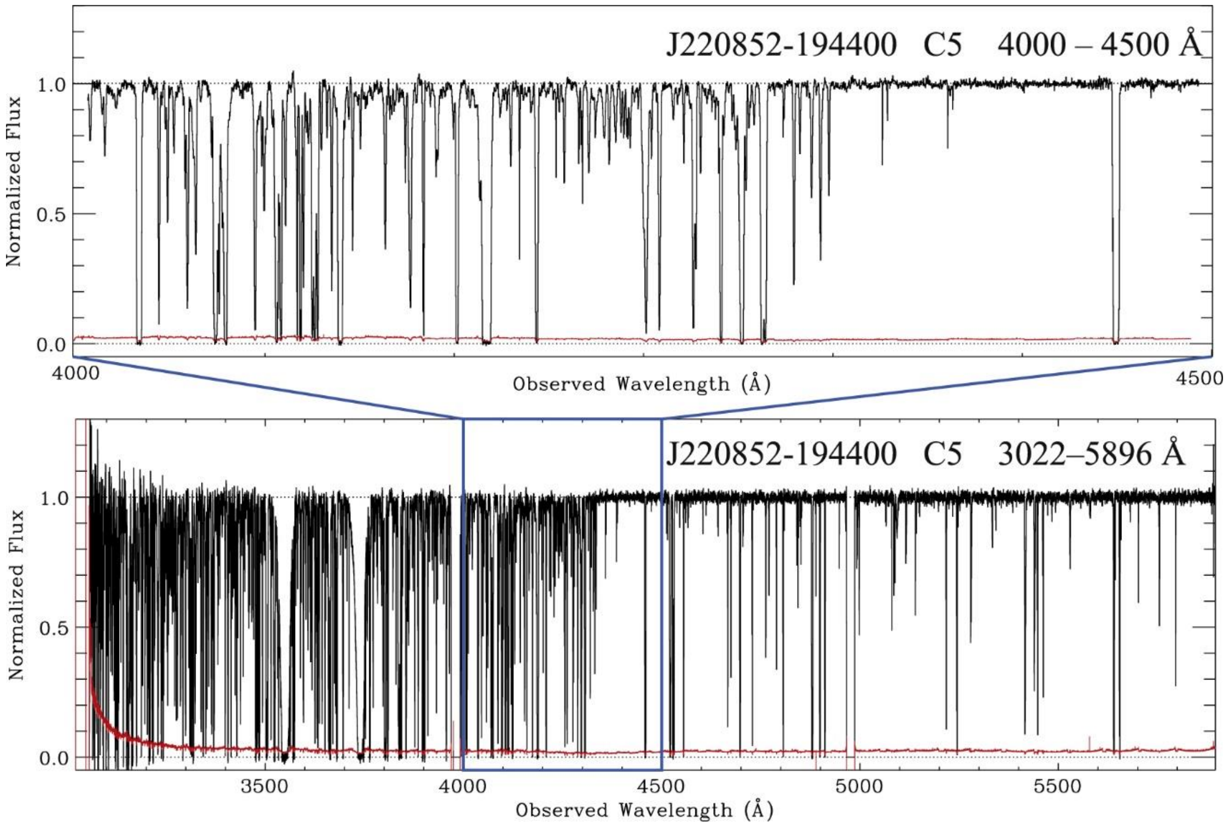

DESI Instrument

- Multi-object spectrograph
- Optical system redirect light from 5000 targets to 10 spectrographs
- Targeting done with a focal plane system composed of automated positioners
- Spectrographs composed of 3 spectral band each, receive 500 fiber light

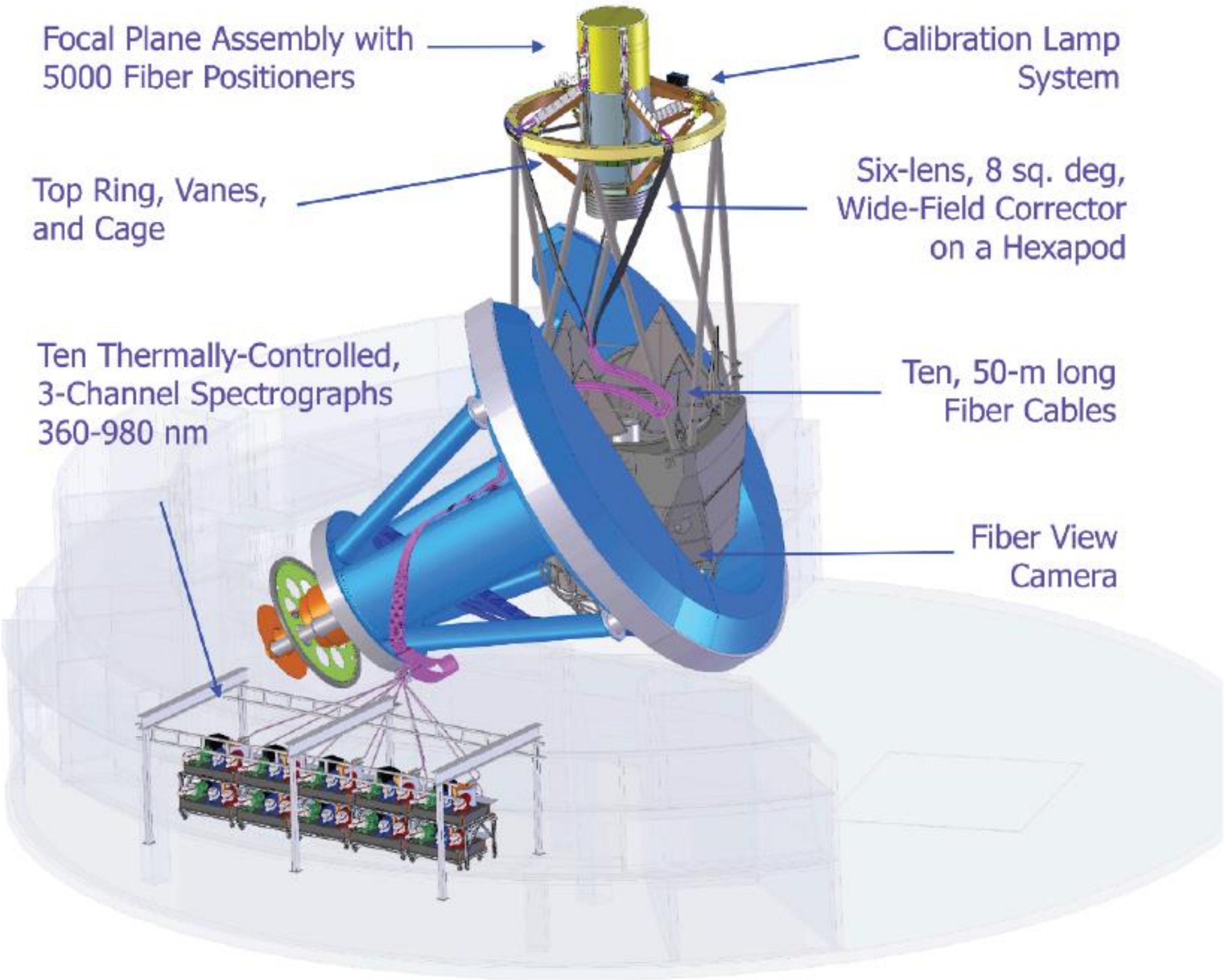

DESI Instrument

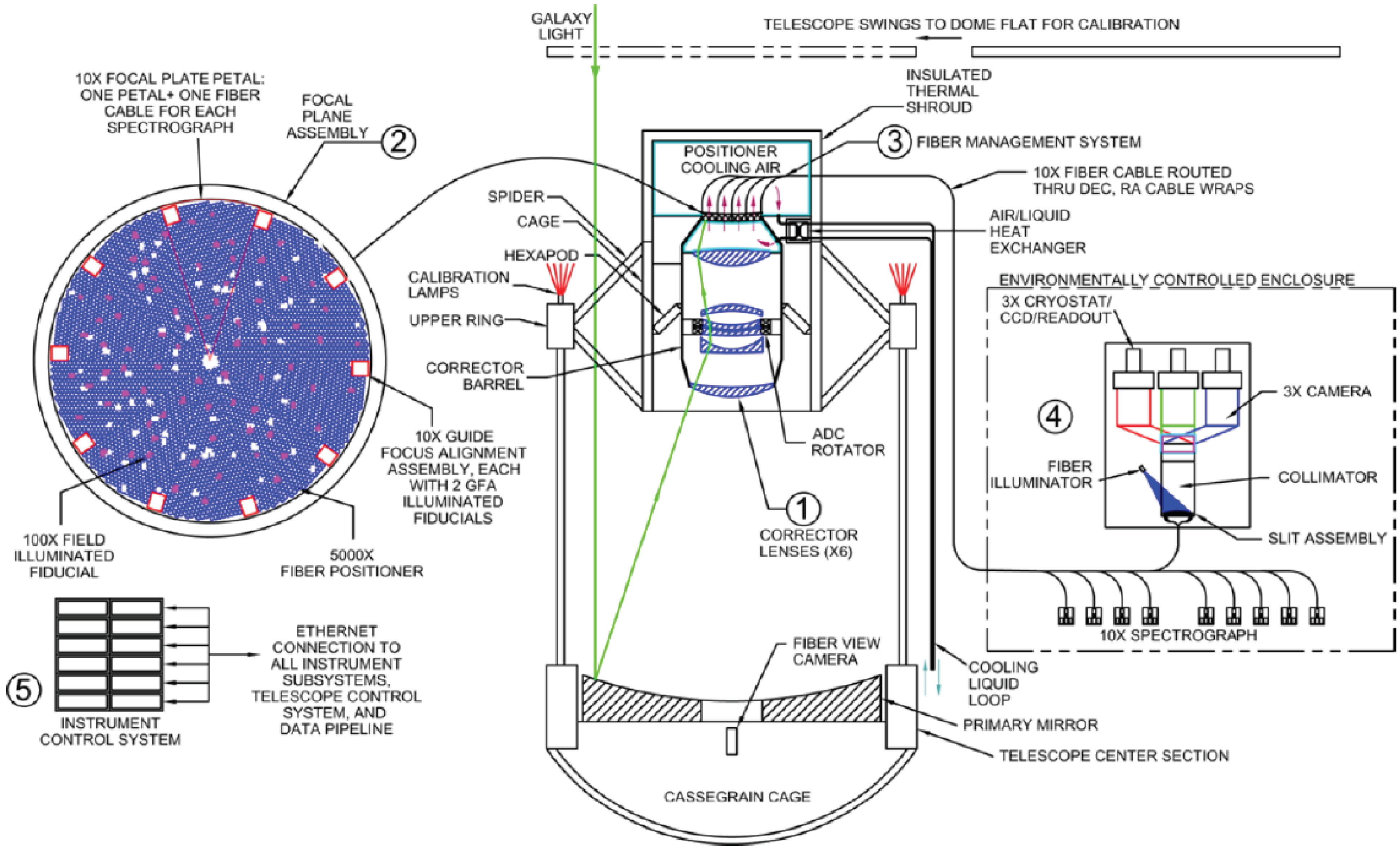

DESI Focal plan

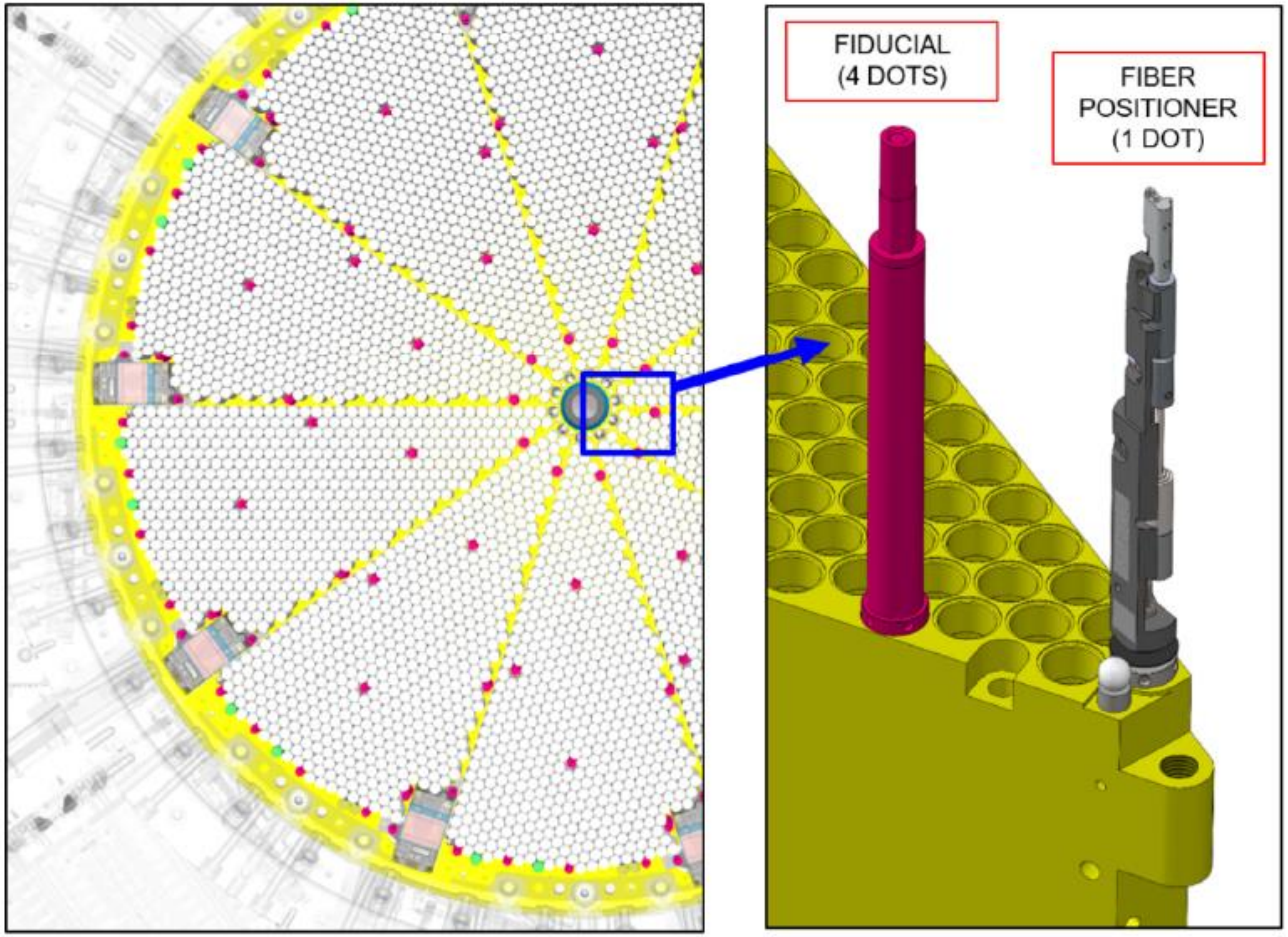

DESI Spectrograph

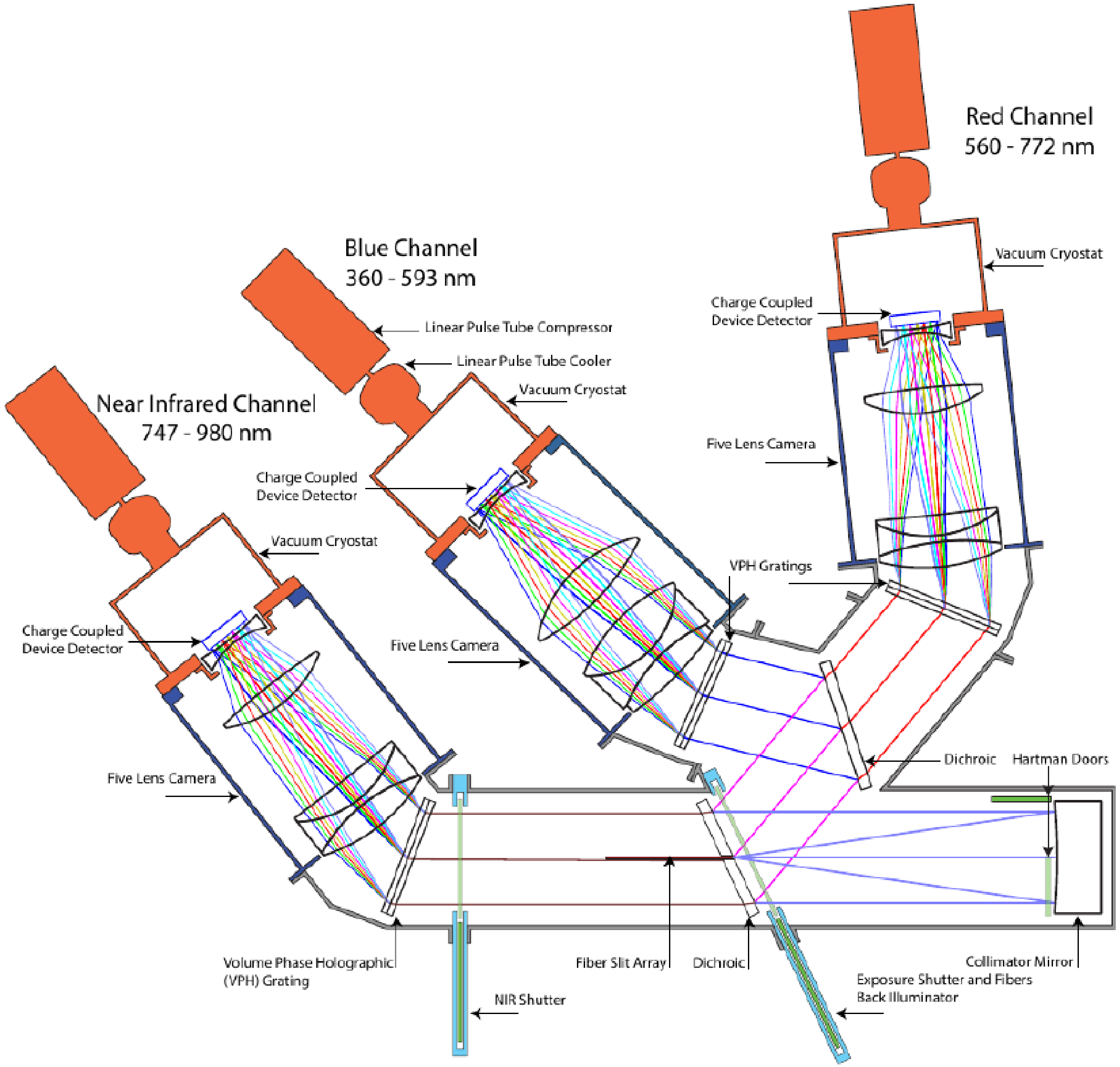

DESI shift

- DESI zero, dark, flat and arc frames on my observing night (from left to right, top to bottom).

- Used for calibrating spectrograph CCD, sky level, sky lines, wavelength grid…

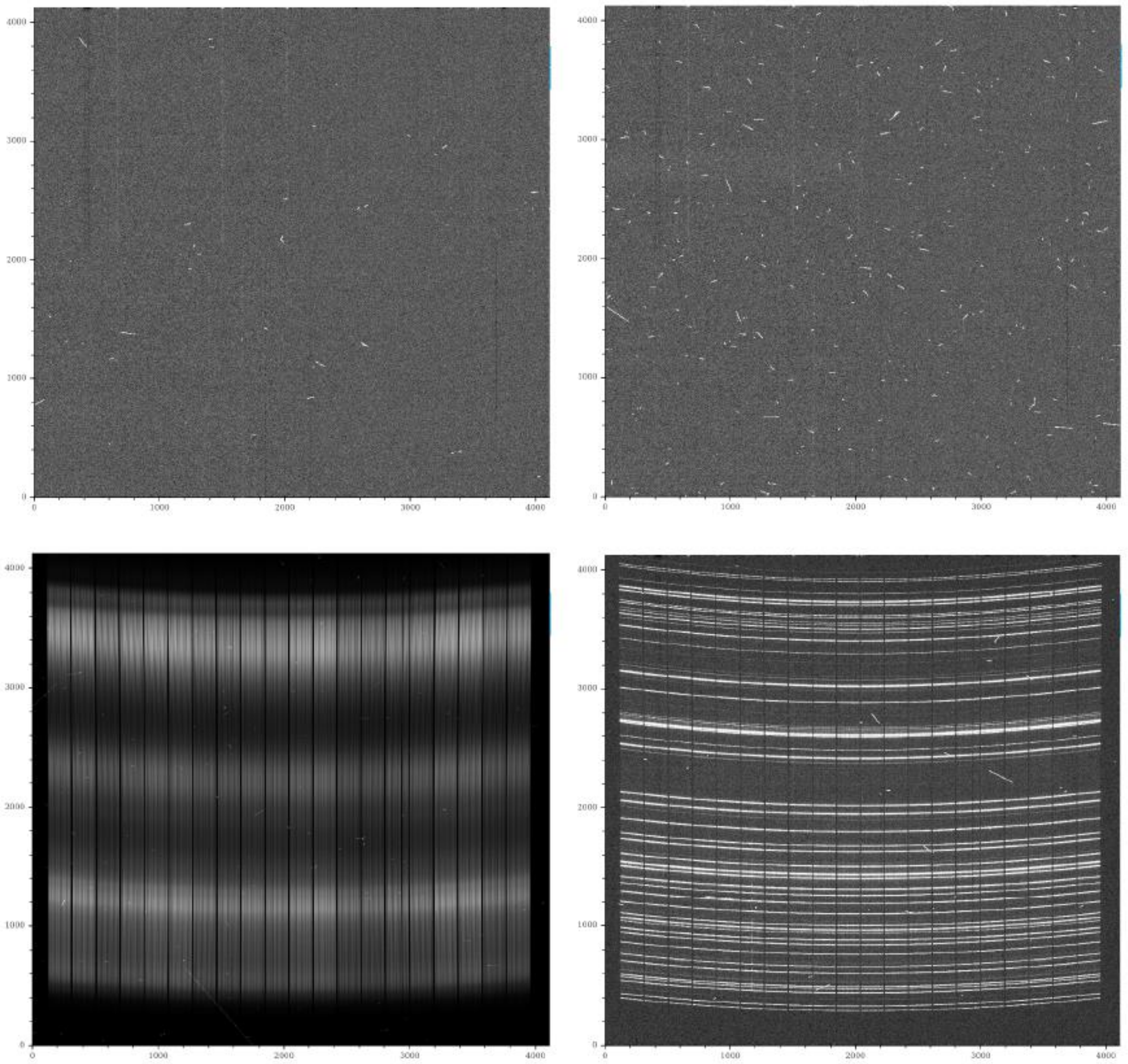

DESI shift

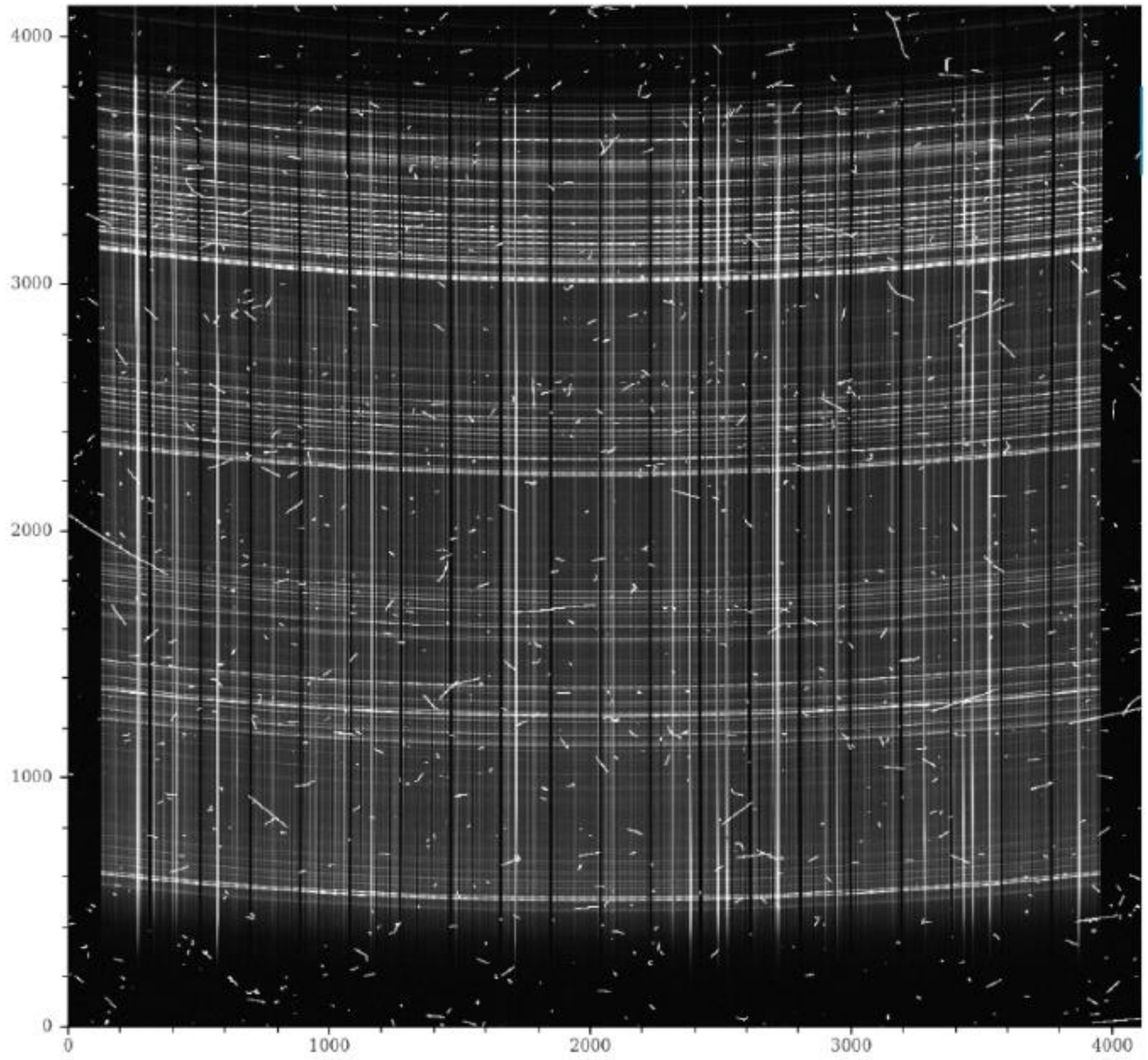

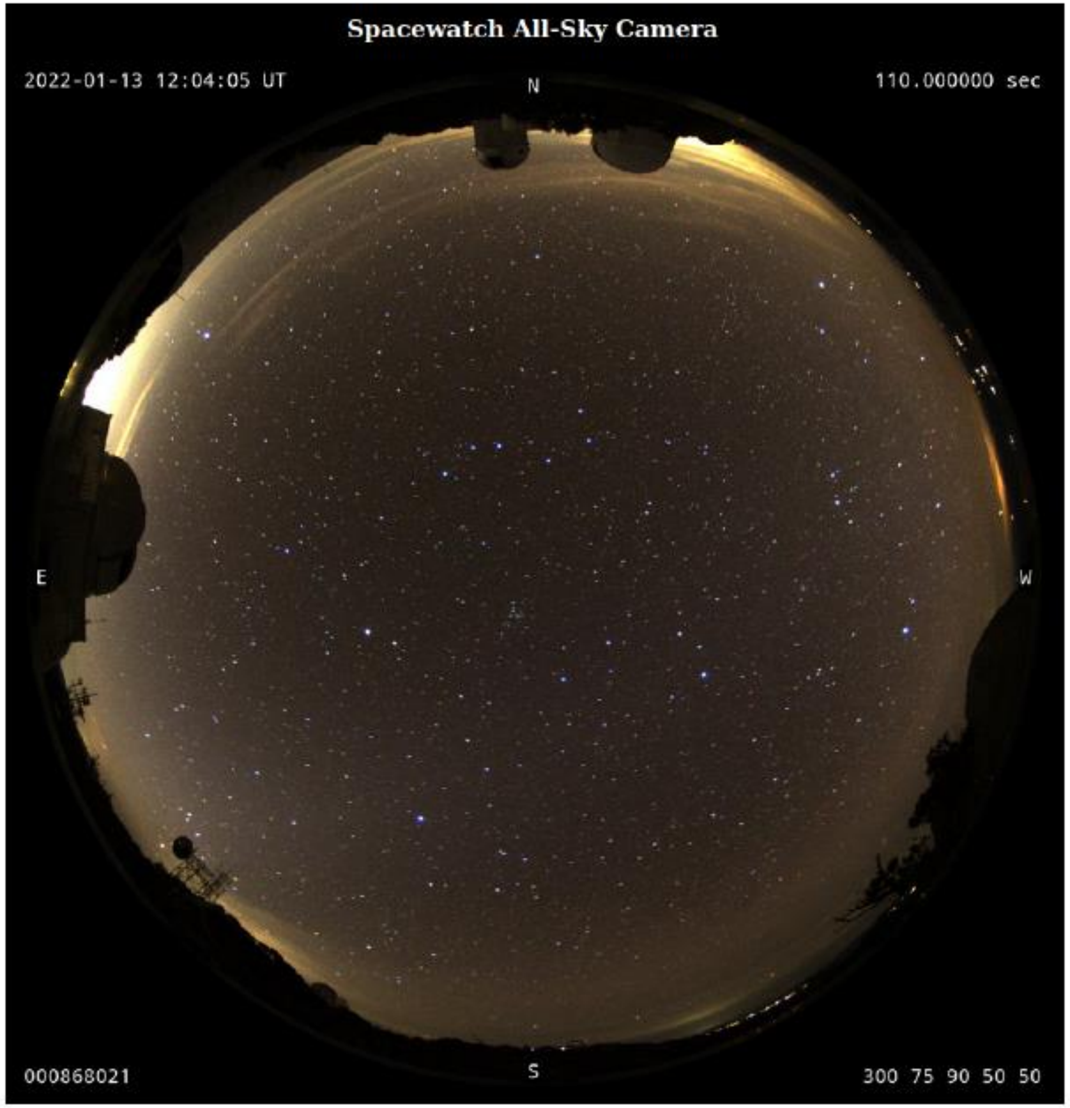

500 spectra distributed on the spectrograph CCD

Small-scale Lyman-α tomography

- 3D map of Lyman-α absorption from 1D spectra (*Pichon et al. 2001*)
- CLAMATO (*Lee et al. 2018*):
  - Small and dense field in COSMOS, 0.157 deg^2, 1455 objects/deg^2
  - Use LBG and quasar spectra

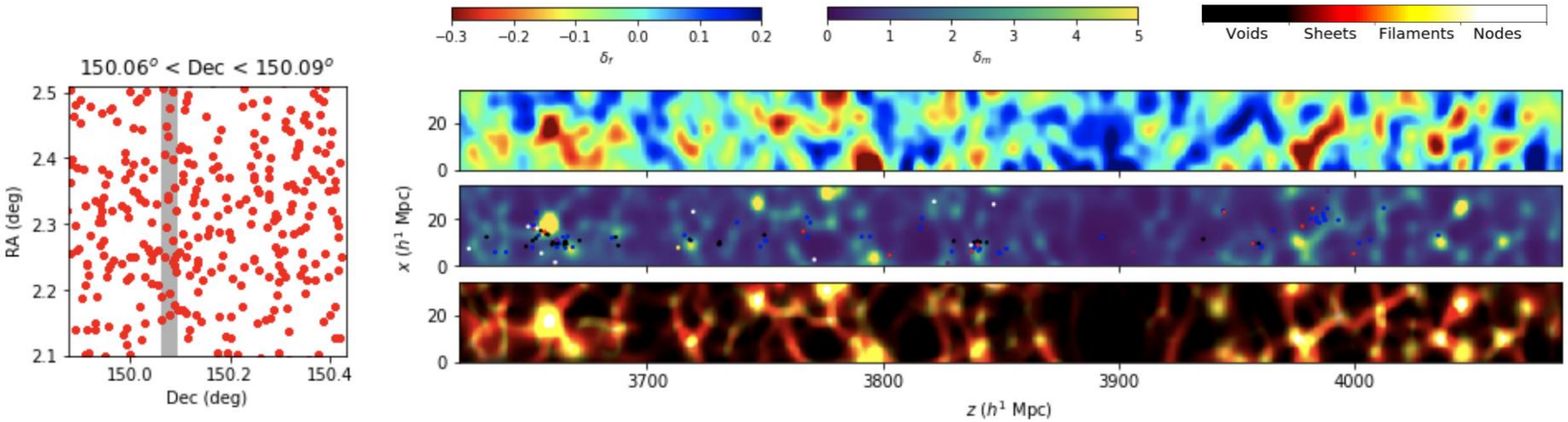

- Goal: Map the cosmic web, reach Mpc scale
  - Might be achievable with ELT (*Japelj et al. 2019*)

Wiener filter

- Input data:

$$\vec{d} = \vec{s}_{\rm p} + \vec{n}$$

- Minimization of

$$\epsilon = E\left[\left|\vec{s}_{\rm m} - \hat{\vec{s}}\right|^2\right]$$

sm = « true » map signal
s = estimator
(Assumption on sm)

- Minimal error estimator:

$$\hat{\vec{s}} = \left(\mathbf{S}_{\rm mp}(\mathbf{S}_{\rm pp} + \mathbf{N})^{-1}\right) \cdot \vec{d}$$

- Gaussian kernels:

$$\mathbf{S}_{ij} = \sigma_F^2 \exp\left(-\frac{(r_{i\|} - r_{j\|})^2}{2L_\|^2}\right) \exp\left(-\frac{(r_{i\perp} - r_{j\perp})^2}{2L_\perp^2}\right)$$

Large-scale Lyman-α tomography with eBOSS

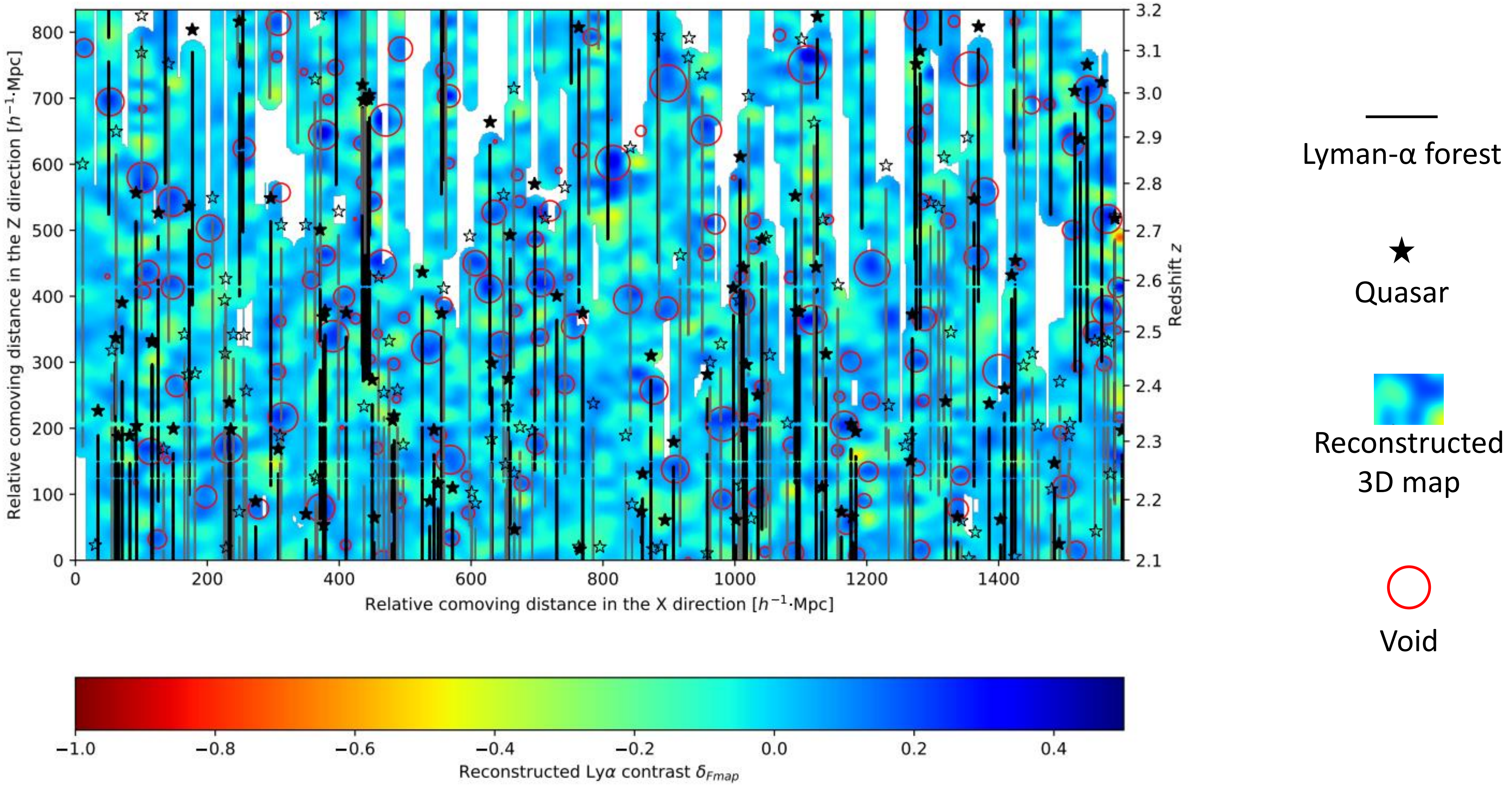

Correlation with matter density

- Use dedicated simulations (mocks)
- Production of Lyman-α forest samples with the same properties as Stripe 82
- Test of tomographic algorithms
- Comparison of underlying matter field with reconstructed Lyman-α contrast

$$\boldsymbol{r = 34\%}$$

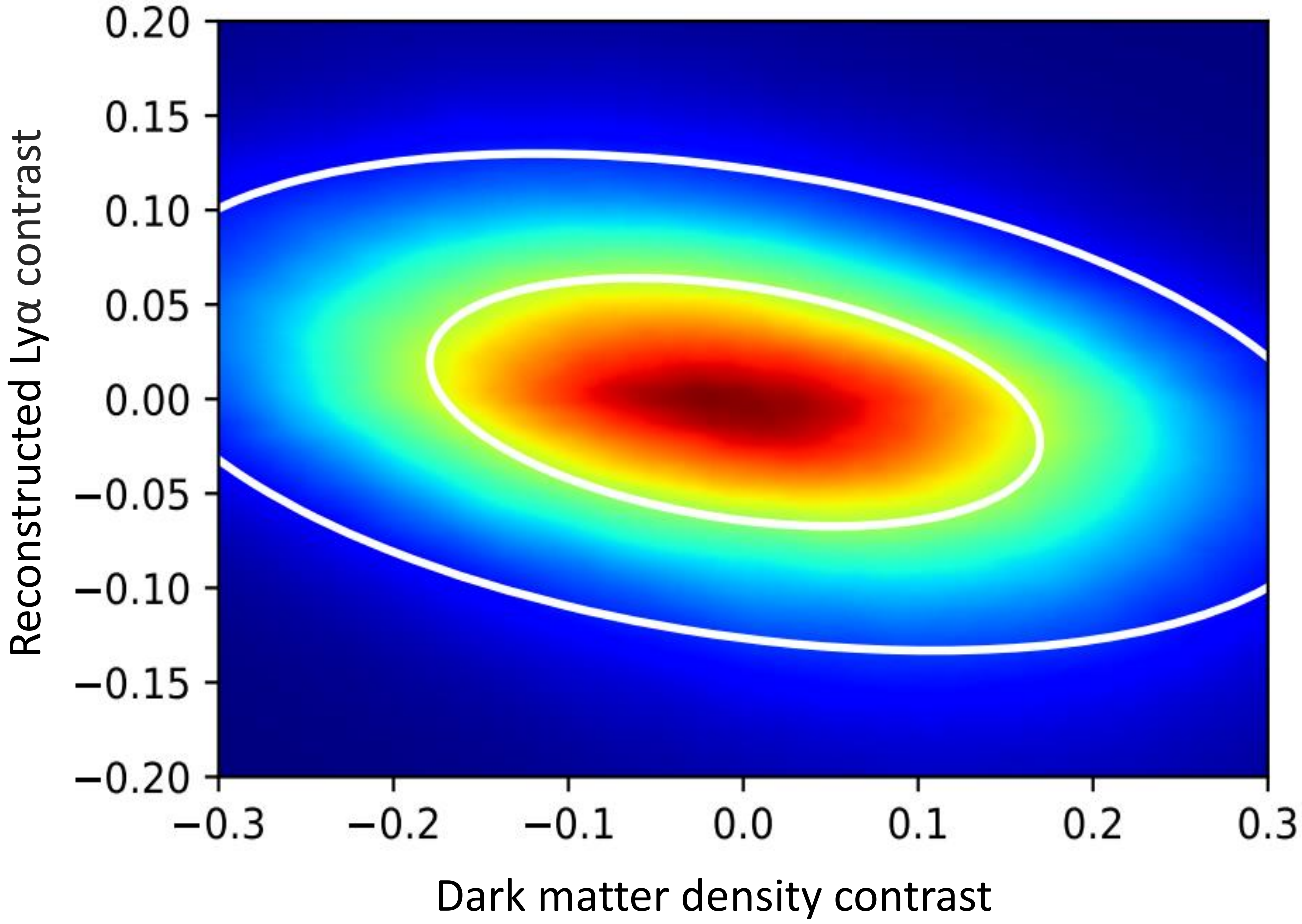

Void finder details

- Spherical void finder:
  - Select all pixels with reconstructed Lya contrast larger than δ_{th}=0.14
  - Sphere grown around this pixel until the mean reconstructed Lya contrast inside reaches δ_{av}=0.12
- Watershed void finder:
  - All pixels with a reconstructed Lya contrast larger than are selected and sorted into groups of neighboring pixels.
  - Centers defined with the largest contrast
  - Radius defined by the total volume of pixels $R = (3N_{\rm pix}V_{\rm pix}/4\pi)^{1/3}$

- Voids with radius lower than R_{min} removed
- Overlapping void removed by iteration or clustering

Void statistics

- Radius and redshift histograms

- Distribution of radius as a function of redshift rather stable.

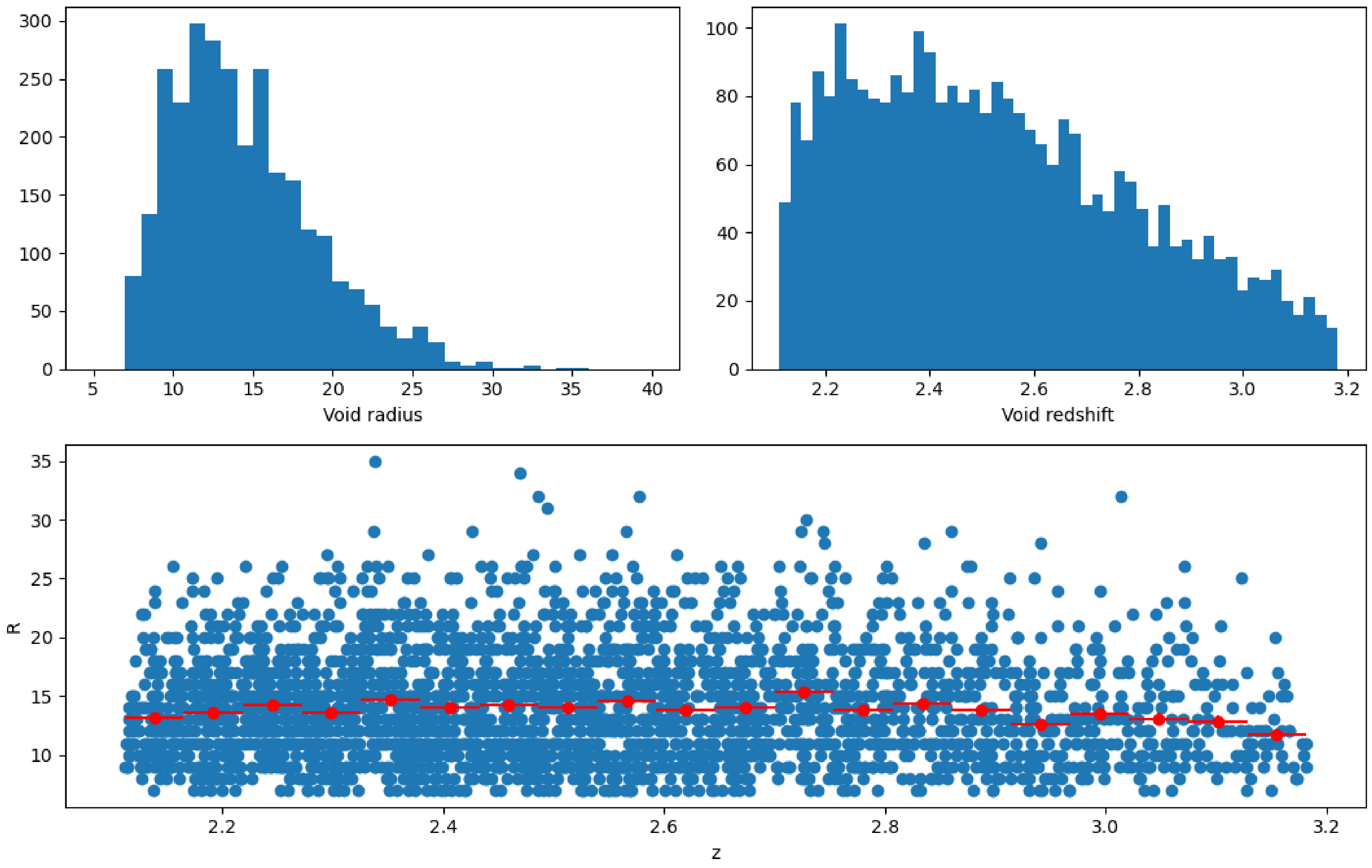

DESI-LBG: Secondary target program

- Secondary project to test DESI ability to observe Lyman-break galaxies:
  - Tracers
  - Lyman-alpha absorption
- Tomographic map with quasars only on COSMOS field
- Stacking on LBG positions on the tomographic map yields an over-dense signal with 3σ statistical significance.

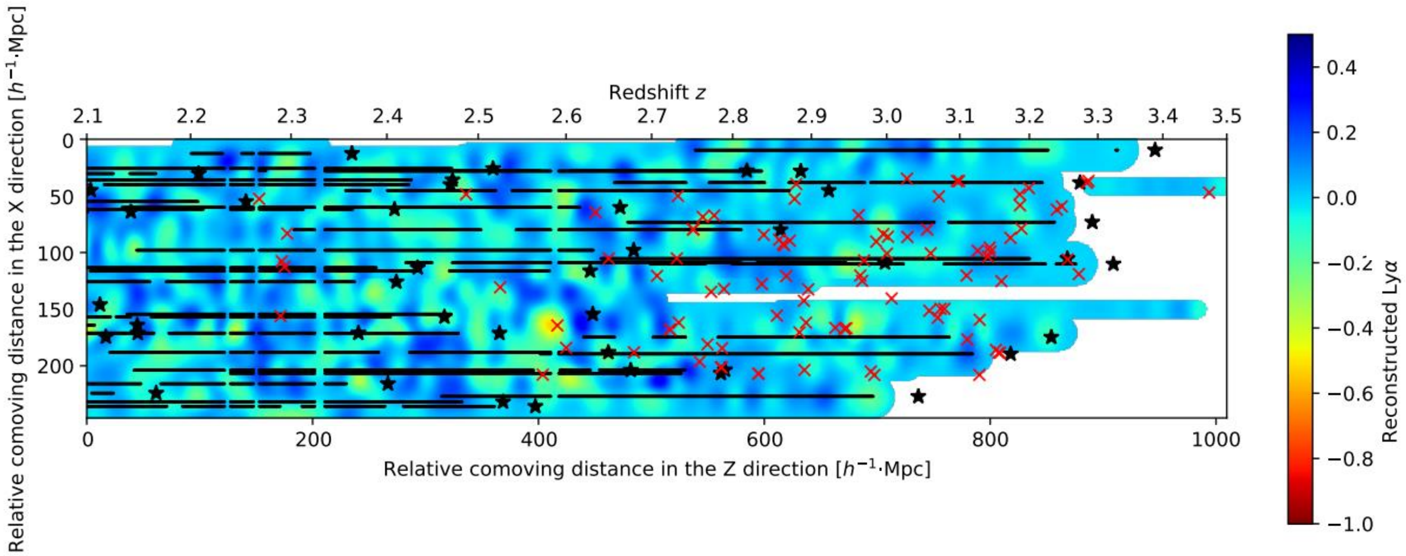

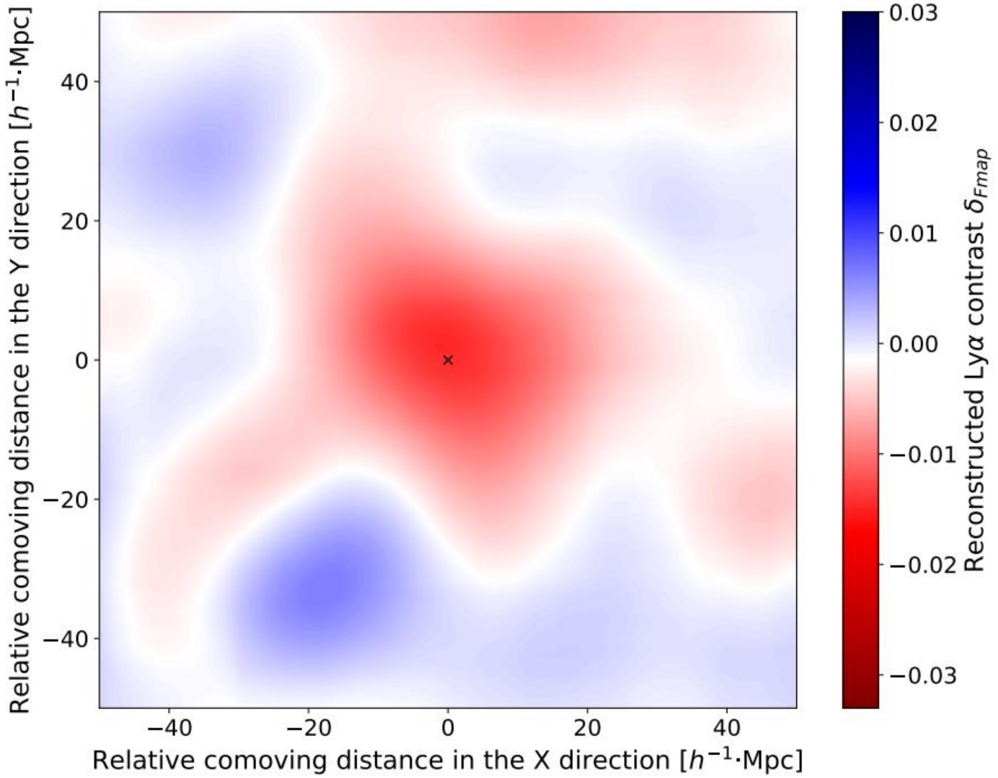

DESI-LBG: Secondary target program

- Stacked spectra of 2200 DESI LBGs (credits: Christophe Yèche)

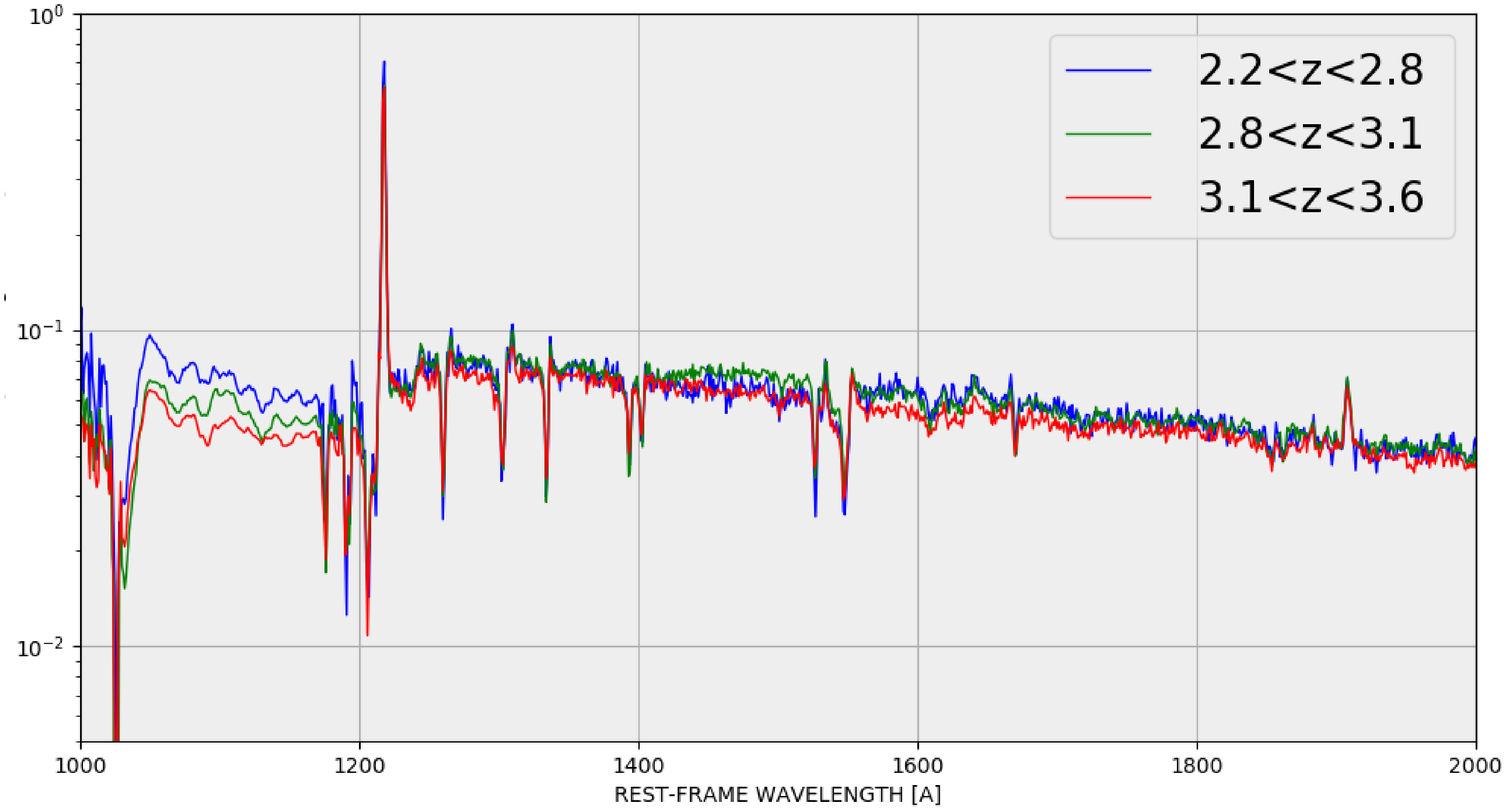

RSD void model

- Velocity:

$$\vec{u} = -\frac{1}{3}\frac{fH}{1+z}\overline{\delta}(r)\vec{r} \qquad \overline{\delta}(r) = \frac{3}{r^3}\int_0^r \delta(r')r'^2 dr'$$

- RSD transformation:

$$\vec{s} = \vec{r} + (1+z)\frac{\hat{X}\cdot(\vec{u}-\vec{U})}{H(z)}\hat{X}$$

- Optical depth conservation:

$$\tau_\alpha^s(\vec{r}) = \tau_\alpha(r)\left|\frac{d^3\vec{r}}{d^3\vec{s}}\right| = \tau_\alpha(r)\left[1 + \frac{f}{3b}\overline{\delta}(r) + \frac{f}{b}\mu^2\left(\delta(r) - \overline{\delta}(r)\right)\right]$$

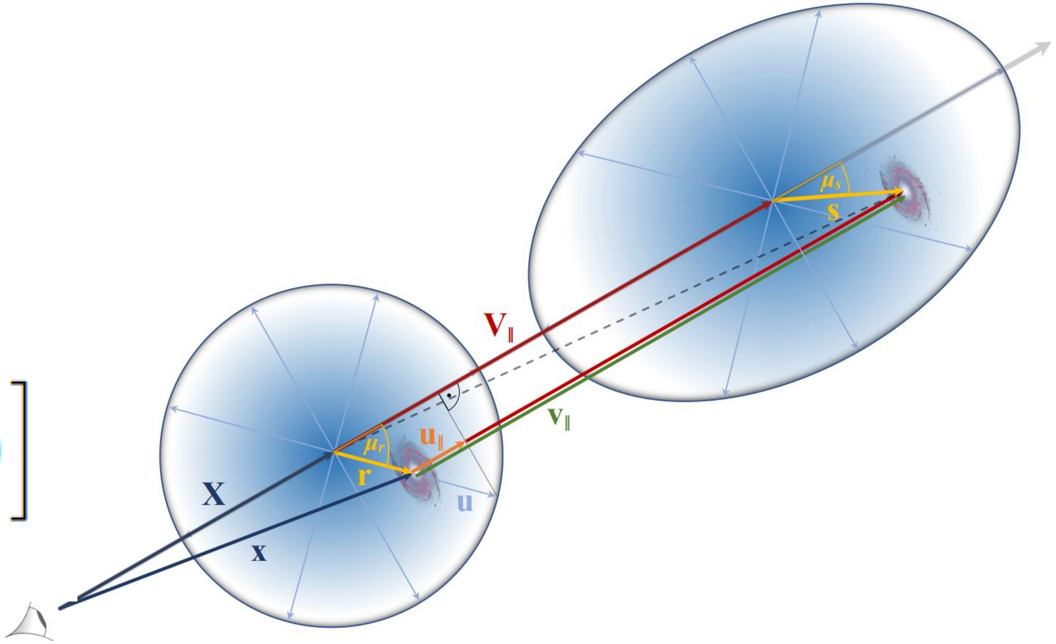

RSD void model

- Taylor expansion:

$$F[\tau_\alpha^s(\vec{k})] = \sum_{n=0}^{\infty} \frac{F^{(n)}[0]\left(\tau_\alpha^s(\vec{k}) - 0\right)^n}{n!}$$

- At linear order and introducing velocity bias:

$$F[\tau_\alpha^s(\vec{r})] = F[\tau_\alpha(r)] + b_\eta f \overline{F}\left[\frac{1}{3}\overline{\delta}(r) + \mu^2\left(\delta(r) - \overline{\delta}(r)\right)\right]$$

$$b_\eta = \tau_\alpha \left.\frac{\partial \delta_F}{\partial \tau_\alpha}\right|_{\tau=0} = \tau_\alpha \frac{F^{(1)}[0]}{\overline{F}}$$

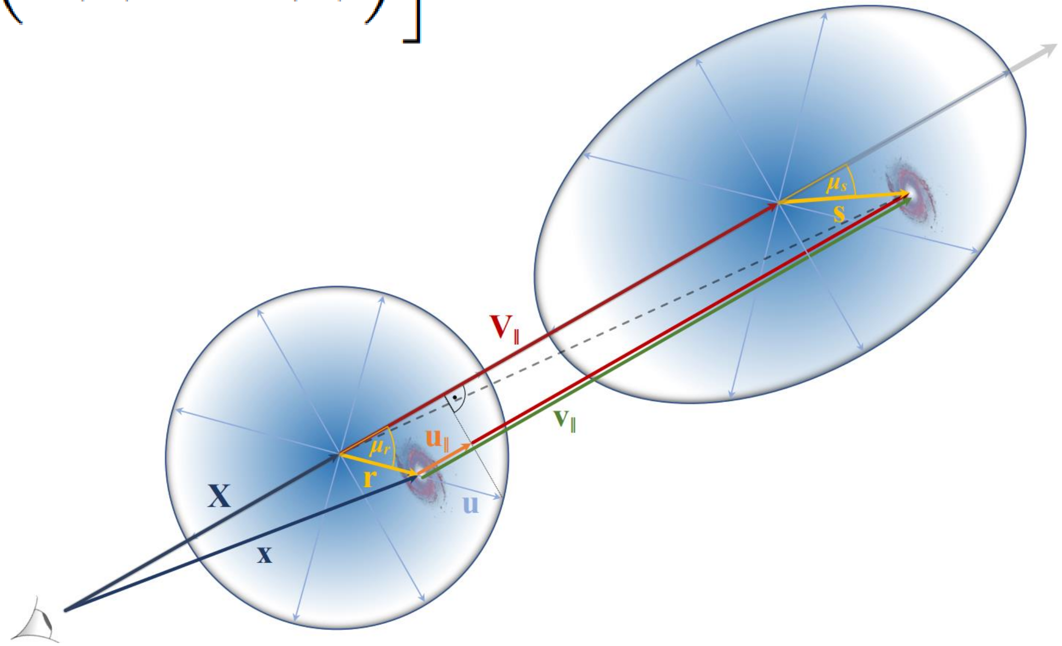

RSD void model

- Lyman-α contrast: $$\delta_F^s(\vec{r}) = \delta_F(r) + b_\eta f\left[\frac{\bar{\delta}(r)}{3} + \mu^2\left(\delta(r) - \bar{\delta}(r)\right)\right]$$

$$\beta = \frac{b_\eta f}{b}$$

- Linearity: $$\xi_{\text{v}\alpha}(r) = b\delta(r)$$

$$\bar{X}(r) = \frac{3}{r^3}\int_0^r X(r')r'^2 dr'$$

- Model:

$$\xi_{\text{v}\alpha}^s(\vec{r}) = \xi_{\text{v}\alpha}(r) + \beta\left[\frac{\bar{\xi}_{\text{v}\alpha}(r)}{3} + \mu^2\left(\xi_{\text{v}\alpha}(r) - \bar{\xi}_{\text{v}\alpha}(r)\right)\right]$$

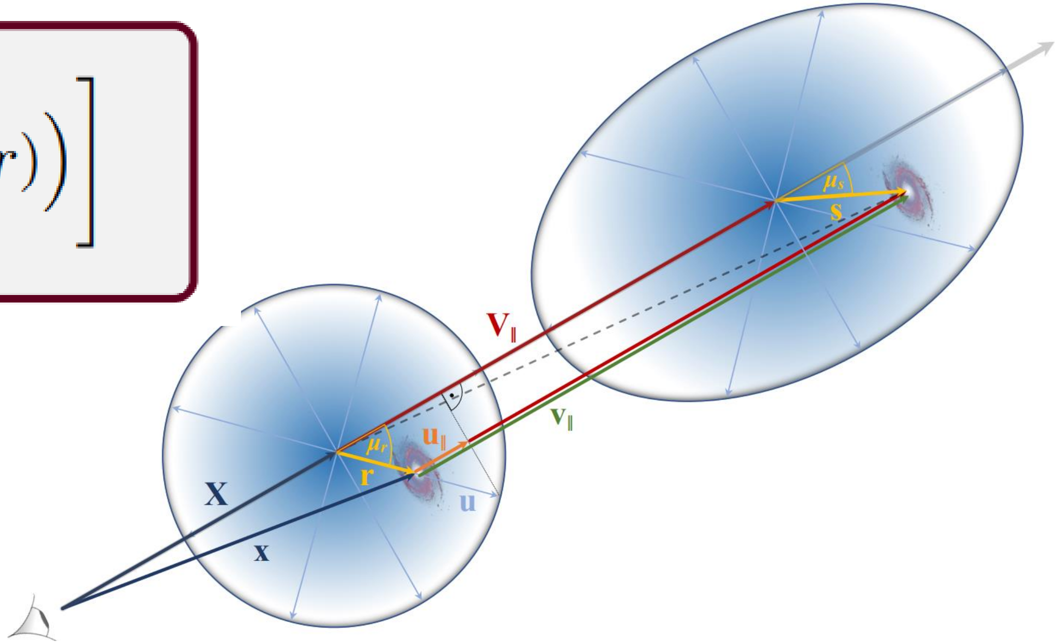

RSD void model

- Multipoles:

$$\xi^s_{\mathrm{v}\alpha,0}(r) = \left(1 + \frac{\beta}{3}\right) \xi_{\mathrm{v}\alpha}(r)$$

$$\xi^s_{\mathrm{v}\alpha,2}(r) = \left(\frac{2\beta}{3}\right) \left(\xi_{\mathrm{v}\alpha}(r) - \overline{\xi}_{\mathrm{v}\alpha}(r)\right)$$

$$\xi^s_{\mathrm{v}\alpha,2}(r) = \left(\frac{2\beta}{3+\beta}\right) \left(\xi^s_{\mathrm{v}\alpha,0}(r) - \overline{\xi}^s_{\mathrm{v}\alpha,0}(r)\right)$$

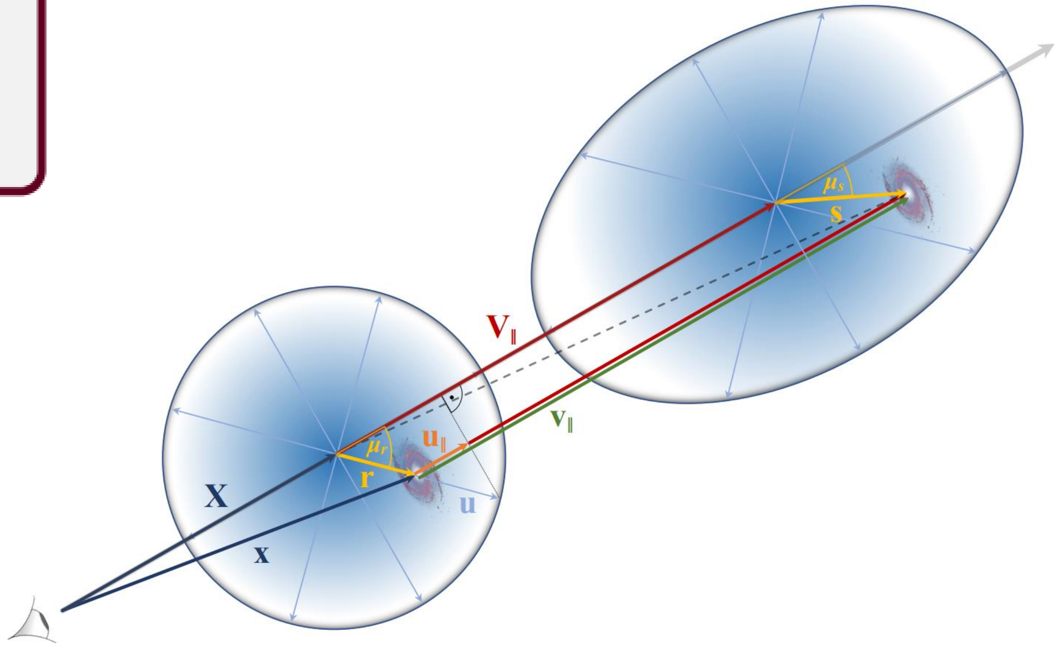

Possible sources of tomographic effect

- First source:
  - With sparse LOS geometry, the void position is biased toward the LOS which generates it on the transverse plan
- Second source:
  - Map flux-contrast signal higher near to the LOS and decrease following a Gaussian kernel along transverse direction
  - Along the LOS, field is statically over-dense after an under-density (void). Not necessary the case for transverse direction
  - Difference between these two effects generate a quadrupole

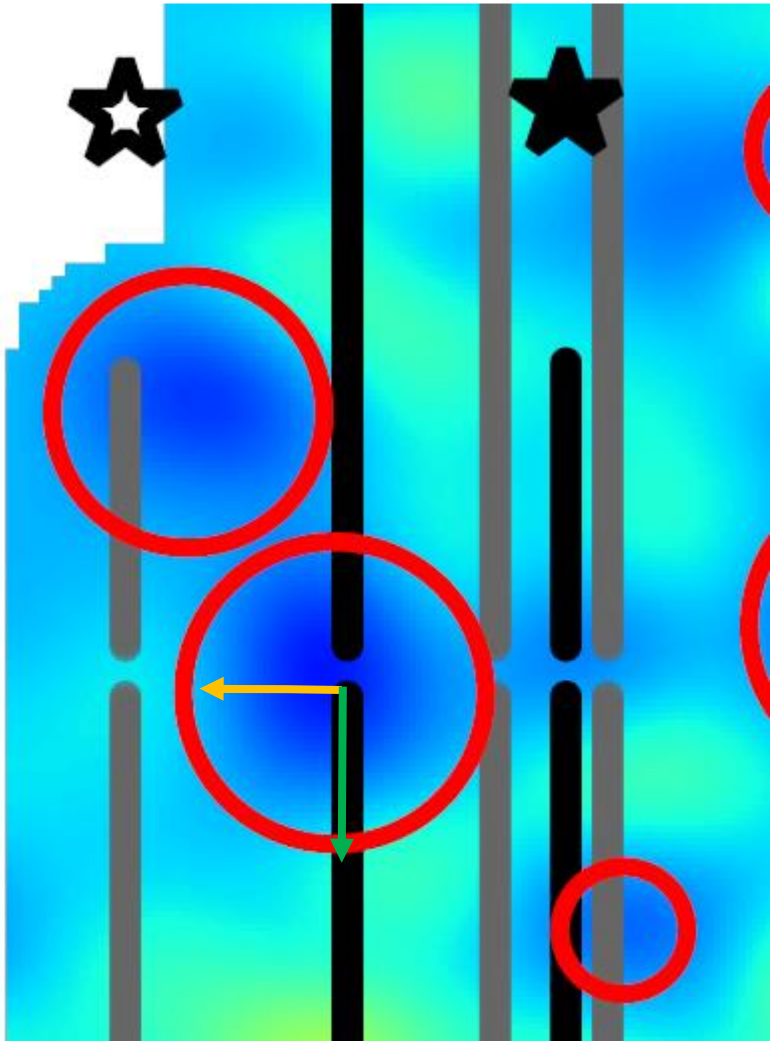

Tomographic effect model

- Two toy models created:
  - Biasing of void position $\vec{s} = s_{\parallel}\hat{X} + s_{\perp}\hat{Y} = r_{\parallel}\hat{X} + (r_{\perp} - \epsilon(r_{\perp}))\,\hat{Y}$
  - Void finder efficiency $\xi^{s}_{\mathrm{v}\alpha}(\vec{r}) = \xi_{\mathrm{v}\alpha}(r) \times \frac{n_{\mathrm{los}}(r_{\perp})}{\overline{n_{\mathrm{los}}}}$
- Similar results:
  - Create monopole, quadrupole and hexadecapole
  - All poles proportional to a function which only depends on r. The proportionality coefficient depends on the toy model considered

$$\xi_{\mathrm{tomo},\ell} = A_{\ell} f(r)$$

Comparison mocks with and without RSD

- Removal of the tomographic effect with no RSD mock

- Linear relation as in the Kaiser model

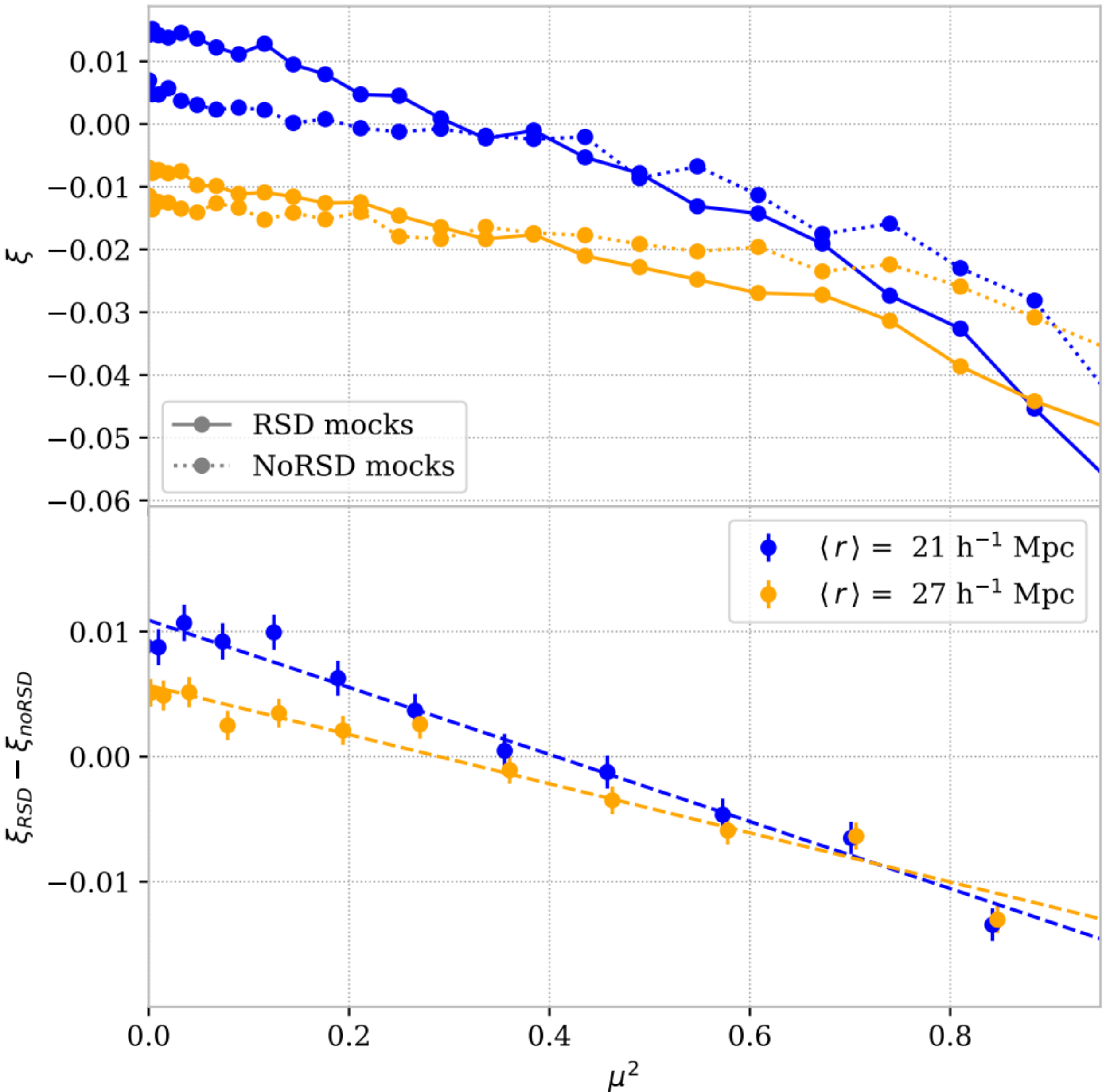

Comparison mocks with and without RSD

- Impact of RSD on the monopole: 6% difference, 17% expected with the RSD model
- Several effect can change this difference (void finder, tomographic mapping)

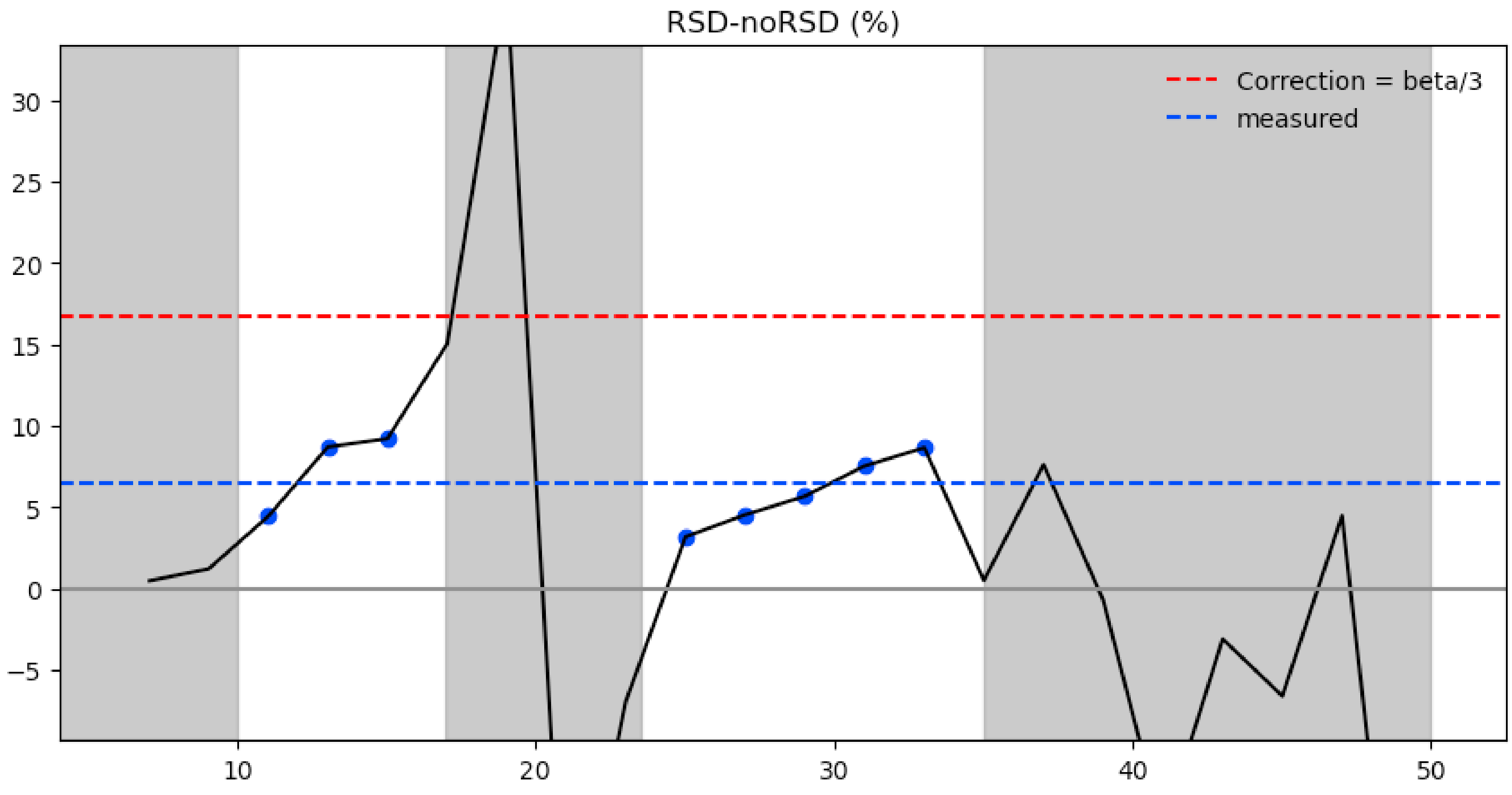

Measuring the tomographic effect

- Cumulative histogram ratio between randomly placed voids and voids obtained on the tomographic map

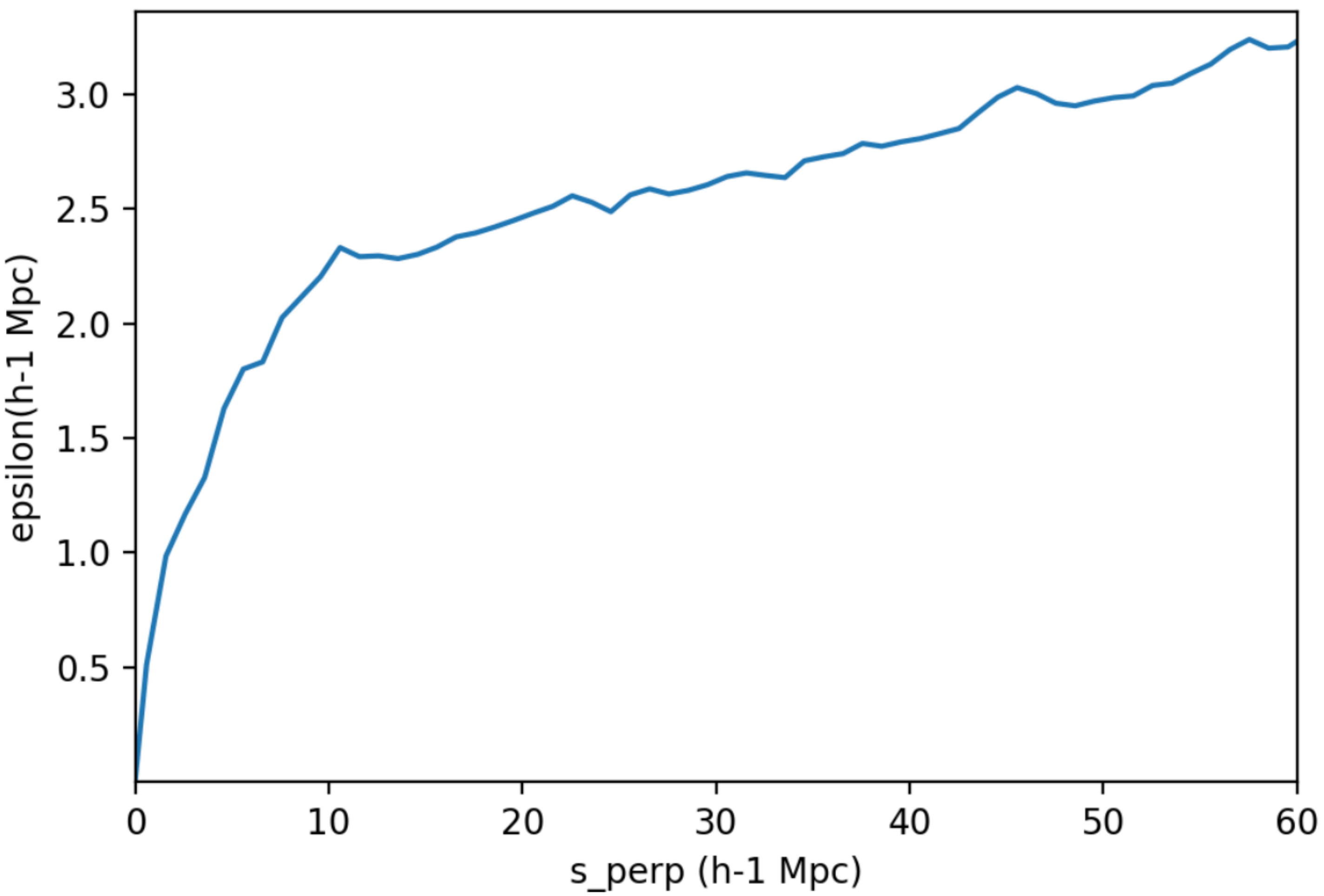

Effect of void and tomographic parameters

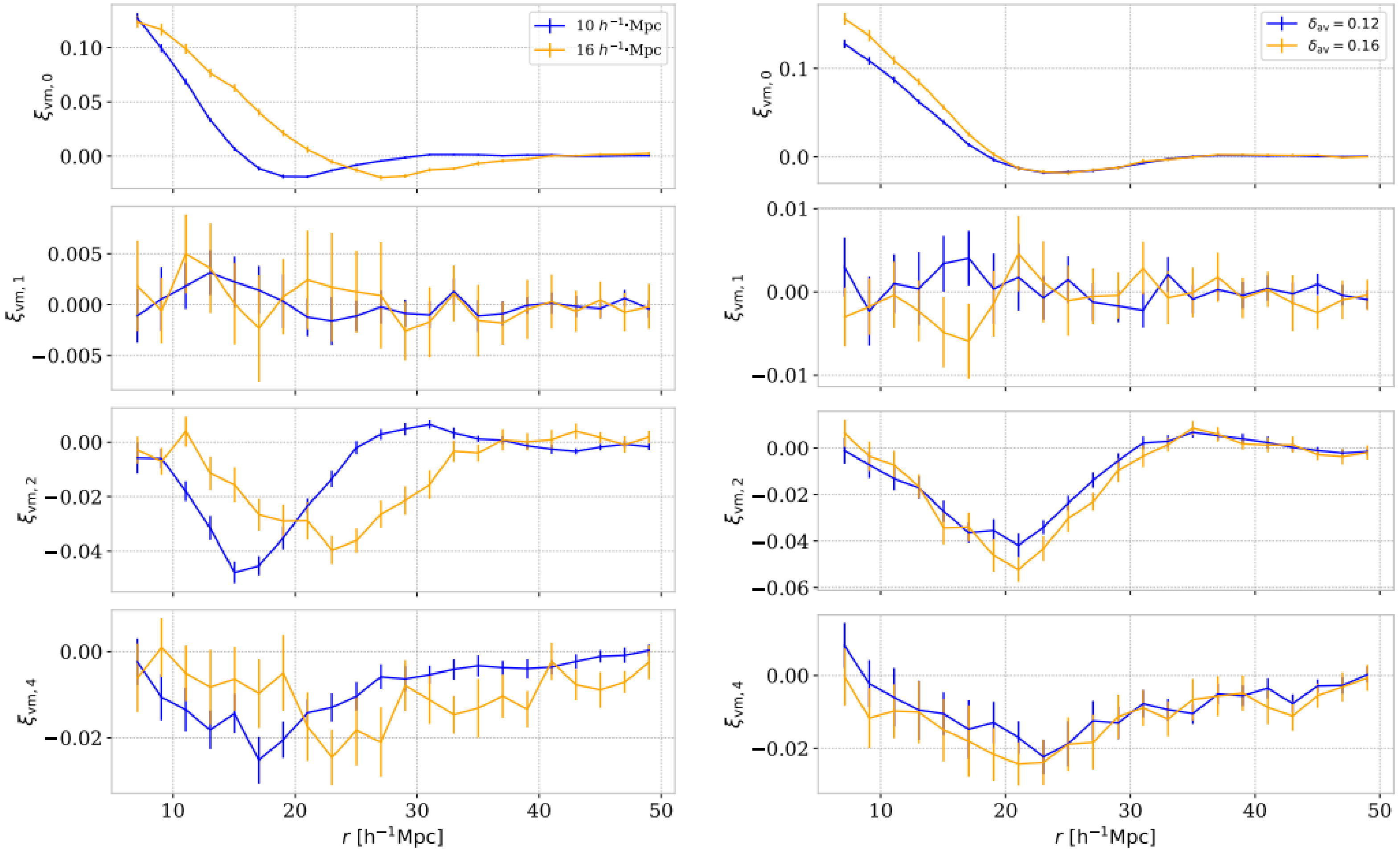

FIGURE 7.13 – Impact of analysis parameters on the *raw-noRSD* mock multipoles. (left) Variation of both $L_\perp$ and $L_\parallel$ correlation lengths from 10 to 16 h^{-1}·Mpc. (right) Variation of spherical void finder parameter δ_{av} from 0.12 to 0.16.

Fit variations

- Different estimates of the error bars (picca, diagonal covariance matrix, picca corrected by mocks)
- Change of fit interval
- Change of nuisance parameter

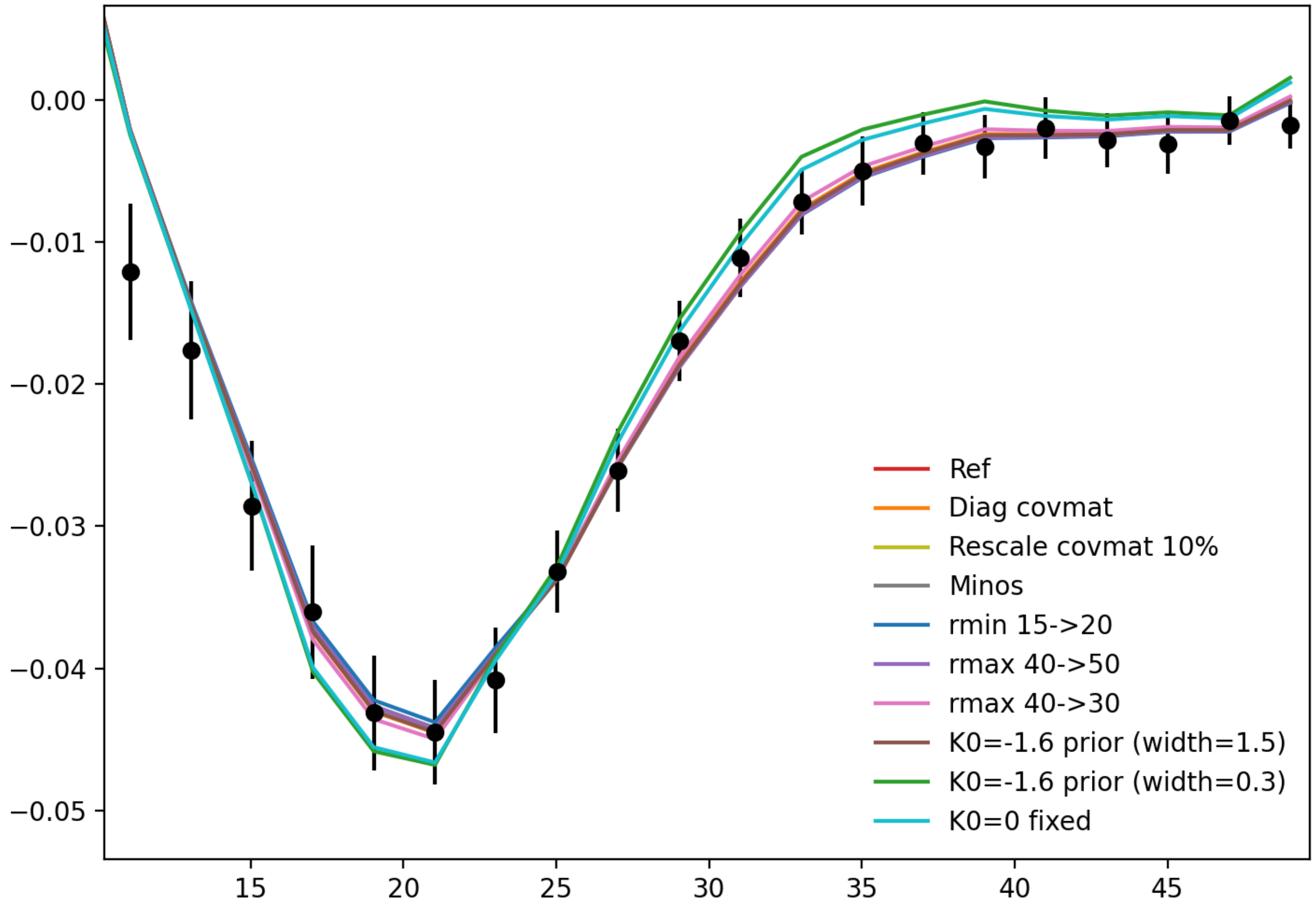

Fit contours

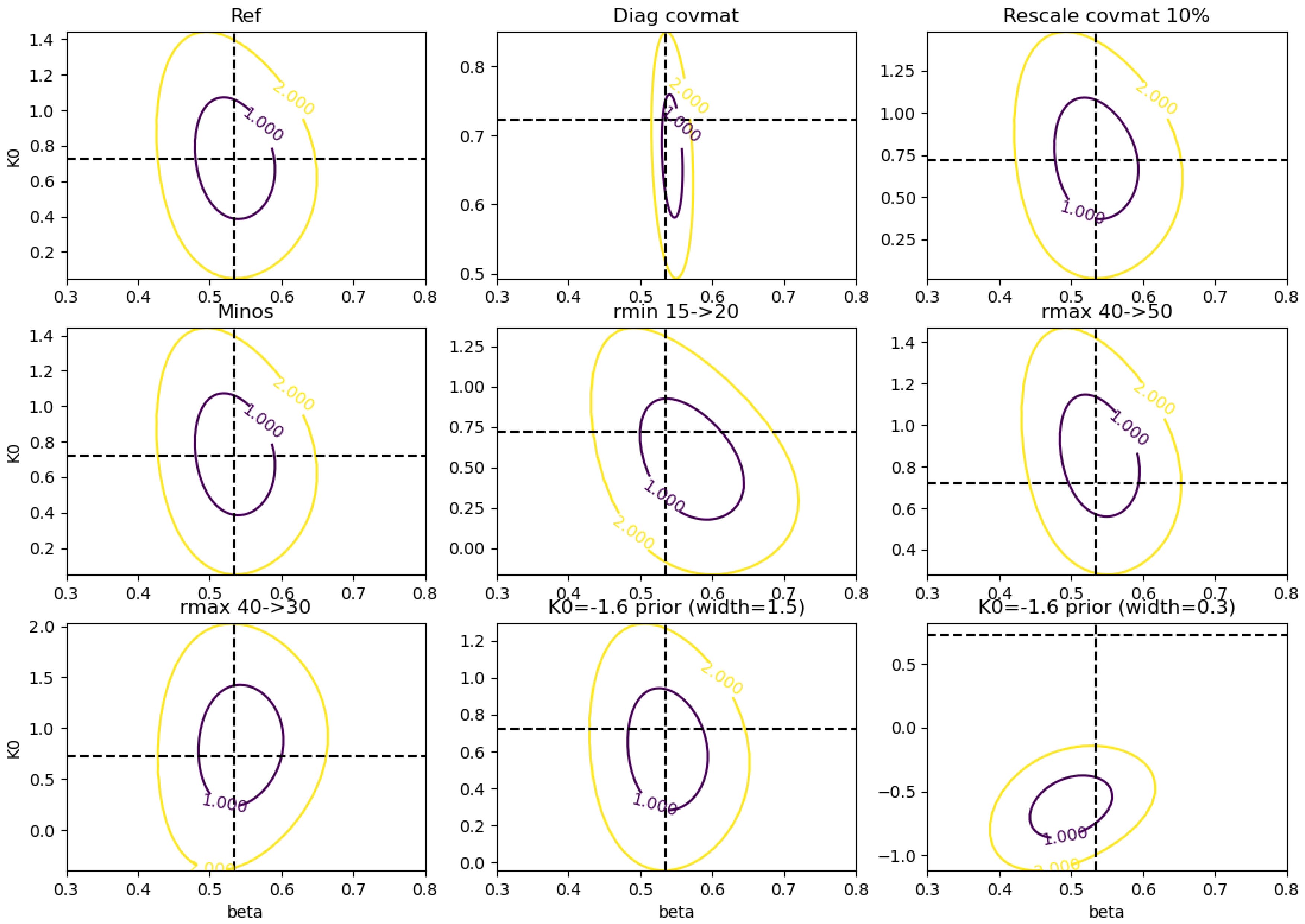

Other tests

- Using shuffle instead of mocks to correct tomographic effect quadrupole result in a 1σ bias of the β value (increase of 0.06)

- Measurement of β on raw mocks decreases β by 1σ (0.05)

Mgii afterburner

- Algorithm to retrieve low-z quasar missed by the main redshift algorithm of DESI
- Included in DESI pipeline
- Increasing completeness of quasars up to 98%

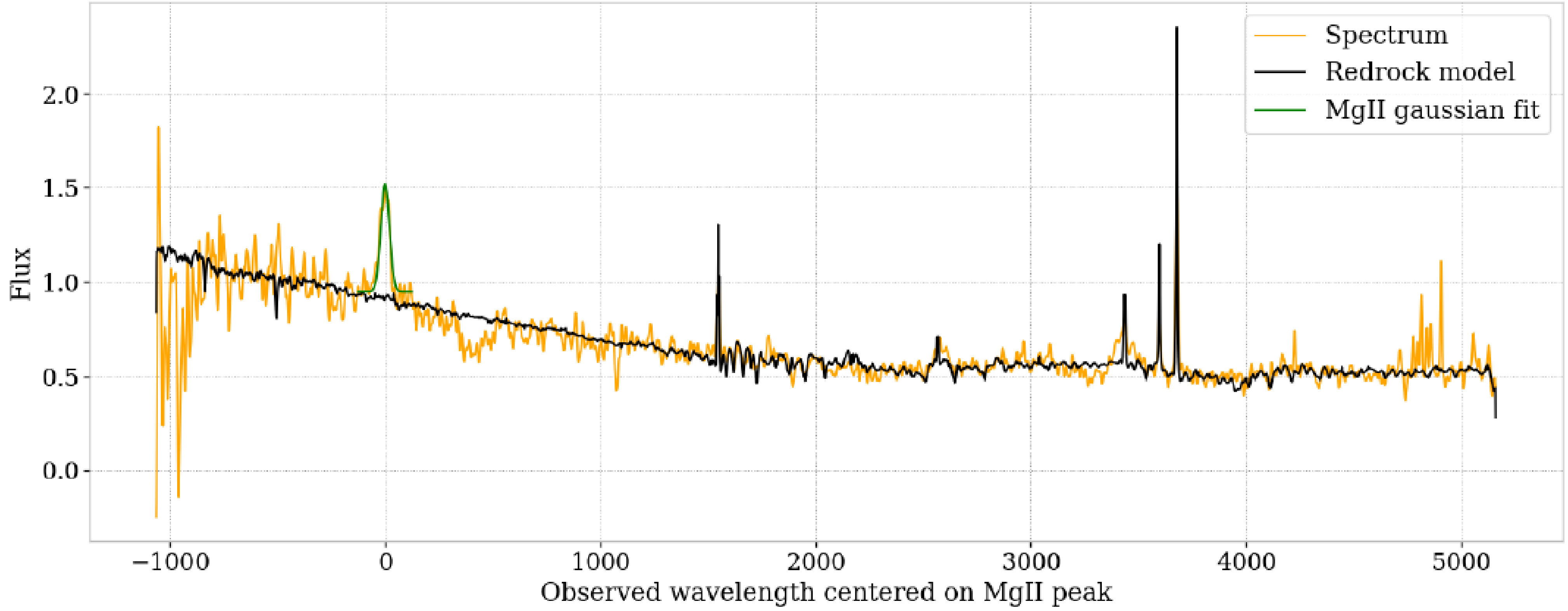

Quasar continuum fitting procedure

- Continuum model

$$C_q(\lambda, z_q) = (a_q + b_q\Lambda)\, C\left(\lambda_{rf} = \frac{\lambda}{(1+z_q)}\right)$$

$$\Lambda = \begin{cases} \log(\lambda) & \text{logarithmic binning (SDSS)} \\ \lambda & \text{linear binning (DESI)} \end{cases}$$

- Likelihood minimization

$$\mathcal{L} = -\sum_i \frac{\left[f_i - \overline{F}(\lambda_i) C_q(\lambda_i, z_q, a_q, b_q)\right]^2}{\sigma_q^2(\lambda_i)} - \ln\left[\sigma_q^2(\lambda_i)\right]$$

$$\frac{\sigma_q^2(\lambda)}{\left(\overline{F}(\lambda)C_q(\lambda)\right)^2} = \eta(\lambda)\frac{\sigma_{\mathrm{pip},q}^2(\lambda)}{\left(\overline{F}(\lambda)C_q(\lambda)\right)^2} + \sigma_{\mathrm{lss}}^2(\lambda) + \epsilon(\lambda)\frac{\left(\overline{F}(\lambda)C_q(\lambda)\right)^2}{\sigma_{\mathrm{pip},q}^2(\lambda)}$$

- Noise associated:

$$\sigma_{\delta_F}(\lambda) = \eta(\lambda)\frac{\sigma_{\mathrm{pip},q}(\lambda)}{\overline{F}(\lambda)C_q(\lambda)}$$

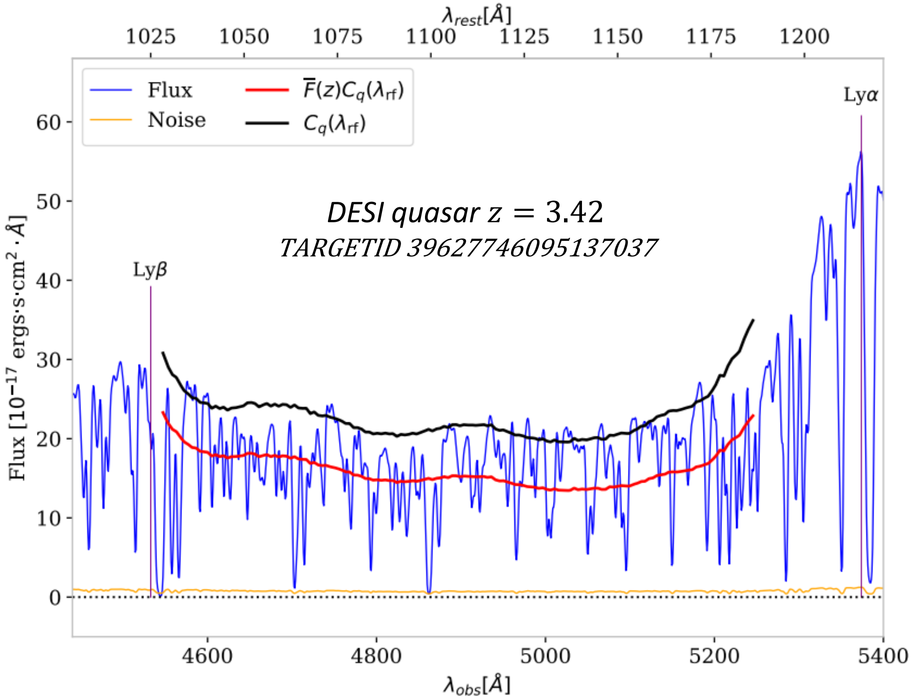

Diff noise on spectra

- Another way to help assessing noise level
- Use quasar and LRG spectra with several exposures:
  - Calculate average difference between exposures
- Improvement between Everest (left) and Fuji (right) data reduction due to accounting CCD position dependence

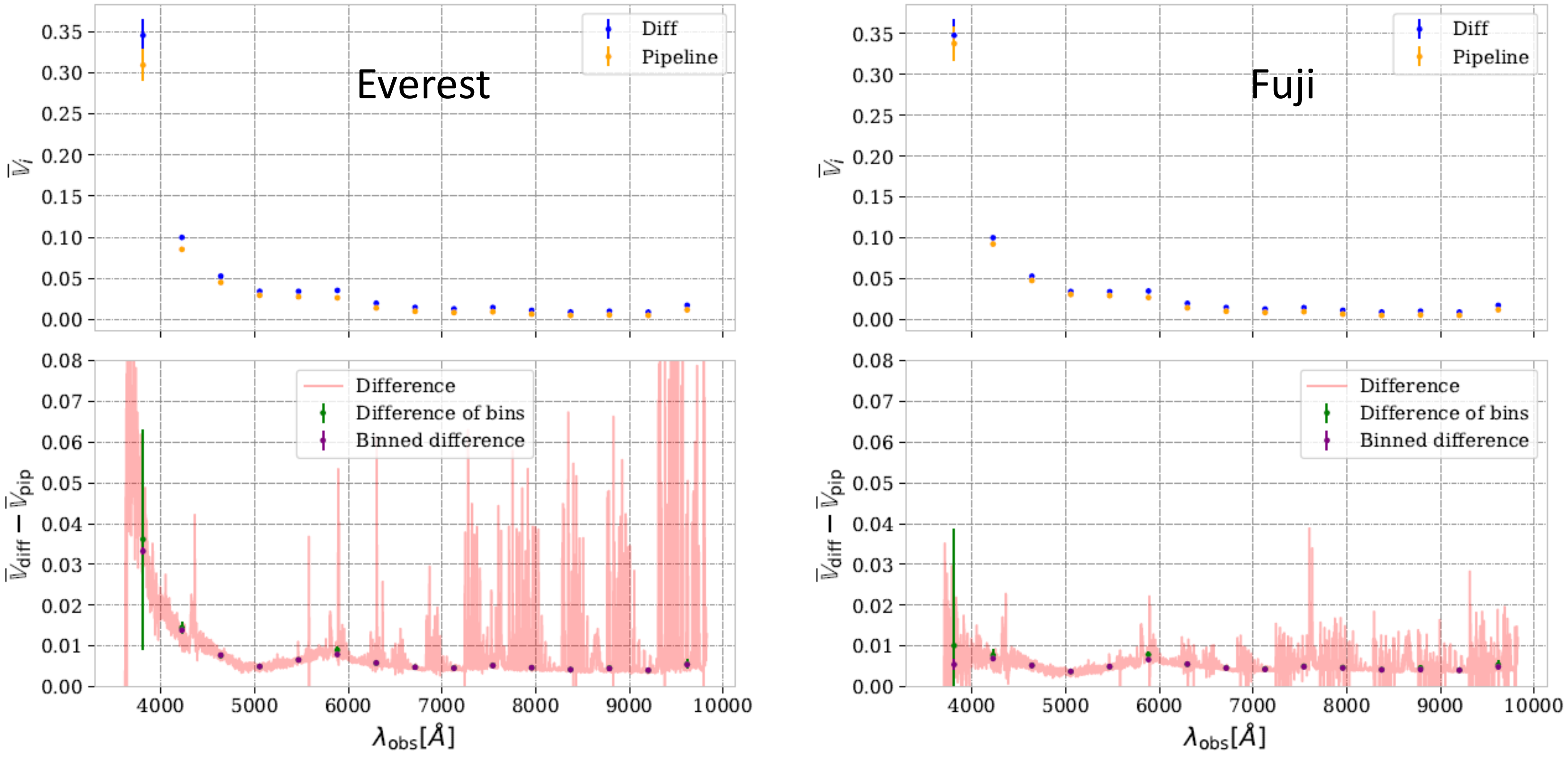

$P_{1\mathrm{D},\alpha}$ diff noise

- Diff noise estimator

$$\Delta f_j = \frac{1}{2}\left(\frac{\sum_{k=1}^{N_{\mathrm{even}}}\left(\mathbb{V}_{\mathrm{pip},k}\right)^{-1} f_k}{\sum_{k=1}^{N_{\mathrm{even}}}\left(\mathbb{V}_{\mathrm{pip},k}\right)^{-1}} - \frac{\sum_{k=1}^{N_{\mathrm{odd}}}\left(\mathbb{V}_{\mathrm{pip},k}\right)^{-1} f_k}{\sum_{k=1}^{N_{\mathrm{odd}}}\left(\mathbb{V}_{\mathrm{pip},k}\right)^{-1}}\right)$$

$$\sigma_{\Delta f_j} = \frac{1}{2}\sqrt{\frac{1}{\sum_{k=1}^{N_{\mathrm{even}}}\left(\mathbb{V}_{\mathrm{pip},k}\right)^{-1}} + \frac{1}{\sum_{k=1}^{N_{\mathrm{odd}}}\left(\mathbb{V}_{\mathrm{pip},k}\right)^{-1}}}$$

$$\Delta f_j^{\mathrm{corr}} = 2\frac{\frac{1}{\sqrt{\sum_{k=1}^{N_{\mathrm{tot}}}\left(\mathbb{V}_{\mathrm{pip},k}\right)^{-1}}}}{\sqrt{\frac{1}{\sum_{k=1}^{N_{\mathrm{even}}}\left(\mathbb{V}_{\mathrm{pip},k}\right)^{-1}} + \frac{1}{\sum_{k=1}^{N_{\mathrm{odd}}}\left(\mathbb{V}_{\mathrm{pip},k}\right)^{-1}}}}\Delta f_j$$

$$P_{\mathrm{diff}}(k) = \left|\mathcal{F}\left[\frac{\Delta f_j^{\mathrm{corr}}(\lambda)}{\overline{F}(\lambda)C_{\mathrm{q}}(\lambda)} - 1\right]\right|^2$$

Detection of DESI pipeline noise issue

Andes

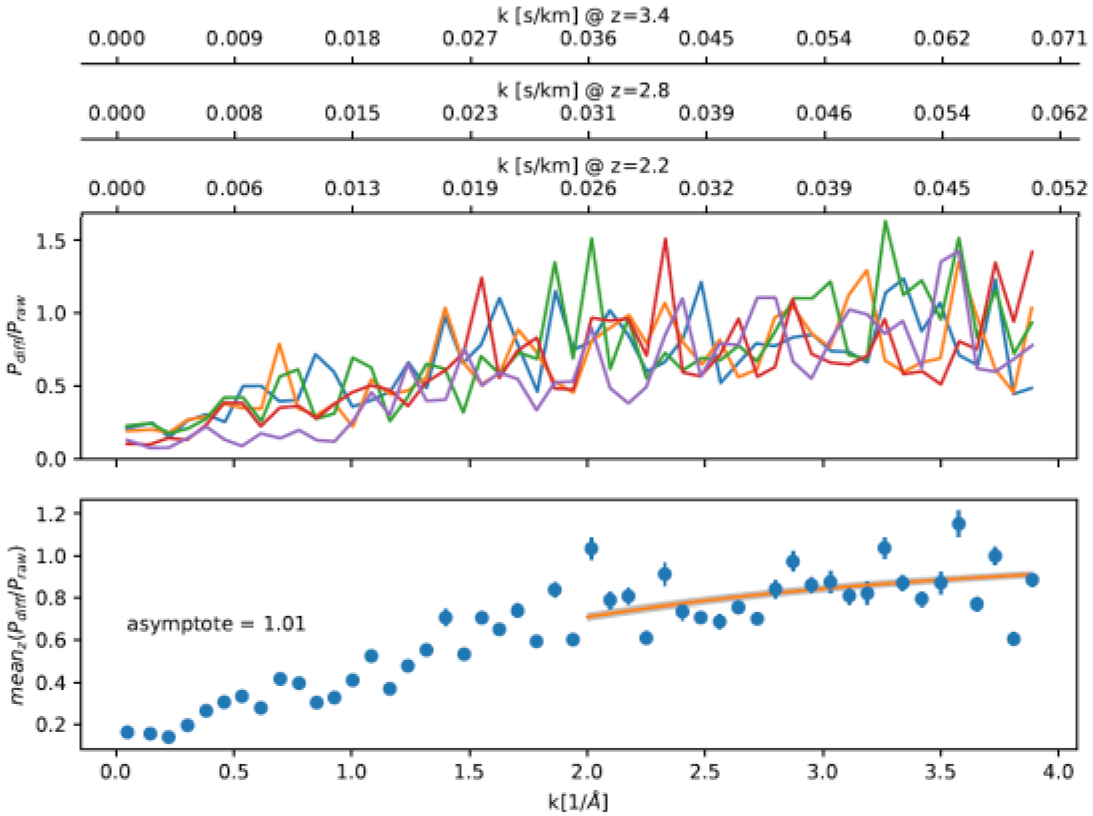

Blanc

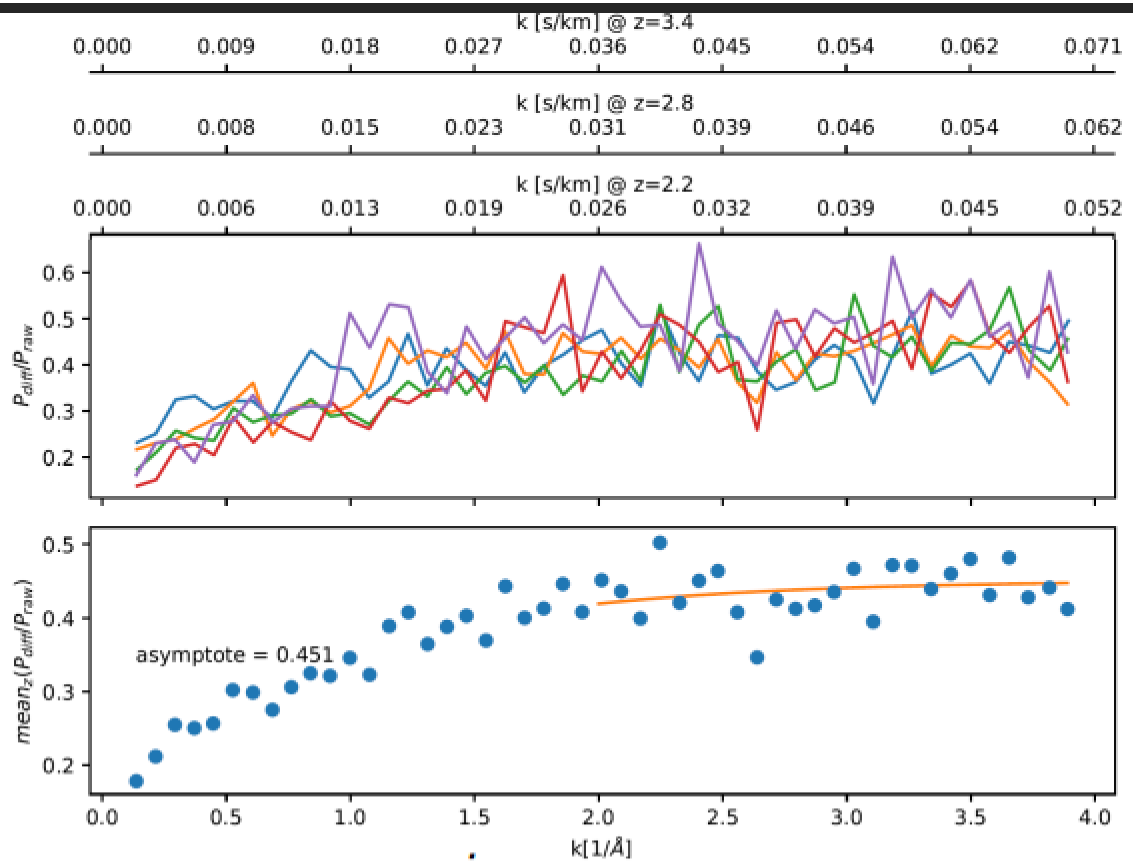

Asymptotic measurement

- Example of measurement on SV3 vs eBOSS

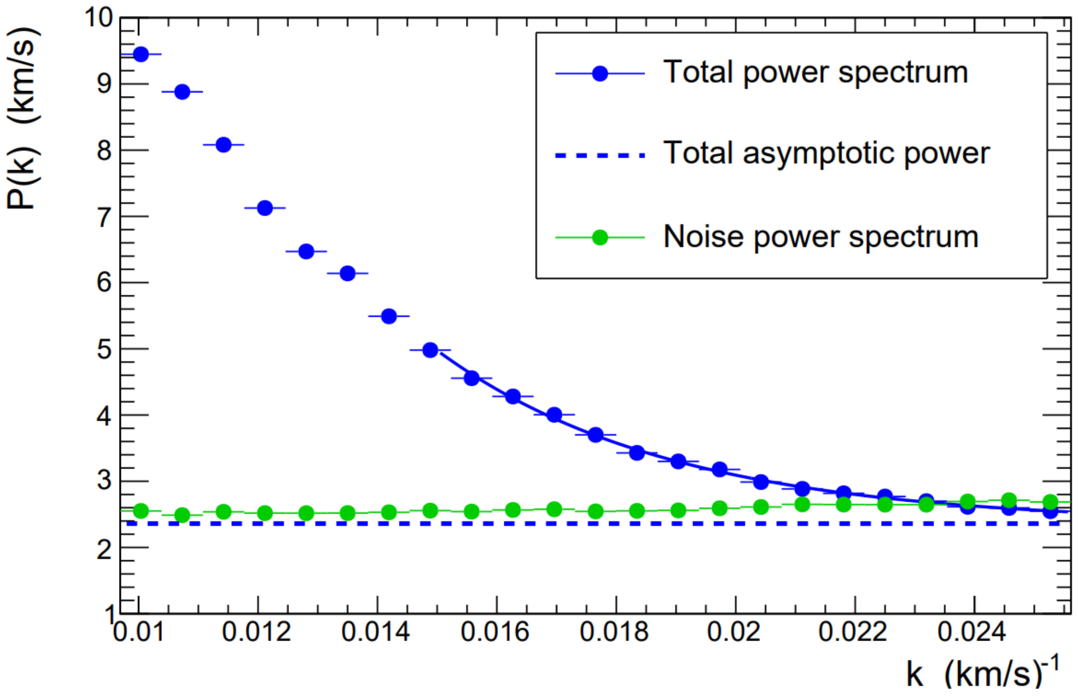

eBOSS

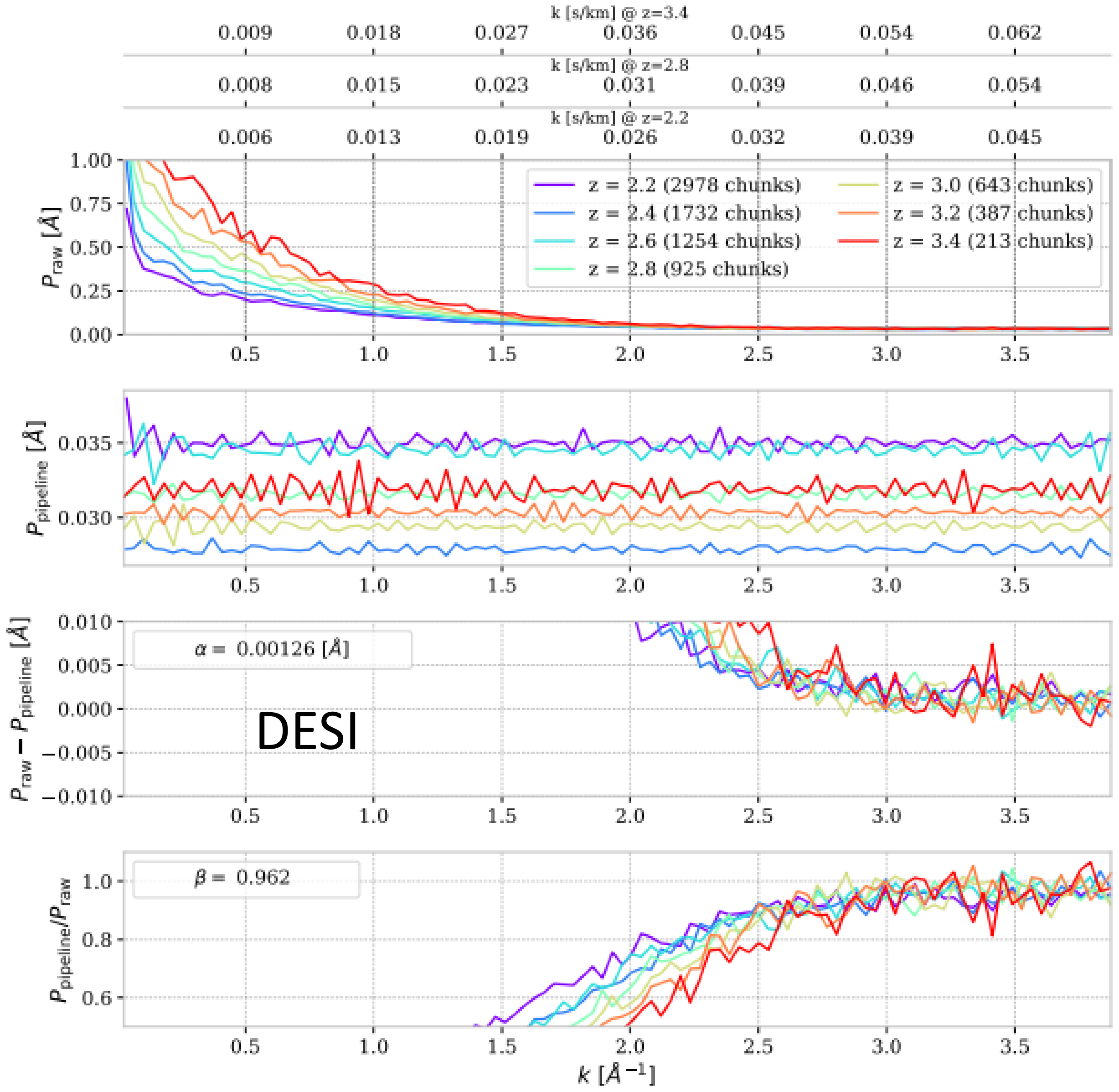

Comparison diff and pipeline noise on last reductions

- Power spectrum difference (raw and noise)

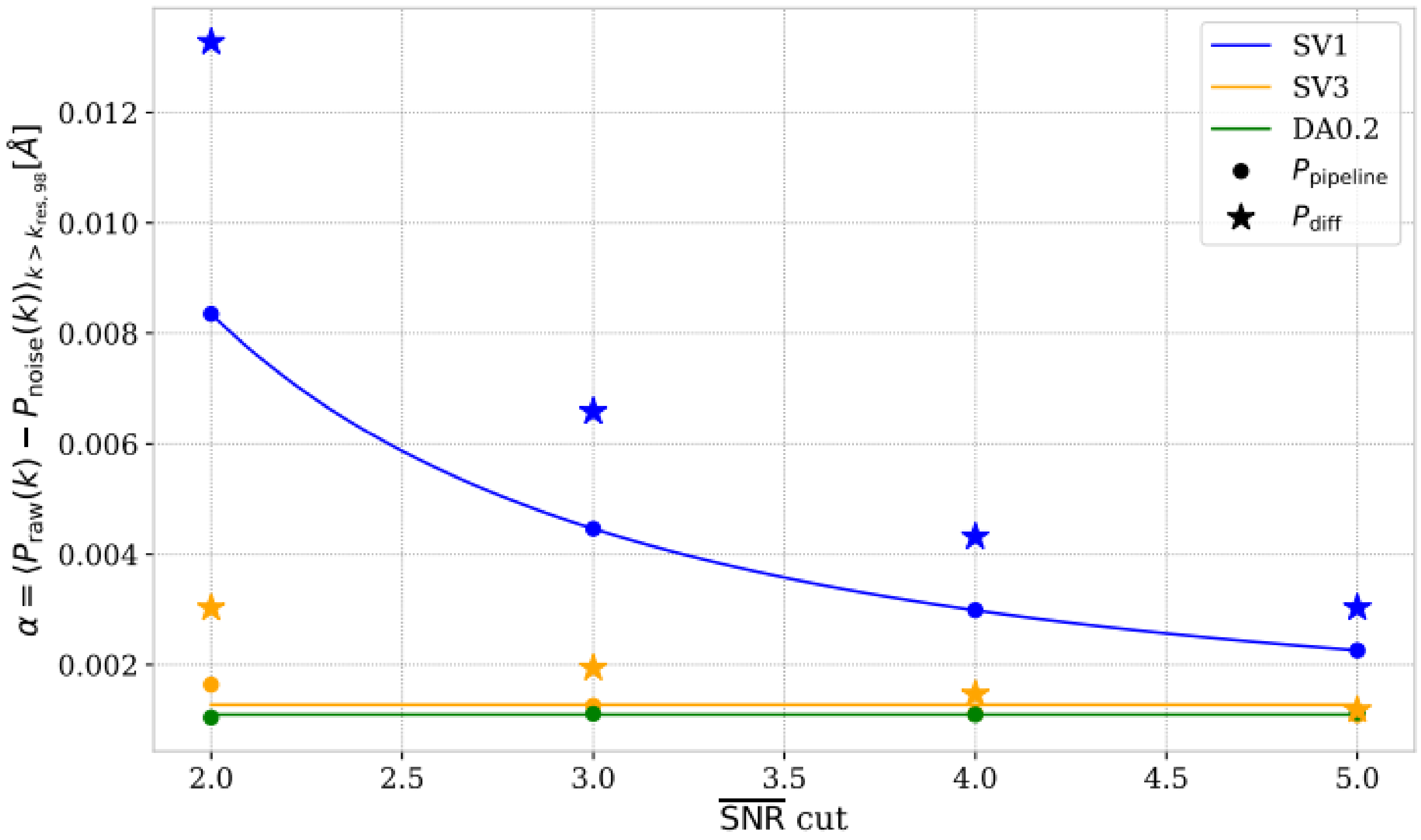

Comparison diff and pipeline noise on last reductions

- Power spectrum ratio and side bands measurements

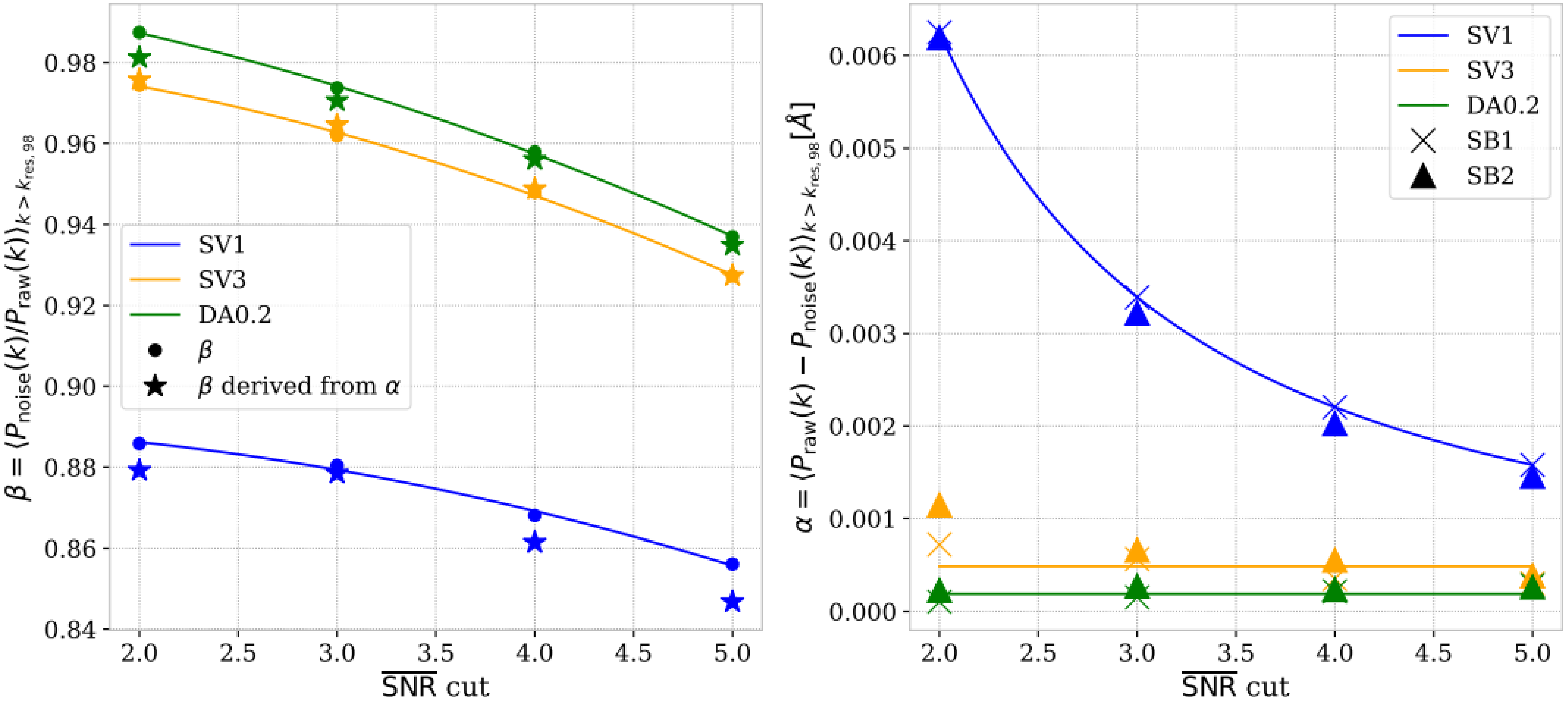

Noise correction: conclusion

- Asymptote results suggest that the correction is:
  - Mostly additive
  - Survey dependent (related to different number of exposures?)
  - SNR cut-dependent for SV1

- Correction applied:

Band	**Data**	$P_{\text{noise,miss}} = \alpha$ [Å]
Lyα	SV1	$0.026 \times \left(\overline{\text{SNR}}\right)^{-1.77} + 0.00076$
	SV3	0.00127
	DA0.2	0.00109

$P_{1D,\alpha}$ side bands

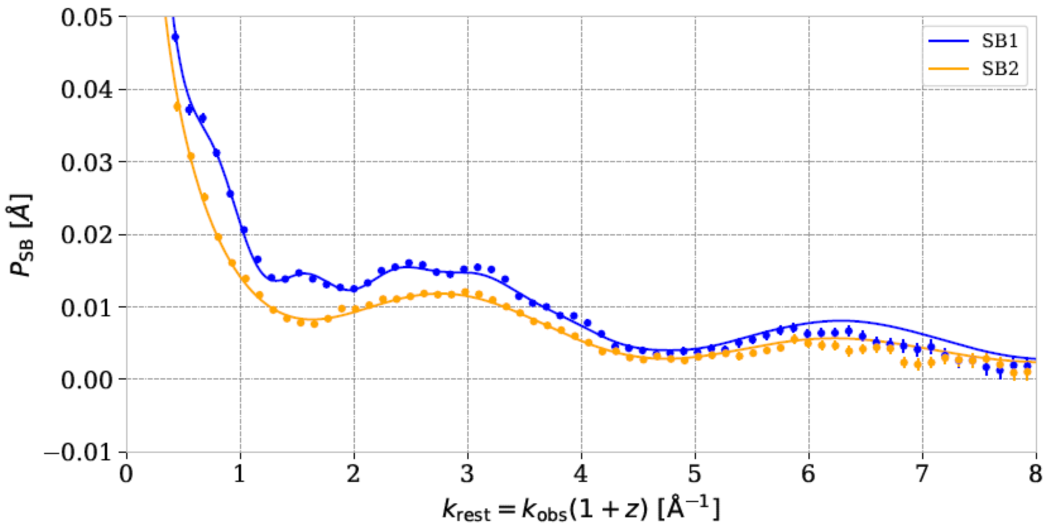

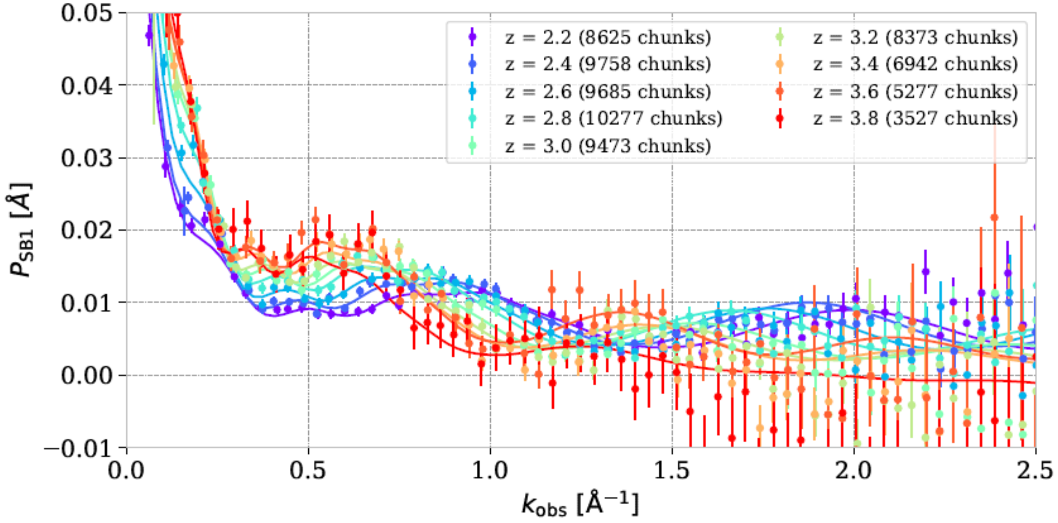

DESI

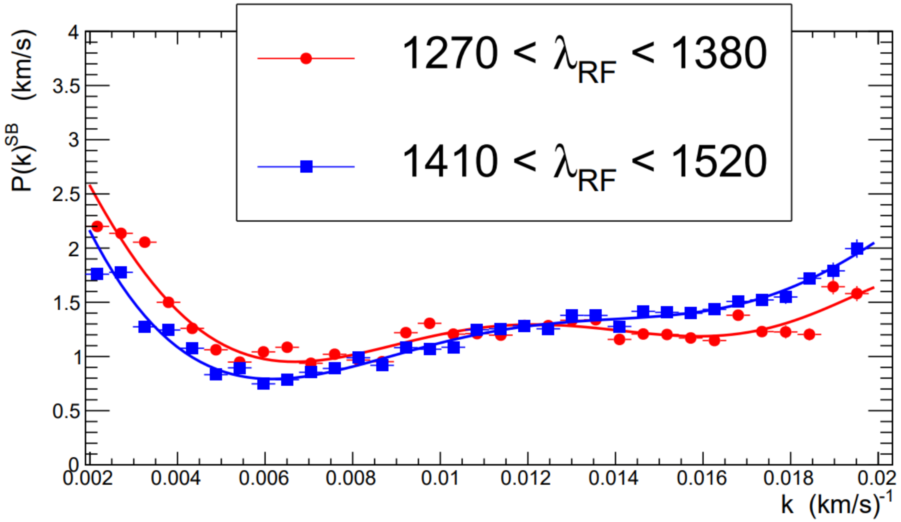

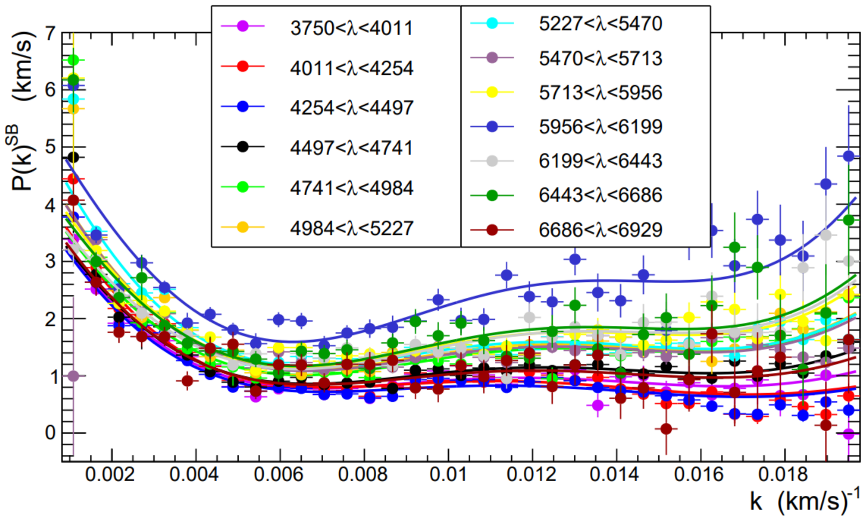

eBOSS

$P_{1D,\alpha}$ mocks

- DLA masking

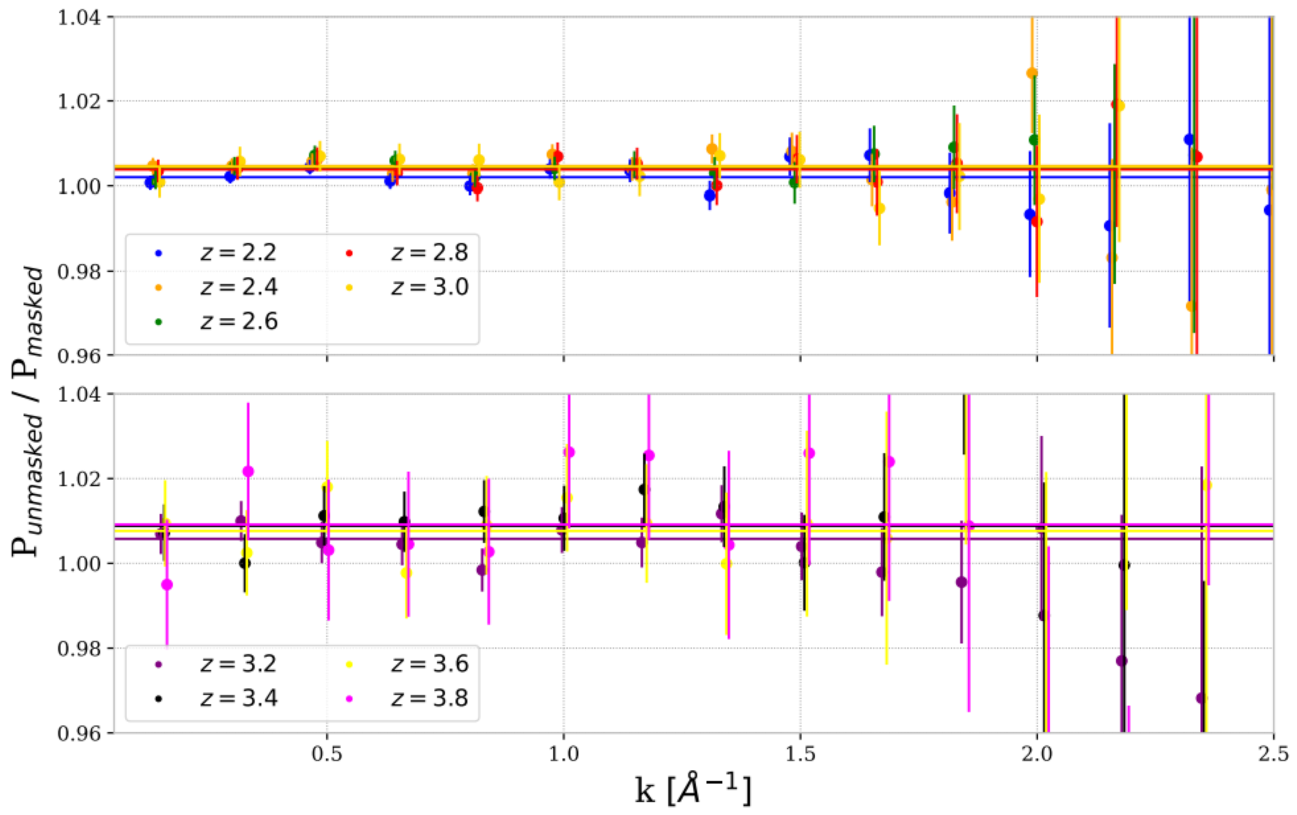

DESI

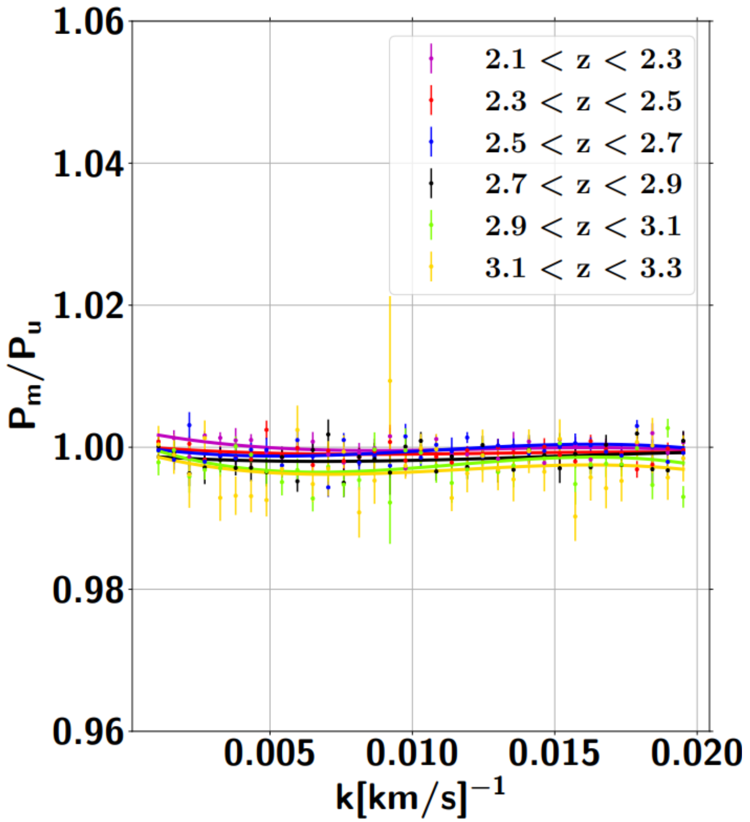

eBOSS

$P_{1D,\alpha}$ mocks

- line masking

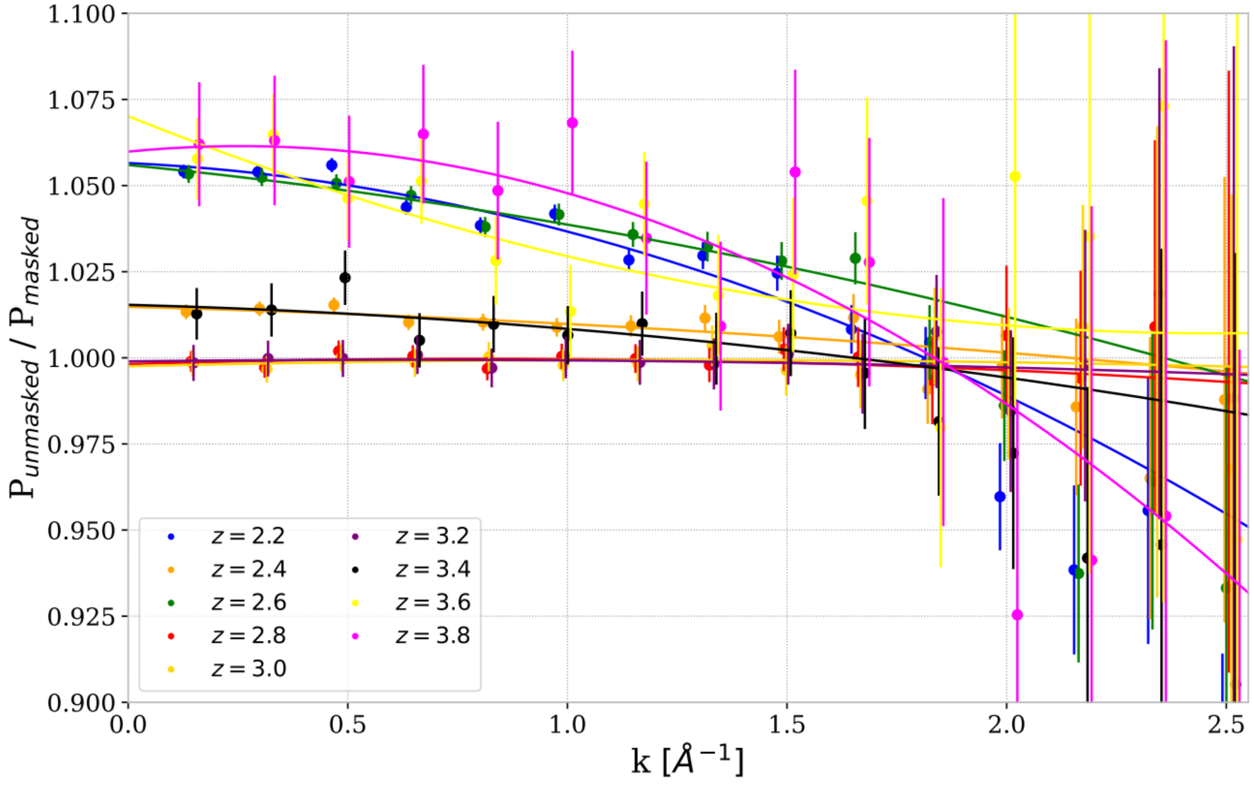

DESI

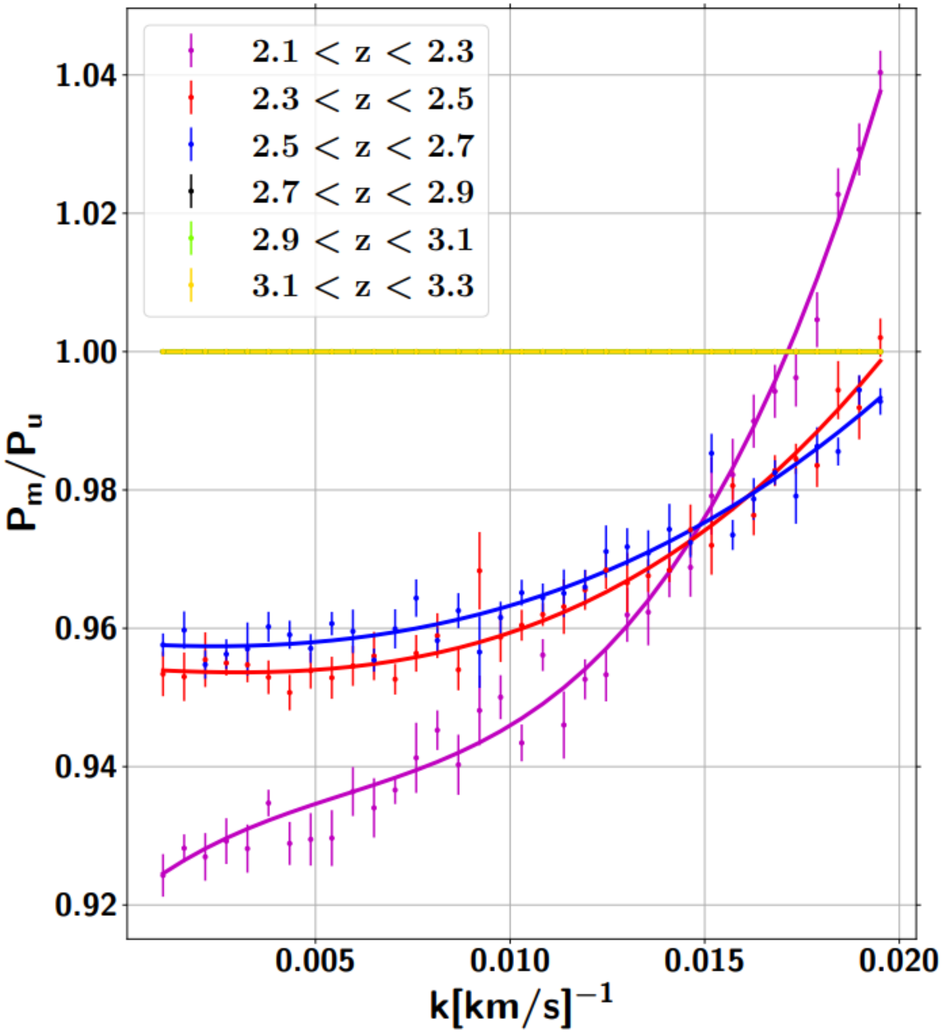

eBOSS

P1D mocks

- Residual correction (work in progress) which includes:
  - Include possible effect of wrong modeling of resolution matrix (mocks)
  - Continuum fitting errors
  - Possible FFT biases

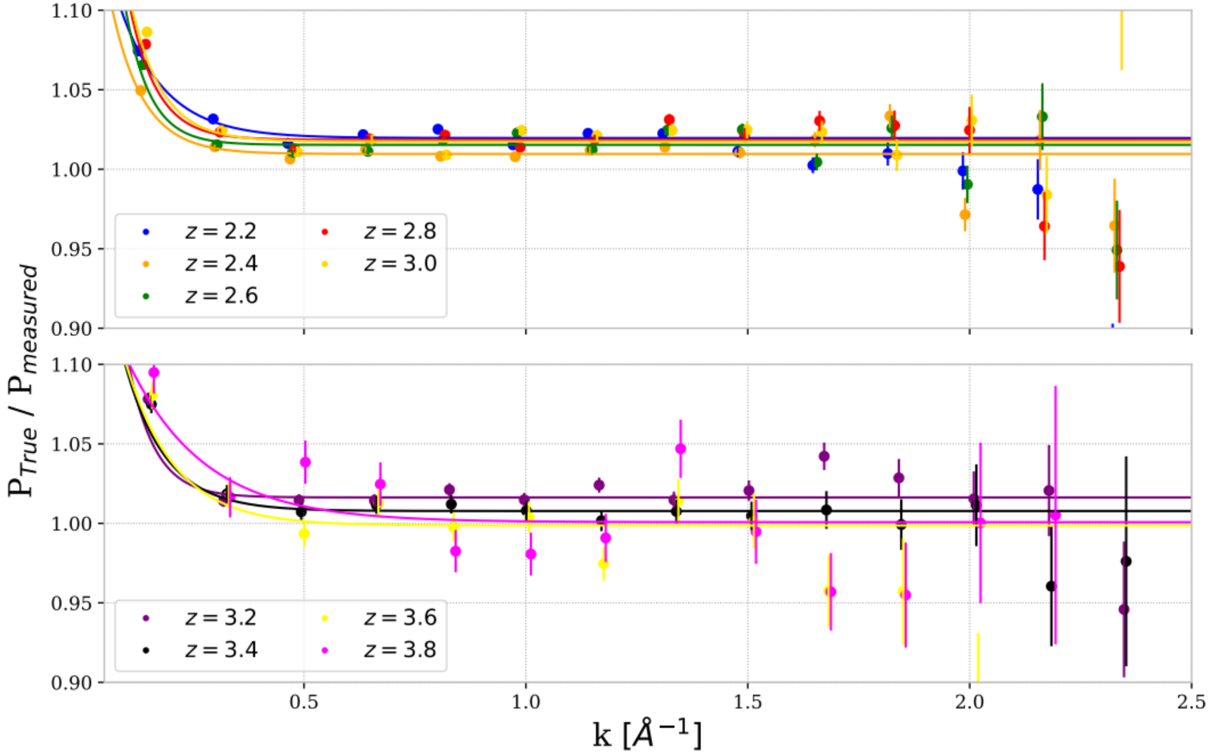

DESI

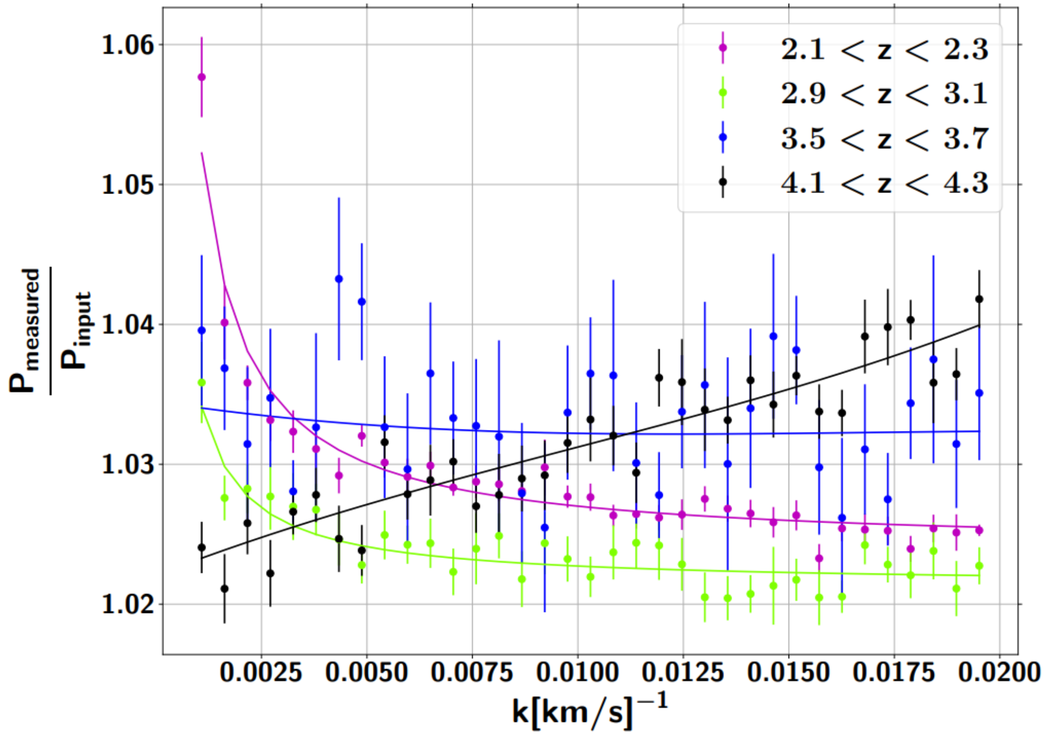

eBOSS

Final $P_{1\mathrm{D},\alpha}$ model

- Final model implemented:

$$P_{1\mathrm{D},\alpha}(k) = A_{\mathrm{sky}}(k,z)A_{\mathrm{residual}}(k,z)A_{\mathrm{hcd}}(k,z)\left(\left\langle\frac{P_{\mathrm{raw}}(k)-P_{\mathrm{noise}}(k)-\alpha(\mathrm{SNR})}{W^2(k,R,\Delta v)}\right\rangle - P_{\mathrm{SB1}}(k)\right)$$

- SNR cut chosen redshift-dependent: used of the eBOSS P1D cuts for now.

Redshift bin	2.2	2.4	2.6	2.8	3.0	3.2	3.4	> 3.6
SNR threshold	4.1	3.9	3.6	3.2	2.9	2.6	2.2	2.0

$P_{1D,\alpha}$ statistical uncertainties

- Larger than eBOSS
- Shape in agreement:
  - Large scales = increasing due to lack of mode with the size of the sub-forest
  - Small scales = noise and resolution

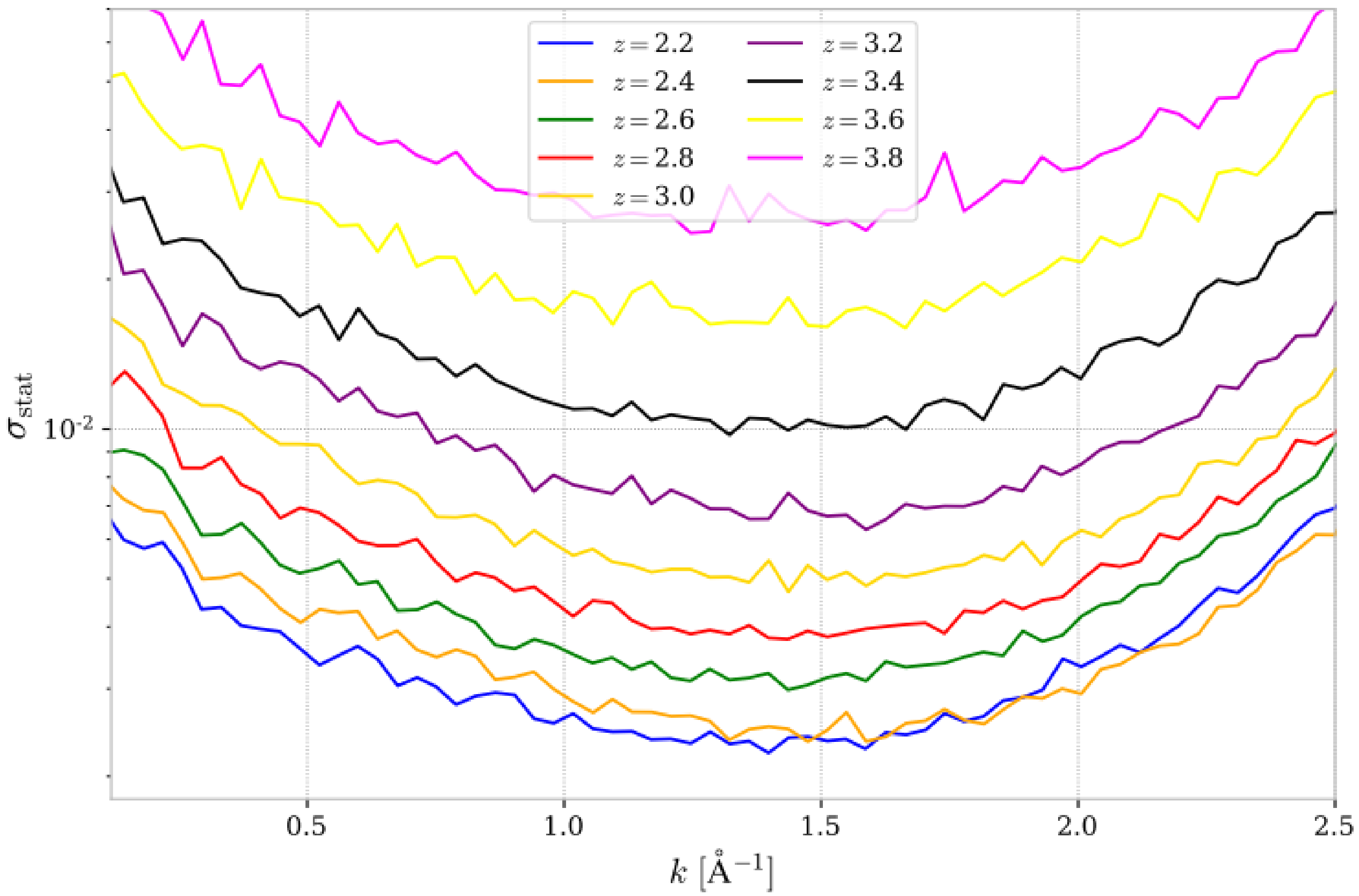

$P_{1D,\alpha}$ DESI systematics and statistics

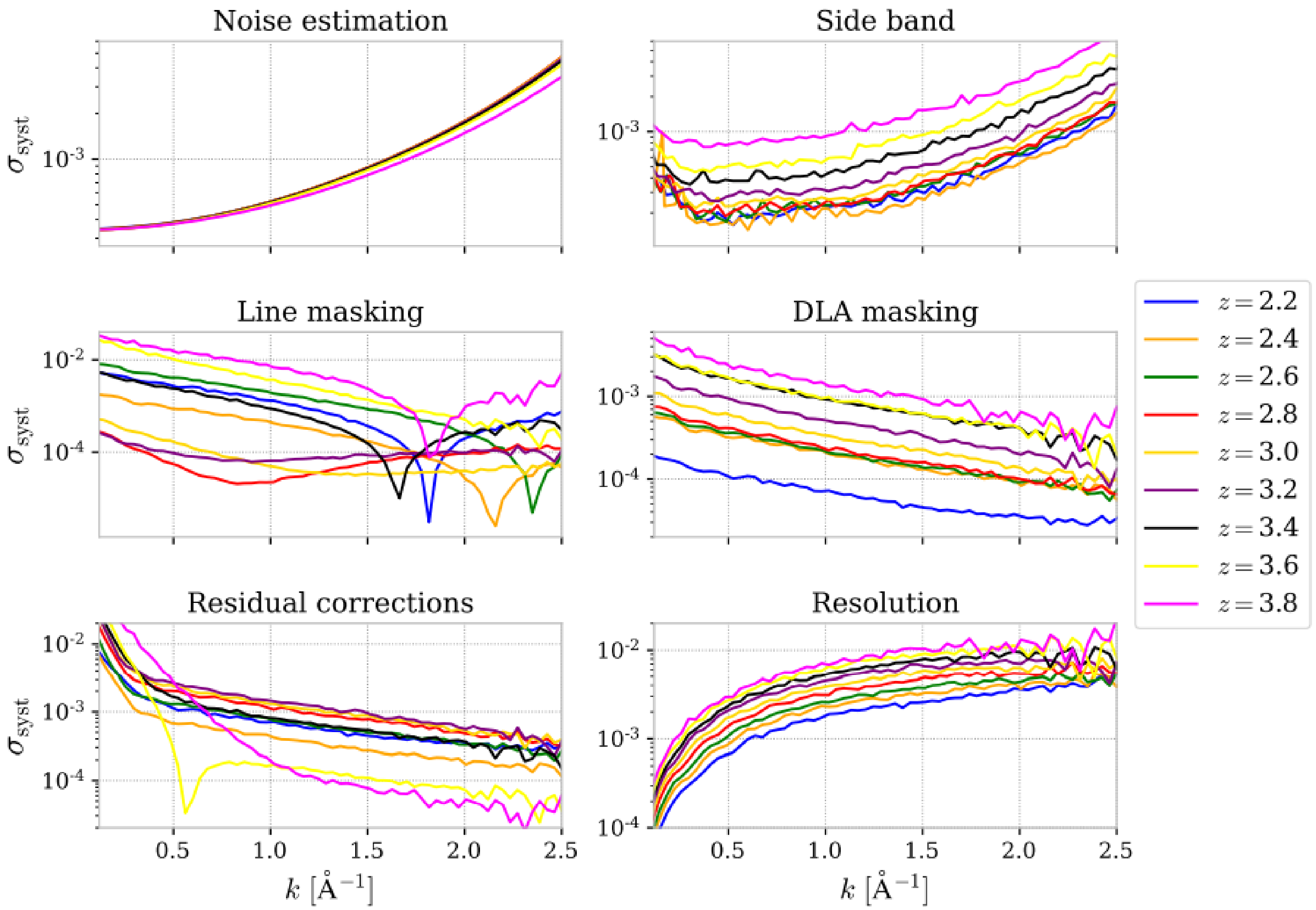

$P_{1\mathrm{D},\alpha}$ eBOSS systematics and statistics

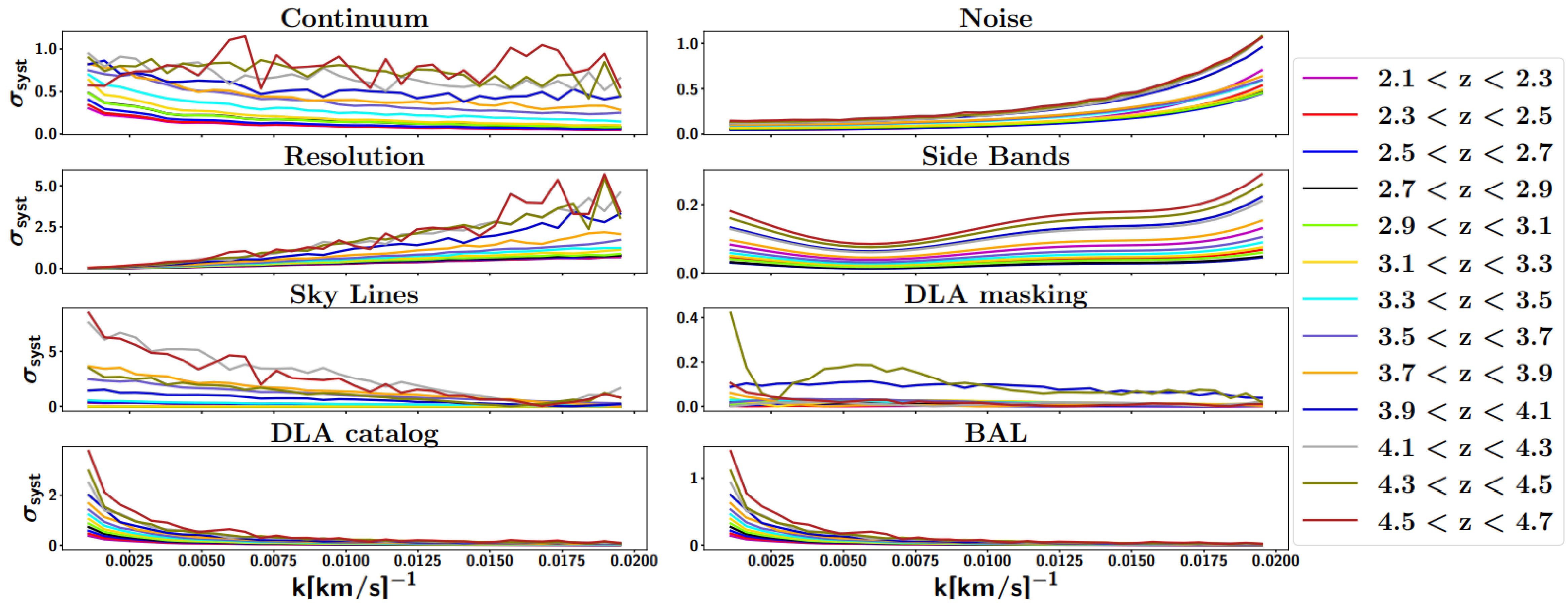

$P_{1\mathrm{D},\alpha}$ DESI systematics and statistics

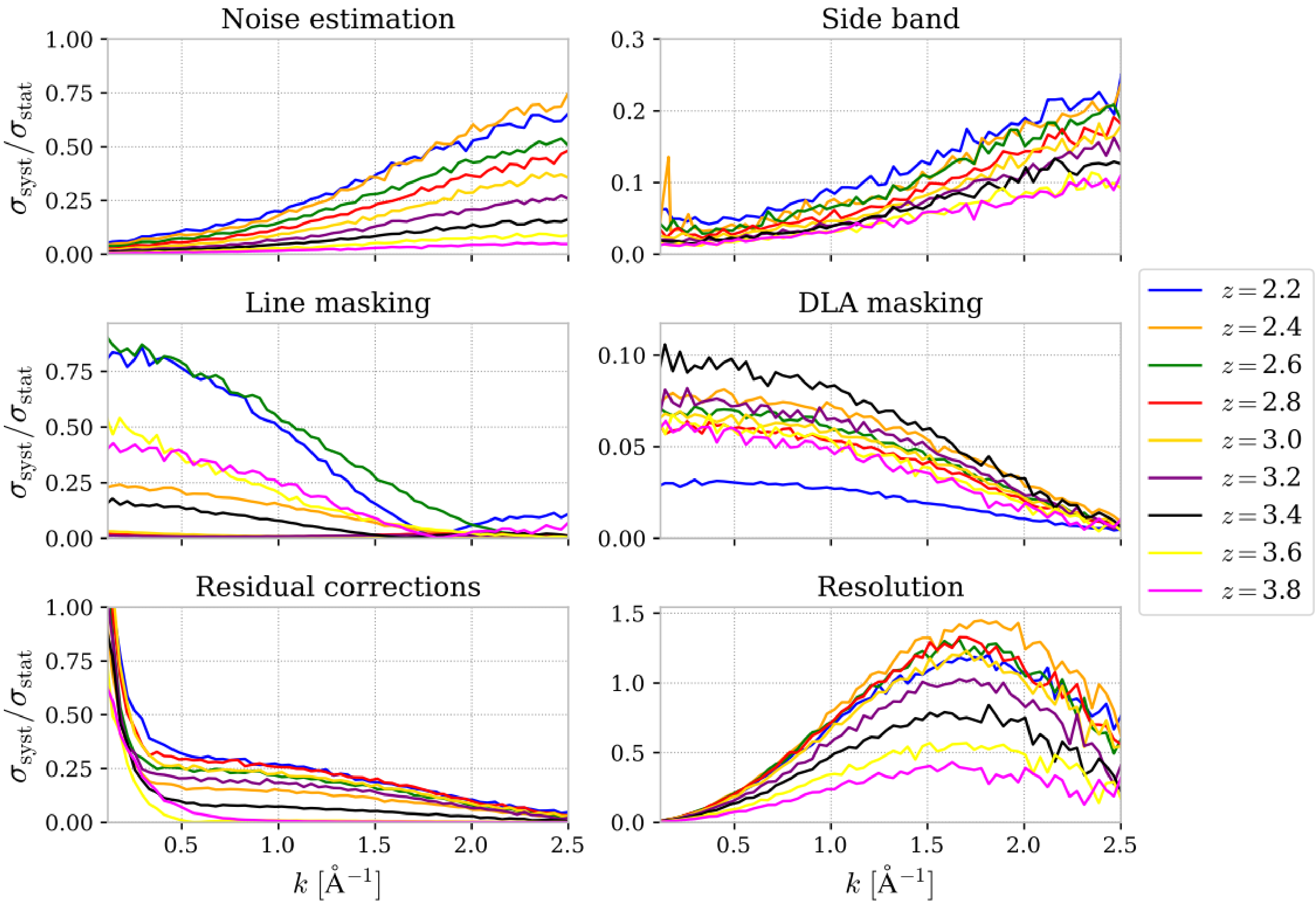

$P_{1D,\alpha}$ eBOSS systematics and statistics

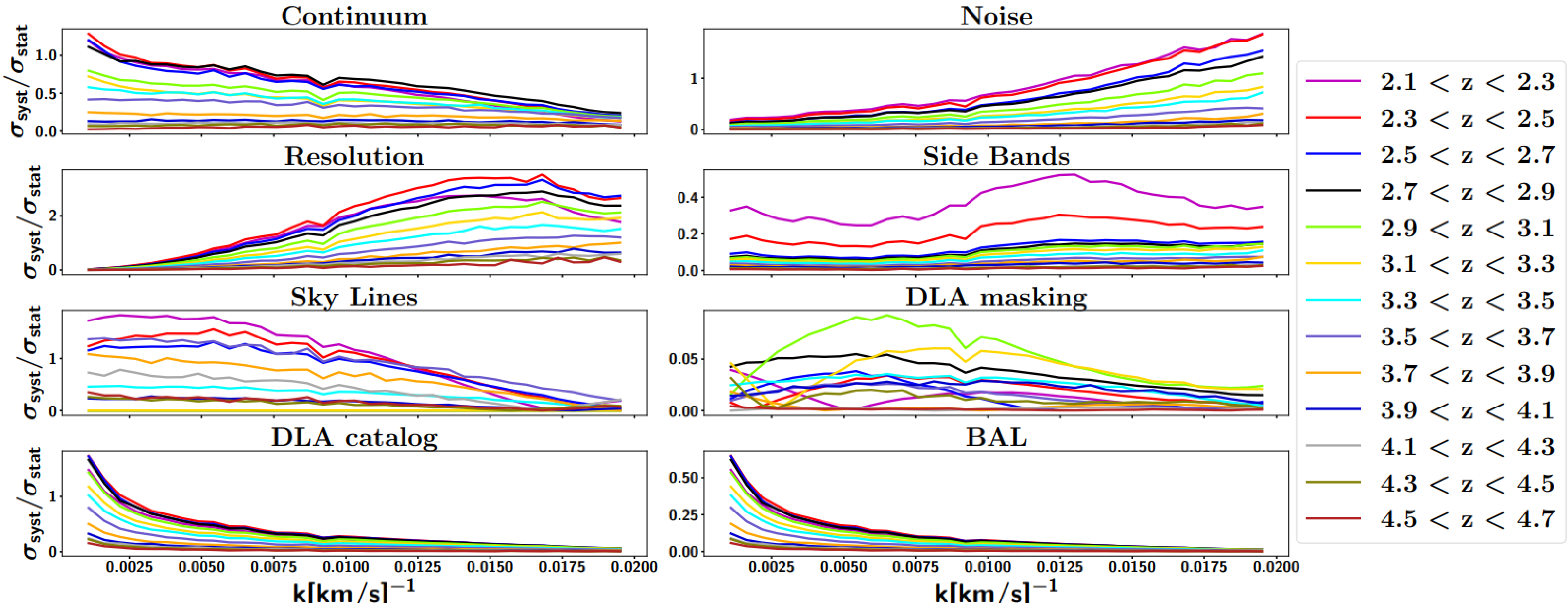

$P_{1D,\alpha}$ comparison eBOSS

- Noise and resolution corrected power spectra
- No other corrections (Metals, masking, …)

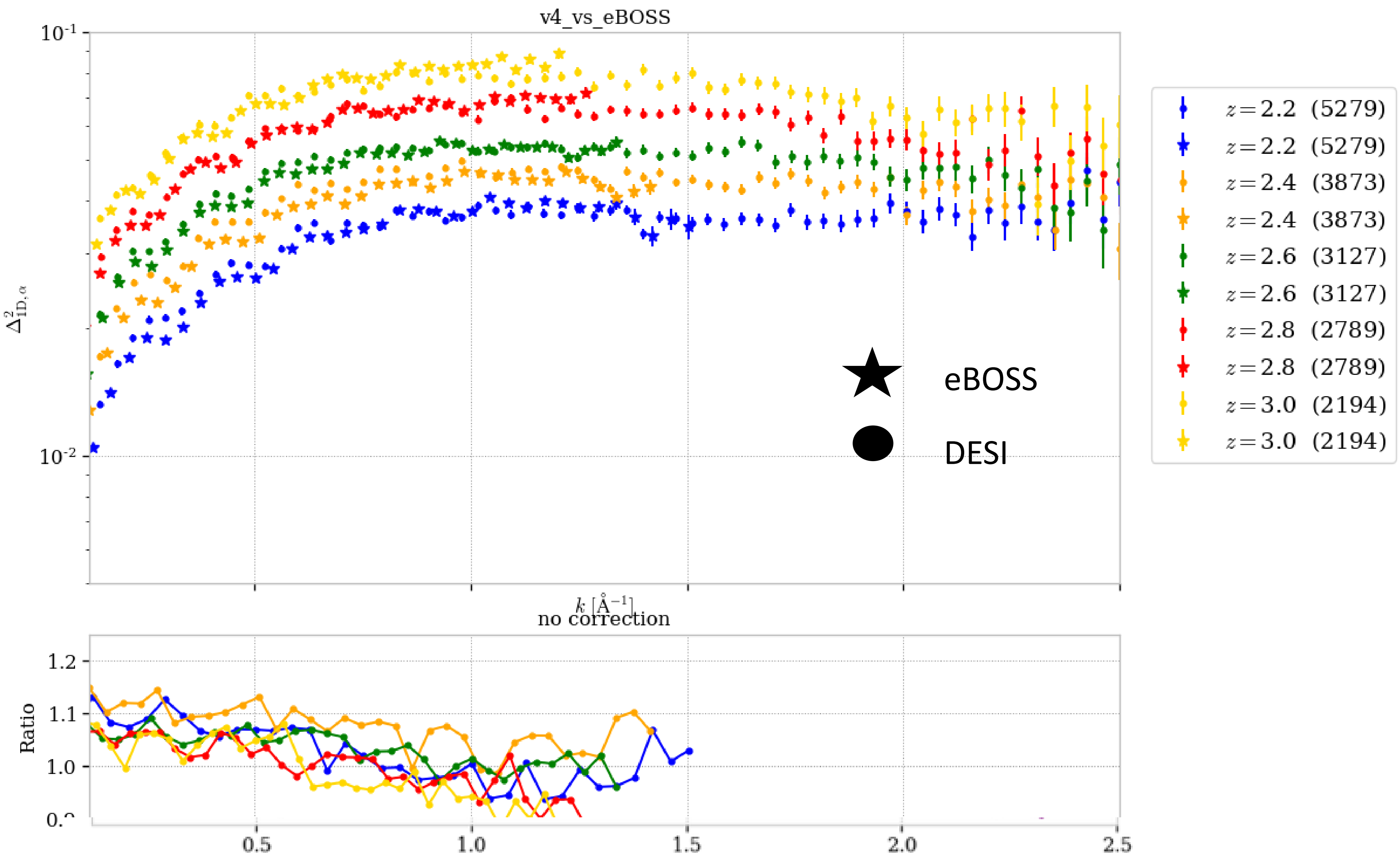

$P_{1D,\alpha}$ comparison high resolution

- High-resolution data from Karaçaylı et al. 2022
- KODIAQ, SQUAD, and XQ-100 data

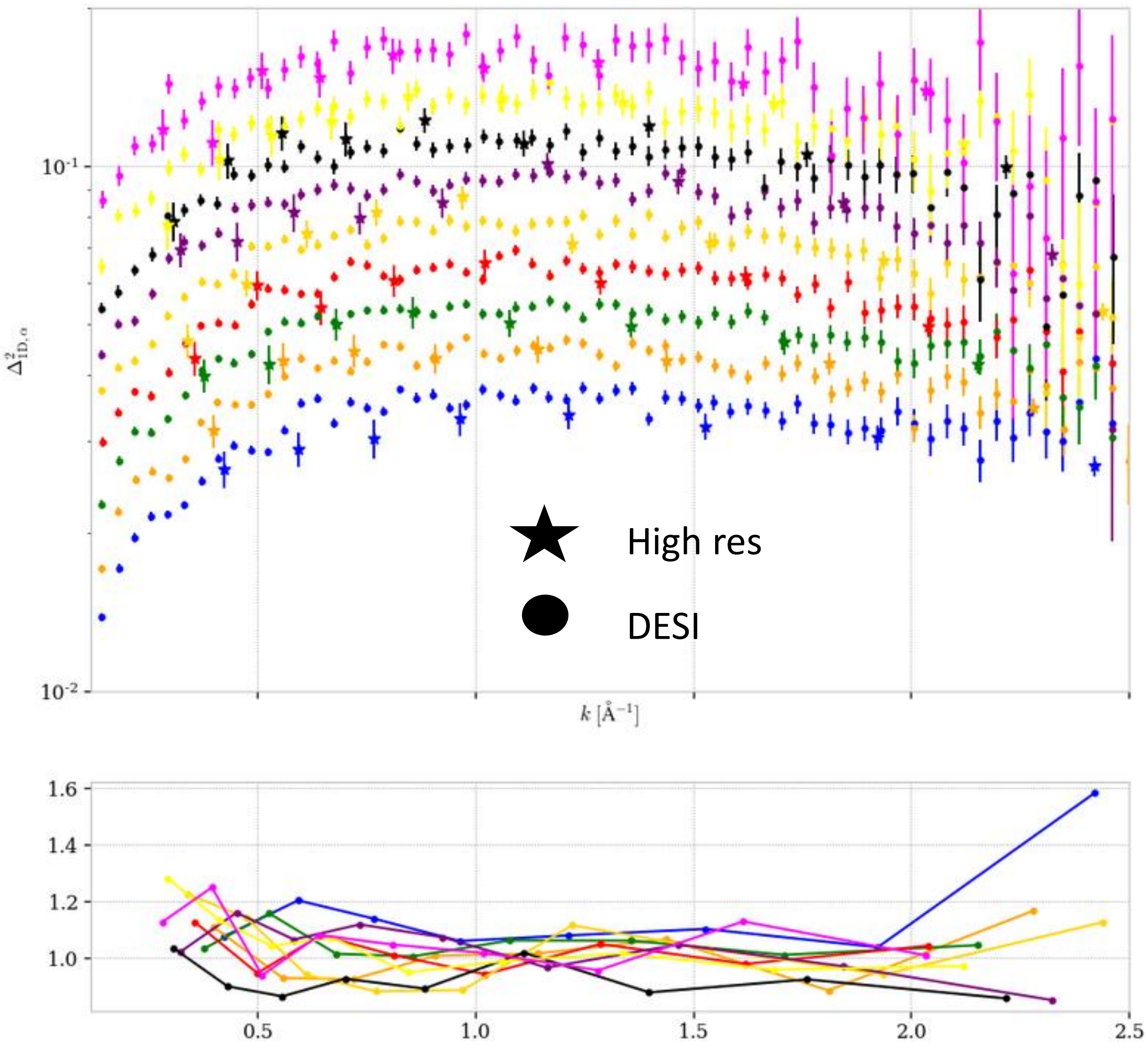

Dark matter properties

Q: Can we test specific dark matter models?

- Matter clustering may be impacted by dark matter properties
- Warm dark matter:
  - Thermal relics from cosmic microwave background
  - Mass-dependent power spectrum cut-off on small scales
- Other models:
  - Fuzzy dark matter
  - Self-interacting dark matter
  - Primordial black holes

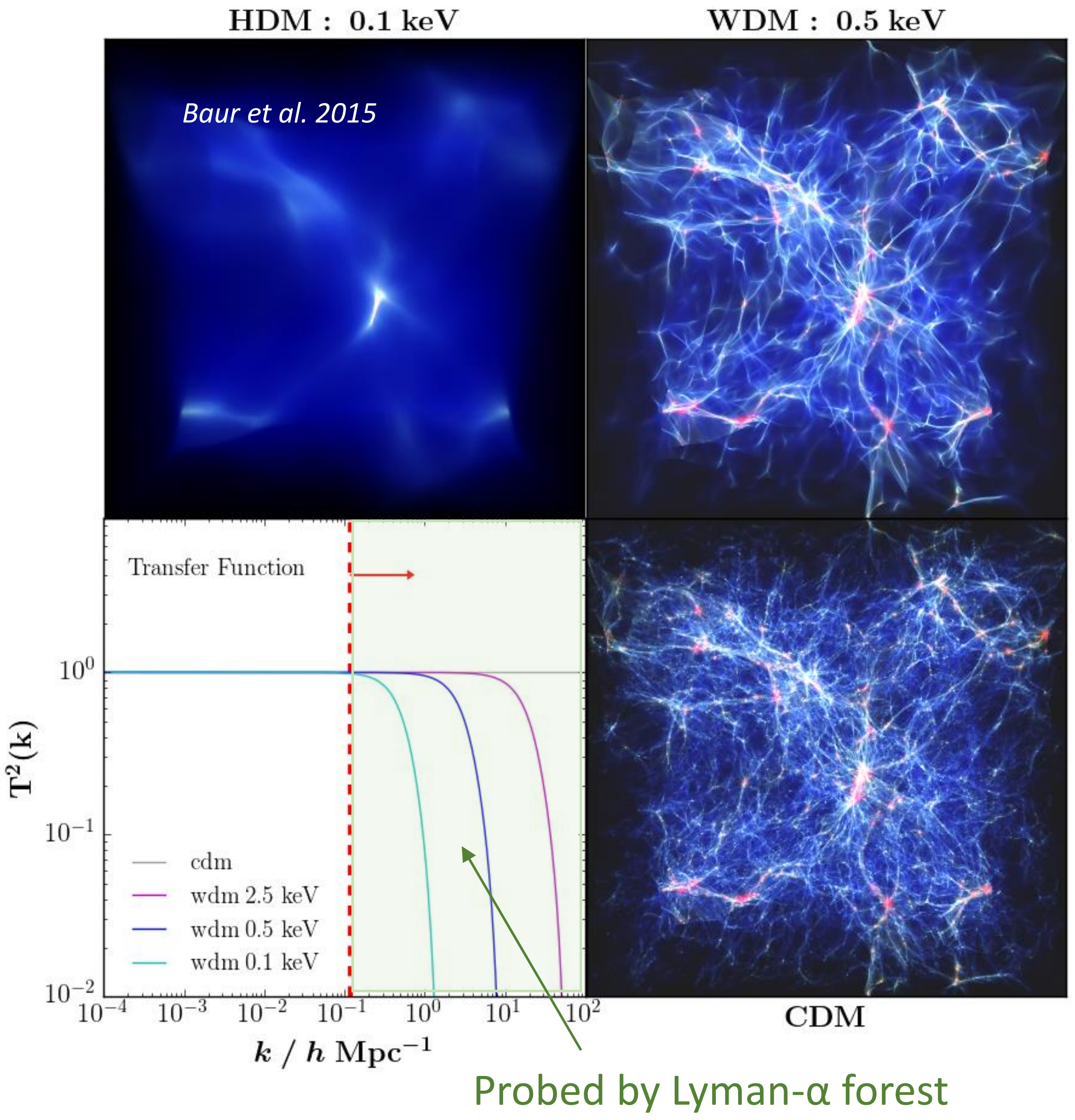

Fuzzy Dark Matter

- Fuzzy Dark Matter (Armengaud et al. 2017, Irsic et al. 2017):
  - De Broglie length close to structure formation and DM halo dynamics
    $$\frac{\lambda_{dB}}{2kpc} \sim \left(\frac{10^{-22} eV}{m}\right)\left(\frac{10\ km/s}{v}\right)$$
  - Smooth the density fluctuation by quantum wave effects
  - Constraint by P1D:

$$m_a > 2 - 3 \times 10^{-21}\ eV$$

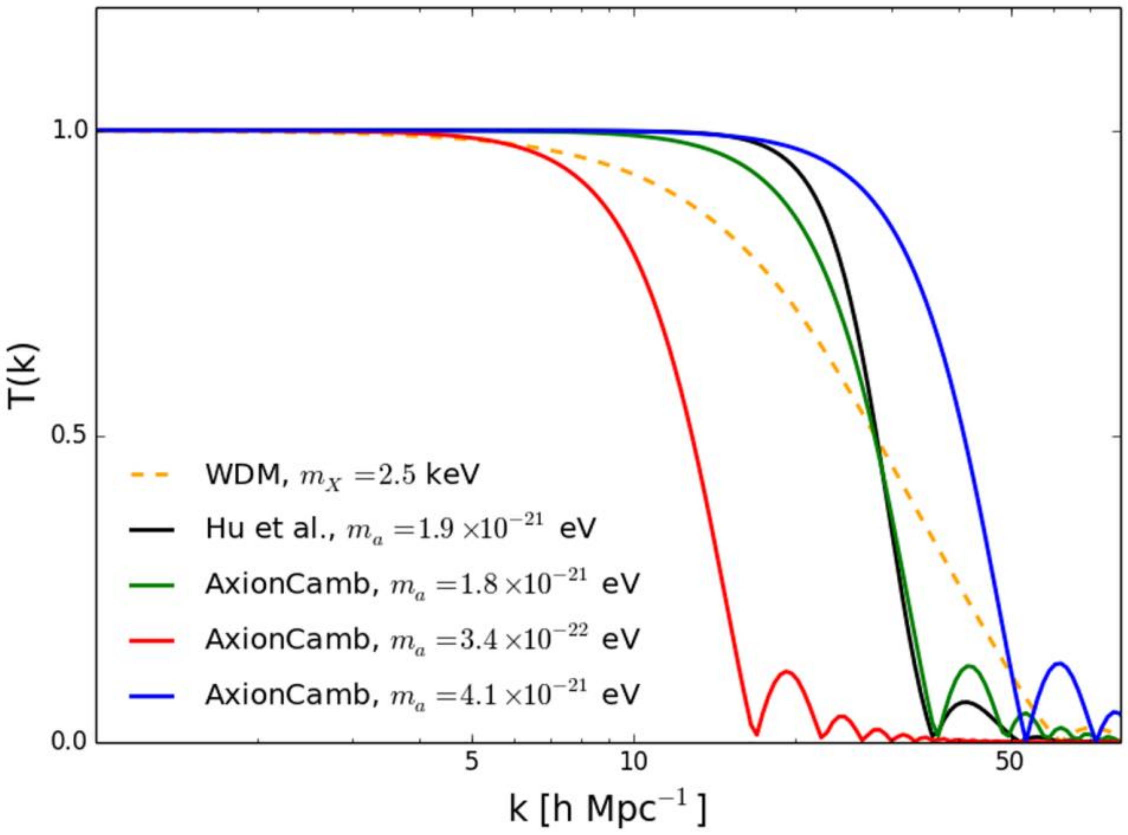

$P_{1\mathrm{D},\alpha}$ simulations

- For BOSS/eBOSS: Taylor expanded grid
- For DESI: Emulated simulation grid with Gaussian Processes (Walther et al. 2021)

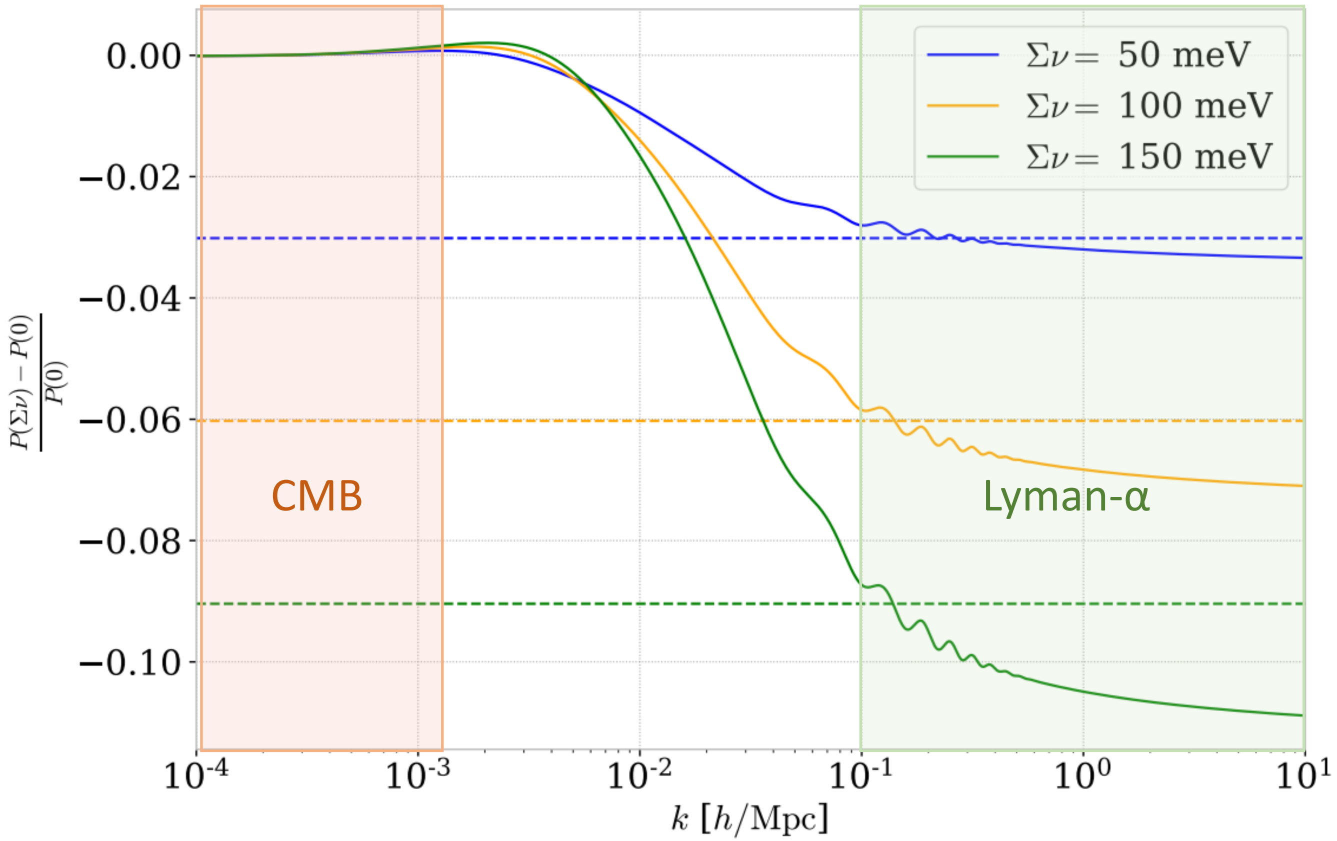

	parameter	*central*	*range*
Cosmology	keV / m_X	0.0	+0.2 +0.4
	$\Sigma m_\nu / eV$	0.0	+0.4 +0.8
	h	0.675	±0.05
	Ω_M	0.31	±0.05
	σ_8	0.83	±0.05
	n_s	0.96	±0.05
	$dn_s / d\ln k$	0.00	±0.04
	z_{reio}	12	±4
	N_{eff}	3.046	±1
Intergalactic Medium	$T_0^{z=3} / K$	14,000	±7,000
	$\gamma^{z=3}$	1.3	±0.3
Optical Depth	A^τ	0.0025	±0.0020
	η^τ	3.7	±0.4

$P_{1D,\alpha}$ simulations

- Interpretation of $P_{1D,\alpha}$ measurement with simulation:
  - At the scales considered, high-resolution hydrodynamical simulations required.
  - Nyx grid $4096^3/120$ Mpc (2M CPU hours)
- Gaussian processes emulator:
  - Covers cosmological parameter space
  - Reduce number of simulations
- Contributed to run simulations and compare codes

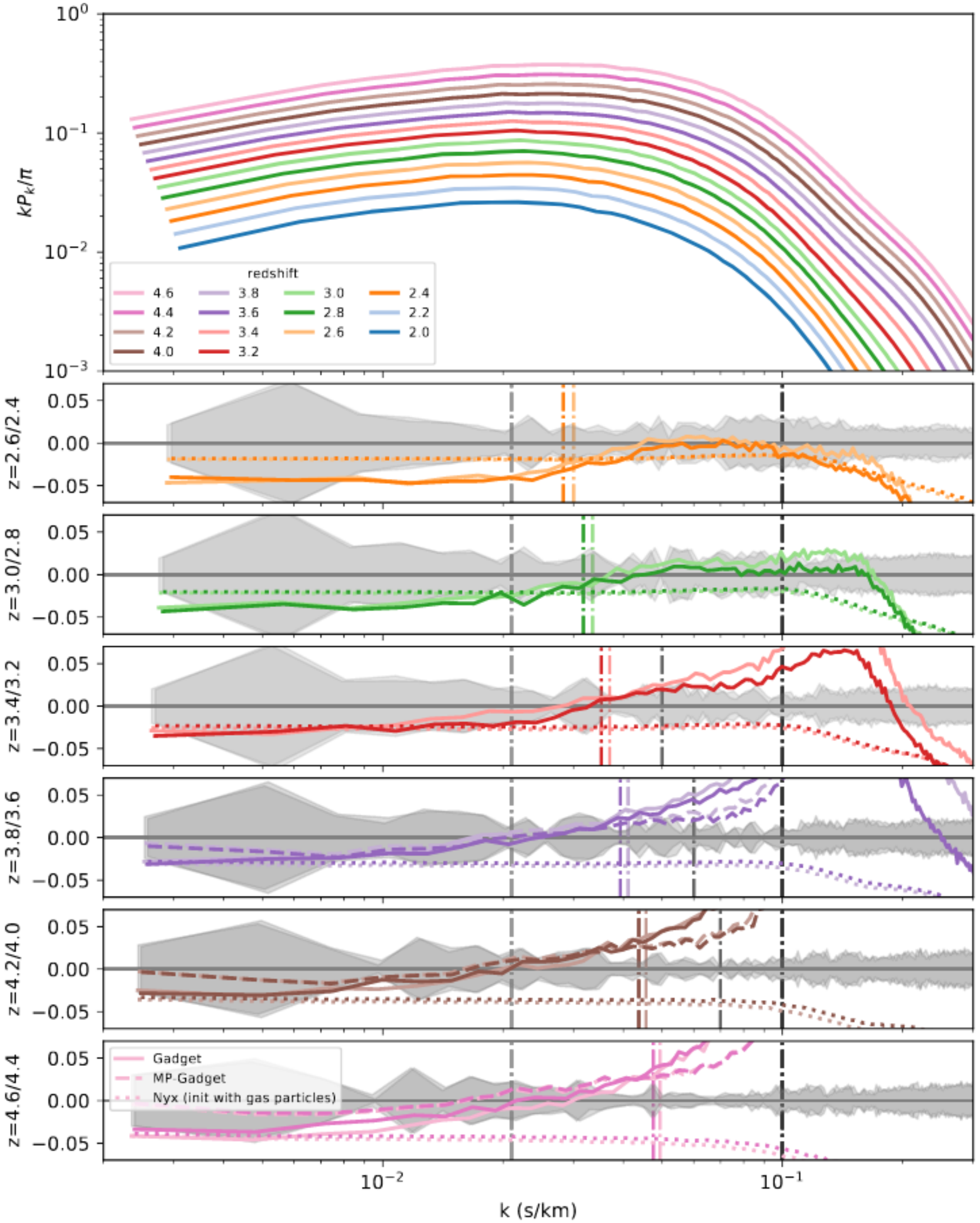

Nyx physics

- Nyx = Hydrodynamical code on grid + Dark matter particles on PM scheme
- Lyman-α forest not very sensitive to very dense IGM regions
  - AMR is not adapted
- Other physical processes modeled in Nyx:
  - Gas chemistry = fixed composition with H and He abundance
  - Inverse Compton + atomic collisional processes
- Effects not included:
  - Thermal feedback from AGN or supernovae
  - Inhomogeneous radiative background (UV)
  - High redshifts: full reionization history (assumed homogeneous)

- Choice: No explicit simulation of these effects but taken into account as a nuisance at the fitting stage
  - Example: AGN effect on P1D accounted for (Chabanier et al. 2020, Horizon-AGN simulation)
  - More modeling effort needed to take into account other effects.

AGN feedback on P1D

- Physical effect = baryons and temperature redistribution in the IGM
- P1D correction, using different feedback parameters with HorizonAGN simulations

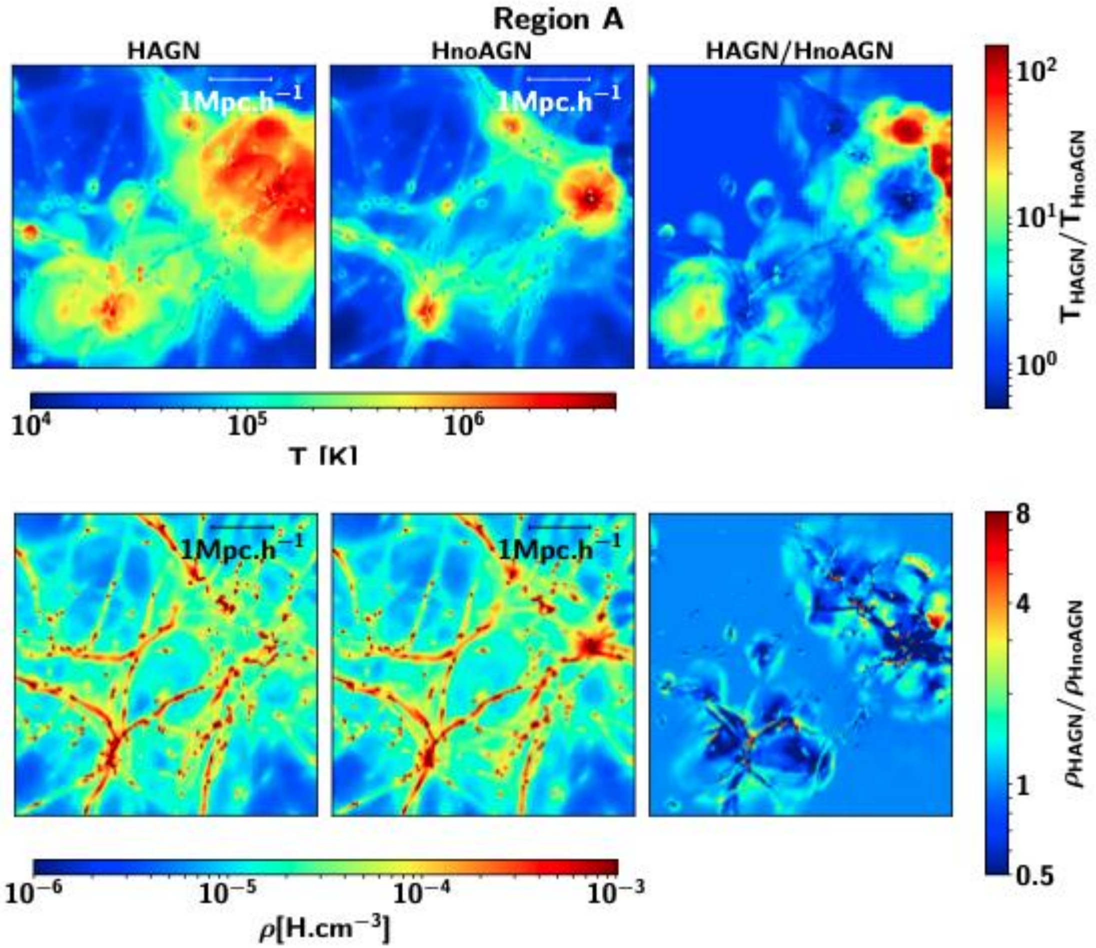

Chabanier et al. 2020

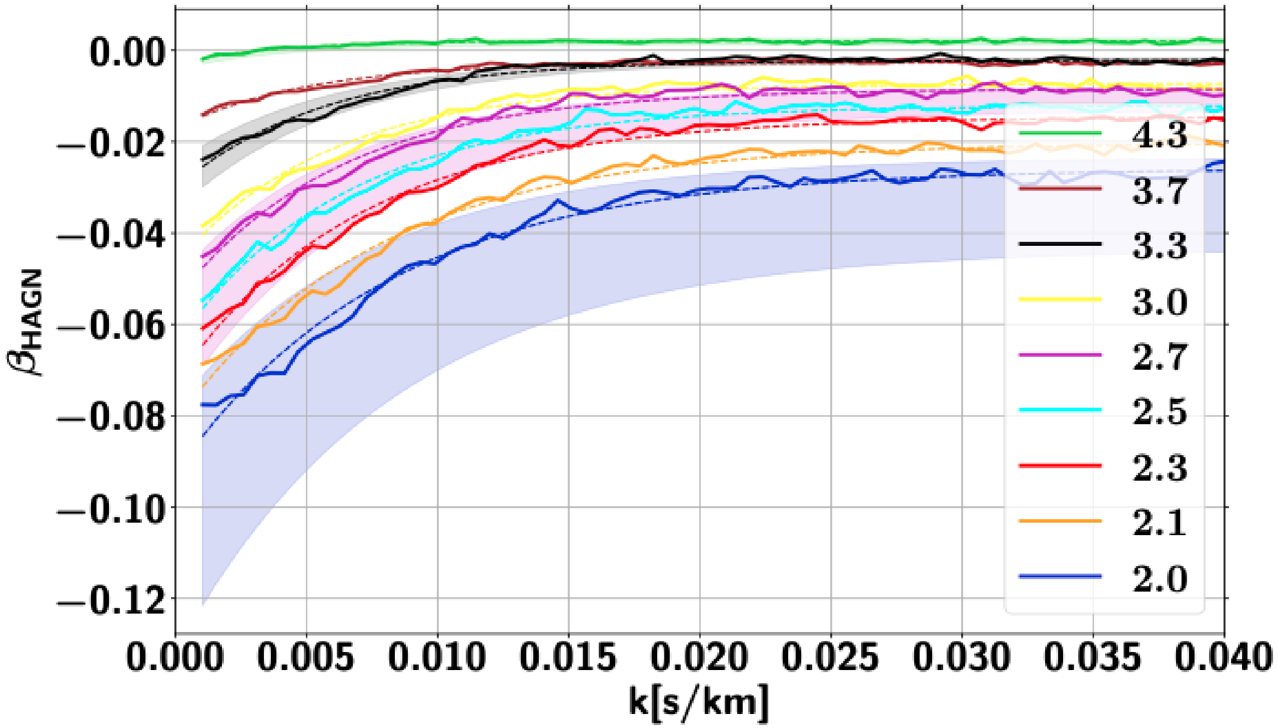

Current neutrino and WDM constraints

- Cosmological constraints using P1D computed on data and simulations (Palanque-Delabrouille et al. 2020)

- Loose constraint by Lyman-α only (Neutrinos simulated)
- Strong constraints combining with CMB data

- DESI: Emulated grid and higher data statistics will improve constraints and their robustness

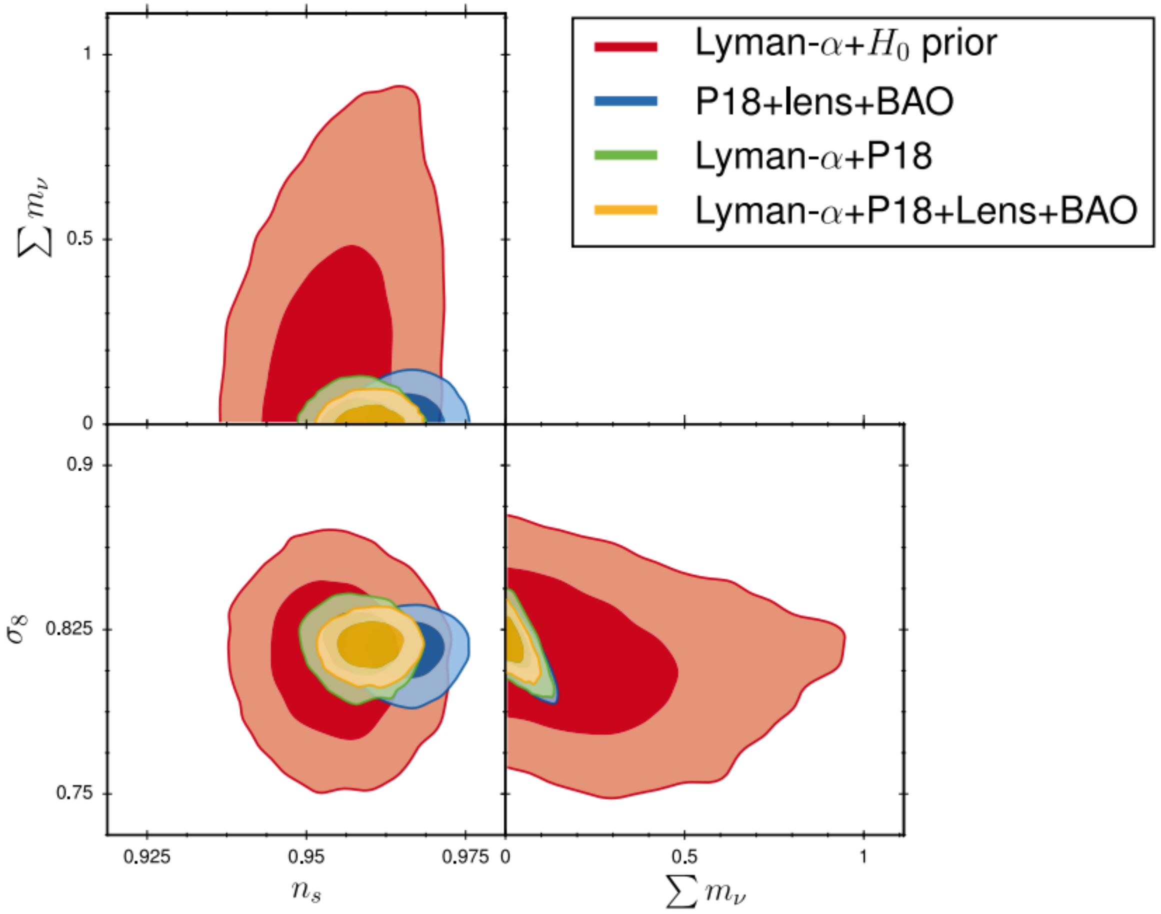

Current neutrino and WDM constraints

- Neutrino mass:

P1D	P1D + CMB	P1D + CMB + BAO + WL
$\sum m_\nu < 0.58\ eV$	$\sum m_\nu < 0.11\ eV$	$\sum m_\nu < 0.09\ eV$

(Palanque-Delabrouille et al. 2020) 95 % CL

- WDM mass (eBOSS + XQ100):

$$m_X > 5.3\ keV$$

95 % CL

- Sterile neutrinos (Baur et al. 2016):
  - Equivalence relation with thermal relics mass (WDM)
  - P1D constraint: $m_s > 34\ keV$ (Non-resonantly produced)
  - X-ray signal at $m_s = 7\ keV$ → in strong tension

Rescaling method for neutrino constraints

- Neutrinos can be accounted into simulation by exploiting the power spectrum level degeneracy

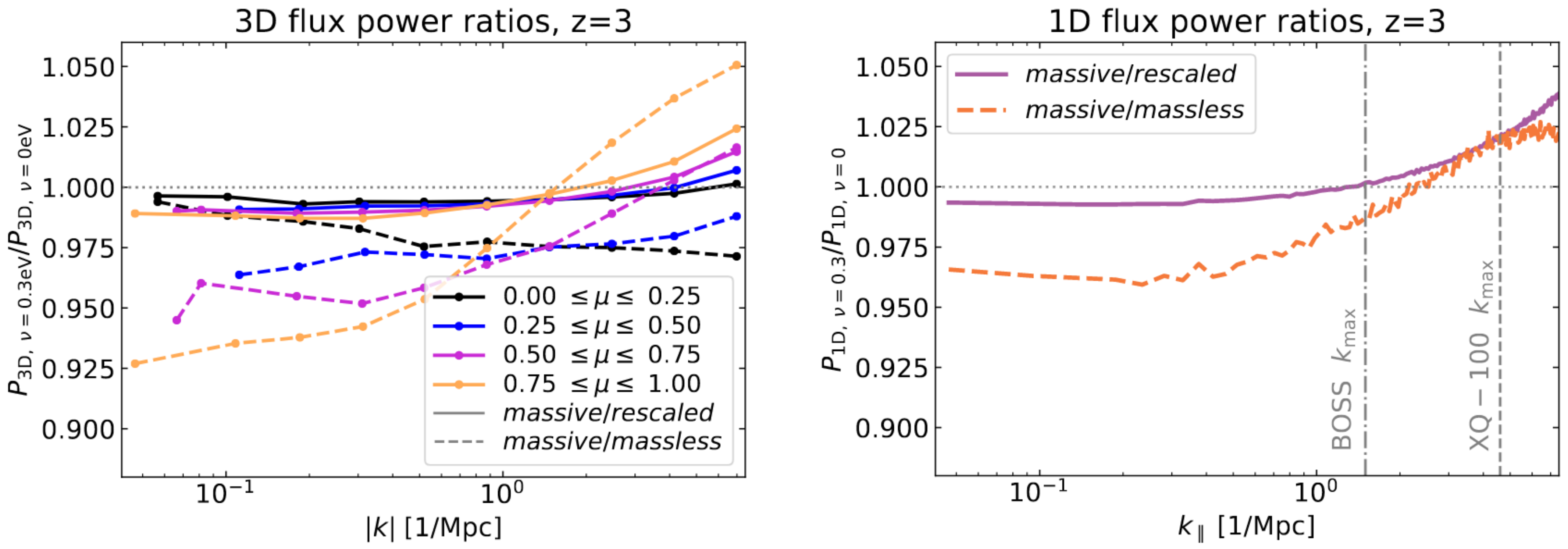

Pedersen et al. 2020

DESI forecast

- DESI collaboration 2016

Data	$\sigma_{\Sigma m_\nu}$ [eV]	$\sigma_{N_{\nu,\mathrm{eff}}}$
Planck	0.56	0.19
Planck + BAO	0.087	0.18
Gal ($k_{\mathrm{max}} = 0.1h\,\mathrm{Mpc}^{-1}$)	0.030	0.13
Gal ($k_{\mathrm{max}} = 0.2h\,\mathrm{Mpc}^{-1}$)	0.021	0.083
Ly-α forest	0.041	0.11
Ly-α forest + Gal ($k_{\mathrm{max}} = 0.2$)	0.020	0.062

Details on $P_{3D,\alpha}$ simulations

- $P_{3D,\alpha}$ predictions on Jean-Zay "grand challenge" simulations
- Variation of resolution and box size

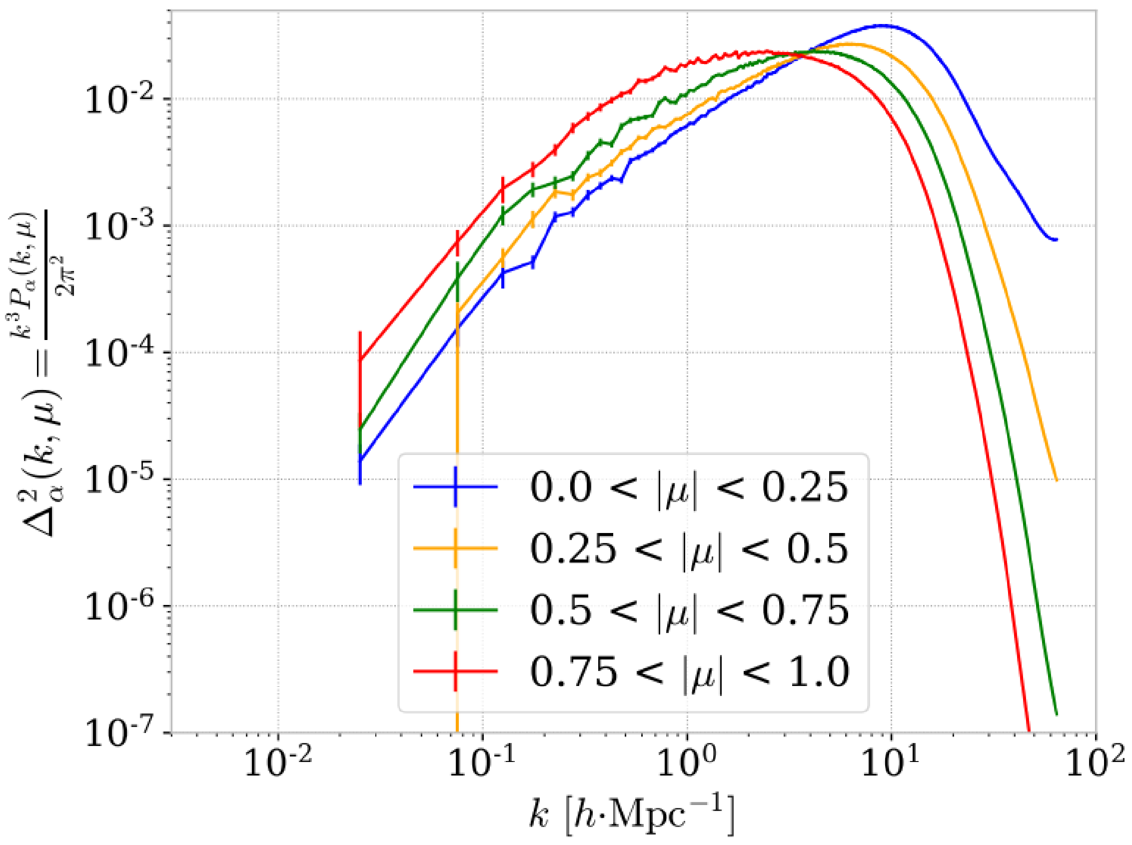

L125

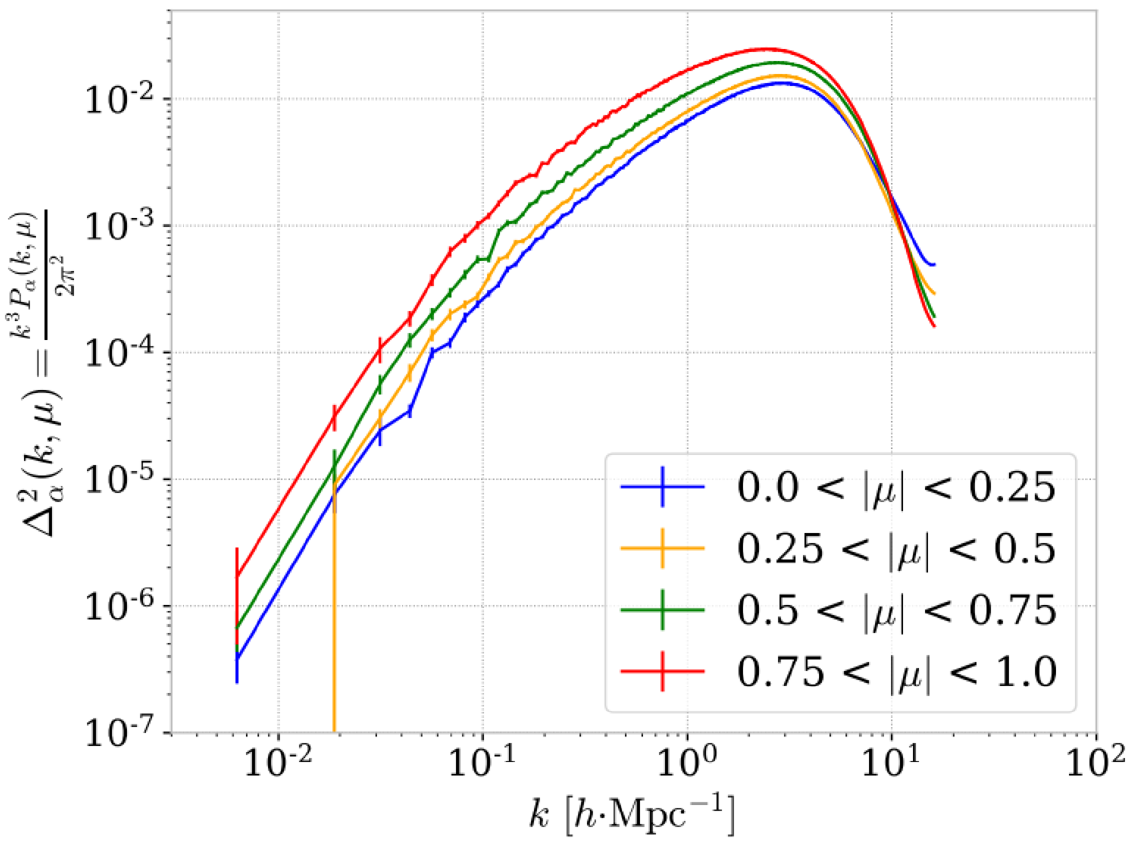

L500

Details on $P_{3\mathrm{D},\alpha}$ simulations

- Splicing: use of high resolution and small boxes, with low resolution and large boxes.

- Verification on boxes for which high resolution/large size box is available.

Mcdonald et al. 2003

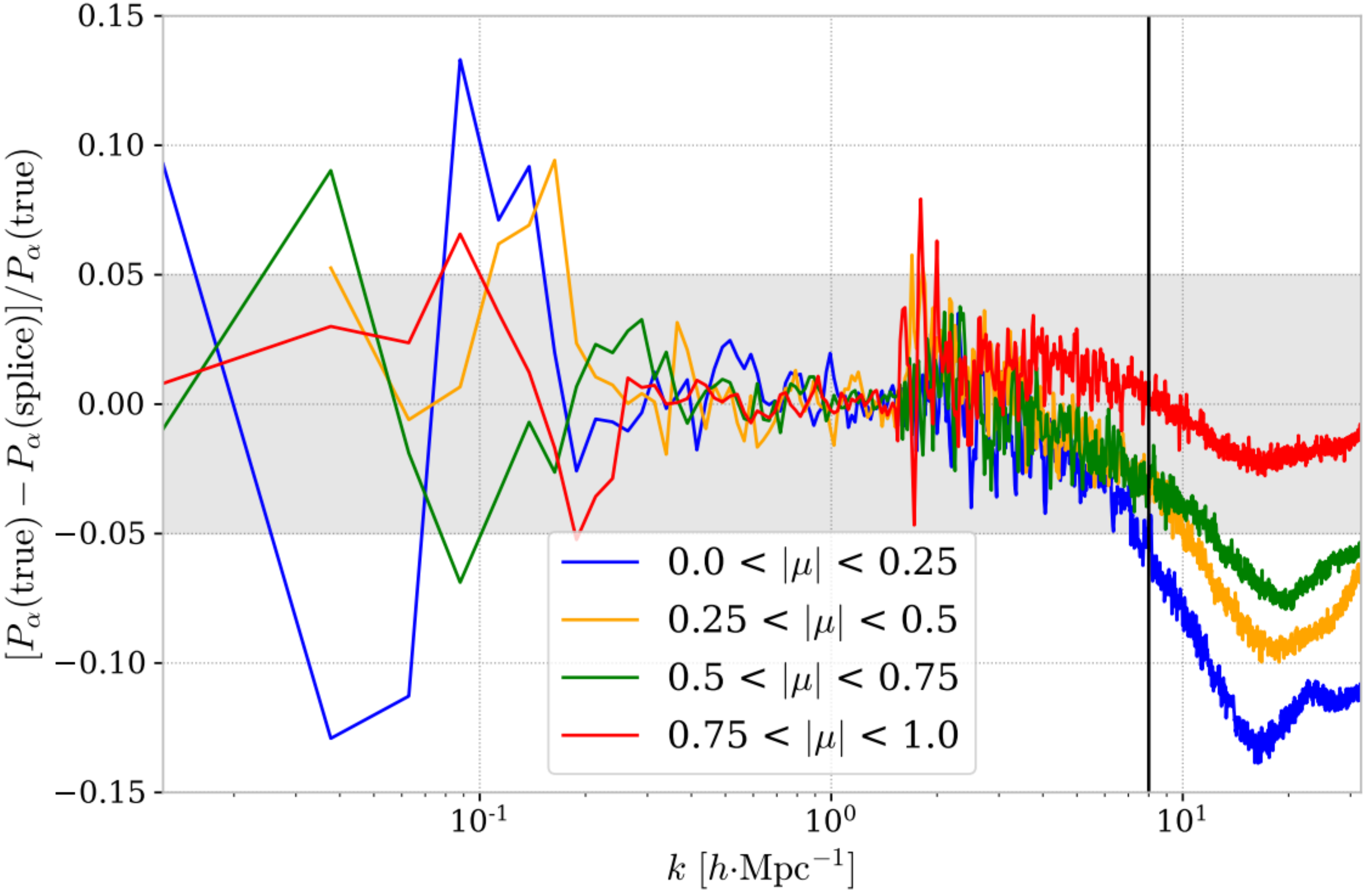

Details on $P_{3\mathrm{D},\alpha}$ simulations

- $P_{3\mathrm{D},\alpha}$ model

$$P_{\mathrm{model},\alpha}(k,\mu) = b_\alpha^2 \left(1 + \beta_\alpha \mu^2\right)^2 P_\mathrm{m}(k) D(k,\mu)$$

$$D_1(k,\mu) = \exp\left\{ \left[q_1 \frac{k^3 P_\mathrm{m}(k)}{2\pi^2} + q_2 \left(\frac{k^3 P_\mathrm{m}(k)}{2\pi^2} \right)^2 \right] \left[1 - \left(\frac{k}{k_\mathrm{v}} \right)^{a_\mathrm{v}} \mu^{b_\mathrm{v}} \right] - \left(\frac{k}{k_\mathrm{p}} \right)^2 \right\}$$

Details on $P_{3\mathrm{D},\alpha}$ simulations

- Fitting of linear parameters

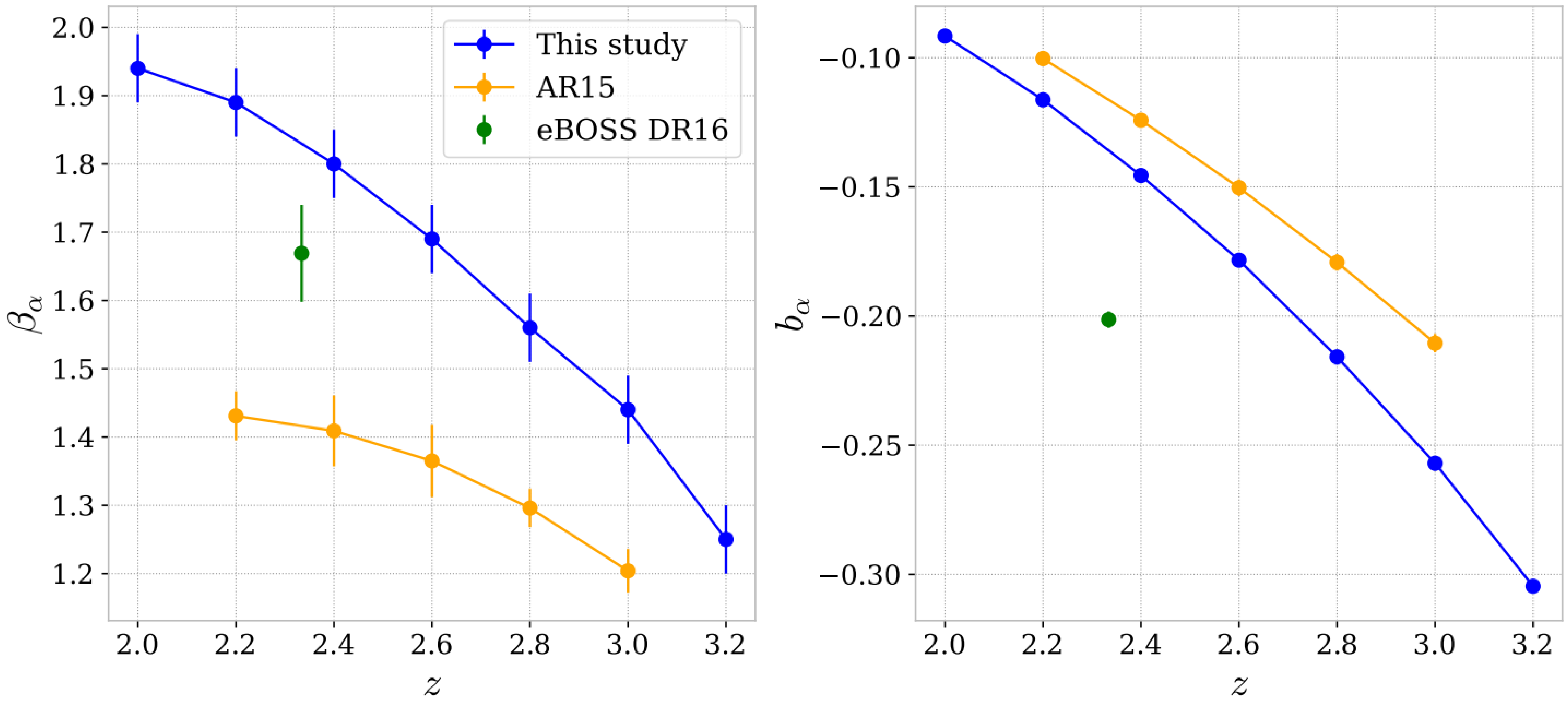

Other $P_{3D,\alpha}$ simulations

- Givans et al. 2022